VIBRATIONAL BAND SHAPE ANALYSIS AND INTERMOLECULAR INTERACTIONS IN SOME COMPLEX MOLECULES

SOMA DATTA
DEPARTMENT OF PHYSICS

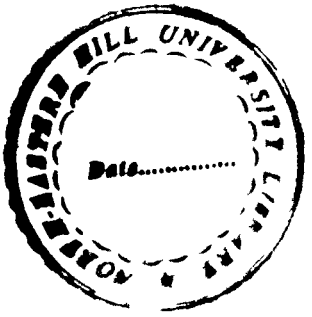

A Thesis
submitted in partial fulfilment of the requirement of the Degree of
DOCTOR OF PHILOSOPHY
in
PHYSICS

of
NORTH-EASTERN HILL UNIVERSITY
SHILLONG
INDIA

PHY

DS
530.6
DAT

DEDICATED TO MY LOVING PARENTS

whose encouragement and affection has been a constant source of inspiration for this thesis. Any accomplishment of mine is due in no small part to their support.

THE NORTH-EASTERN HILL UNIVERSITY
April, 2006

DECLARATION

I, Soma Datta, hereby declare that the subject matter of this thesis is the record of work done by me, that the contents of this thesis did not form basis of the award of any previous degree to me or to the best of my knowledge to anybody else, and that the thesis has not been submitted by me for any research degree in any other University/Institute.

This is being submitted to the North-Eastern Hill University for the degree of Doctor of Philosophy in Physics.

Soma Datta

(Soma Datta) 21/4/06.

P. Nongkynrih

(Dr. P. Nongkynrih)
Professor & Head
Department of Physics

Prof. & Head,
Physics Department,
N.E.H.U, Shillong-793022.

Kamal Kumar

(Dr. Kamal Kumar)
Professor
Department of Physics

ACKNOWLEDGEMENTS

There are many persons to be thanked for their inspiration and support during this study without whom this work would not have been possible.

First of all, I take the opportunity with immense pleasure, to gratefully acknowledge the enthusiastic supervision of Professor Kamal Kumar, department of physics, NEHU. I am indebted to him for introducing me to the subject and for his support and encouragement during the course of the work.

I am grateful to Professor P. Nongkynrih, Head of the physics department for her interest in this work. I acknowledge my sincere thanks to Mr, A.K. Rathore for his adept assistance in recording the Raman spectra. I would also like to thank the staff of the physics department for their help and cooperation.

I am extremely grateful to Dr. Th. Gomti Devi for the fruitful discussions and valuable suggestions, which helped me in completing this work. A special word of thanks to my friends Sandy and Romolus, for their support and interest in the progress of my work.

Finally, I am forever indebted to my parents and my sister Sweta for their understanding, endless patience and encouragement when it was most required during the course of work.

(Soma Datta)

CONTENTS

CHAPTER 1

CHAPTER 1

INTRODUCTION

Laser Raman scattering studies of molecules provide an insight into the understanding of vibrational relaxation mechanism in liquids and detailed information about the molecular environment and the specific dynamic processes in liquids [1-10]. Vibrational lineshapes in condensed phases contain the details of the interactions of a normal mode with its environment. These interactions include the important microscopic dynamics and intermolecular couplings.

The study of dynamical behavior in molecular liquids is very difficult since in the liquid state, the molecules are in state of chaotic motion. The importance of liquid phases in chemical reactions has made liquid science an important and rapidly developing field of research. In recent years, there has been a considerable interest in the study of vibrational relaxation in liquids and considerable progress has been made through experiment, theory and computer simulation. The vibrations of a molecule are sensitive probes of local structure and dynamics in molecular liquids. Raman scattering experiment may be

used to obtain detailed information about the specific dynamic process in the liquid.

Through a study of vibrational relaxation in molecular liquids, it is possible to gain information about the molecular environment and the main intermolecular forces operative in this state of matter. The processes such as chemical kinetics and solution micro-dynamics can be investigated through a study of vibrational relaxation in molecular liquids. The time resolved experiments have been performed, and these studies have allowed accurate information on dynamics in the solid and liquid states. During the past few decades, vibrational relaxation and molecular reorientation processes in liquids have been studied by analyzing the isotropic and anisotropic profiles of the Raman band of the molecule [1-6]. The isotropic component has contribution only from the vibrational process while the anisotropic component has contributions both from vibrational and reorientational processes. Raman bands of molecules are often observed to be sensitive to various environmental effects such as pressure, temperature, density and solvent concentrations. Precise measurements of isotropic Raman line shapes through continuous Raman scattering have allowed a systematic investigation of these aspects of dephasing in liquids [11].

Since intermolecular interactions depend on orientation and distance, the interactions are inherently time dependent. Thus the

eigenvalues and eigenfunctions are time dependent and are constantly fluctuating. These fluctuations are intimately involved in chemical processes, and they are also used to understand dynamics of the solvent and the nature of solute-solvent interactions. The solute-solvent interactions are having implications in drug-drug interactions, adsorption phenomenon, chemical kinetics, ligand-protein interactions, etc.

Vibrational dephasing also known as vibrational phase relaxation refers to the loss of coherence by a collection of oscillators coupled to a solvent bath. Imagine an oscillator whose vibrational motion is perturbed by the fluctuating interactions with the surrounding solvent. The phase of the oscillation will soon go random due to the fluctuation in the intermolecular potential. In this phenomenon, both the time scale and magnitude of force fluctuations are important. Vibrational phase relaxation is a sensitive probe of environmental dynamics around a given bond. In recent years, vibrational dephasing has also been investigated directly in the time domain using ultra fast laser spectroscopies as time-resolved coherent anti-Stokes Raman scattering experiments [12-15]. The dephasing times can also be measured from isotropic spontaneous Raman lines [16-18]. More recently, the development of the picosecond and femtosecond lasers has allowed direct time domain measurements of vibrational coherence [19].

The vibrational relaxation process responsible for line broadening of an isotropic Raman band may be influenced by several mechanisms [20-22]. The two dominant ones are the energy relaxation and phase relaxation. The energy relaxation involves inelastic processes and it may occur due to intermolecular transfer of energy between the vibrational degrees of freedom and the bath. The phase relaxation involves only quasi-elastic interactions of the molecules with their surroundings, leading to perturbation of the phase of the vibrational wave function without changing their quantum states. Both mechanisms have been investigated and it has been found that vibrational phase relaxation (dephasing) in liquids occur much faster than energy relaxation. There are three different relaxation times T_1, T_2 and T_2^* associated with each vibrational normal mode [23]. T_1^{-1} is the rate at which energy is dissipated from the vibrations to the surroundings, T_2^{-1} is decorrelation rate of the vibrations, which is sometimes known as the total dephasing rate.

The decorrelation rate can be written as

$$T_2^{-1} = \tfrac{1}{2} [T_1^{-1} + (T_2^*)^{-1}]$$

which defines the pure dephasing rate, $(T_2^*)^{-1}$. In many situations the decorrelation is dominated by the pure dephasing term.

Different theoretical models have been used to predict the rate constants for vibrational relaxation process. The theories of vibrational

pure dephasing in liquids are based on vibrational-translational coupling and collision induced frequency perturbations and yield results that are related to viscosity. The main theories developed for the dephasing process are the hydrodynamic model [20-22], the isolated binary collision (IBC) model [24], and the model based on resonant energy transfer [25]. Oxtoby [21] has shown that the relaxation time of the random force is responsible for the dependence of the diffusion coefficient. In the IBC model of Fischer and Laubereau, the transition rate is assumed to be the product of the collision rate in the liquid and the transition probability per collision in the gas phase. The dephasing time T^*_2 in this model is related to molecular parameters and temperature. The model relates the bandwidth to dephasing collision probability yielding $1/T^*_2 \propto \eta T/\rho$ where T is absolute temperature, η is viscosity and ρ is the density. The hydrodynamic model of Oxtoby obtains results similar to the IBC model, $1/T^*_2 \propto \eta T$. Lynden-Bell [26] relates vibrational dephasing to translational diffusion within the liquid potential and obtains a temperature dependence $1/T^*_2 \propto \rho\eta/T$. In these expressions, the temperature dependence of the viscosity, η, is the dominant factor.

Experimental data related to the C-H / C-D and C-C stretching modes of many molecular liquids have been explained on the basis of the IBC model of Fischer and Laubereau [24]. Oxtoby [20] developed a

hydrodynamic model to explain the linewidth of the C-I stretching vibration of CH_3I. In this hydrodynamic model collective effects were included and the vibrating molecule was modeled as a microscopic body embedded in a visco-elastic medium. Döge et al [25] showed that the resonant energy transfer via transition dipole – transition dipole (TD-TD) interaction is the main intermolecular coupling mechanism for the ν_2 mode of CH_3I. The vibrational relaxation rate may be determined using the isotropic Raman band width .The broadening of the bands being due to the vibrational dephasing, the band width is a measure of the relaxation rate. Hence the model suggested by Purkayastha and Kumar [27-28] gives a better picture of the phase relaxation in associated liquids (under the condition of high dilution) where the vibrational relaxation rate has been shown to be function of a parameter related to the hydrodynamic and dispersion forces. This model has so far been successfully applied for the carbonyl-stretching (C=O) band of several amides [28], ketones [29], aldehydes [30], as well as for the C≡N bands of nitriles [31]. Later on, the concept of microviscosity instead of dynamic viscosity was included [32] to incorporate the finer details of the solute-solvent systems and microenvironment. This modification has further supported results in several other molecules, successfully [16-18,31-34].

The simultaneous homogenous and inhomogeneous broadening due to the time dependence and the variance of the environments at different reference molecules contribute to the observed line shapes. In binary liquid mixtures, different molecules see different concentrations such that they contribute to the spectrum at different frequencies. The vibrations of neighboring molecules with strong Raman bands arising due to polar bands are coupled by intermolecular interactions. The vibrational relaxation process is mainly responsible for the broadening of the isotropic Raman spectral component. The homogenous and inhomogeneous contribution to the line shape may be separated by time dependent techniques. The two interacting situation, in pure solute and when dissolved in solvents differ markedly. The solvent electric field influences the band shape of a reference mode more significantly. To interpret the experimental results of a study of vibrational relaxation of a particular band in pure liquid, it is useful to perform dilution studies in various solvents with the aim of changing the type of interaction of the active molecules with their neighbors. In this way one can expect to get information about the interaction that influence the band shape in pure liquids.

Solvent induced changes to a solute vibrational spectrum reflect the dynamic aspects of solute-solvent interactions [35-40]. For this reason, vibrational line shape analysis [19,40] and more recently time

domain measurements of vibrational relaxation and dephasing [35,37] have been widely used to probe solvation forces [41]. The dynamic aspects of solute-solvent interactions in dense systems remain an active area of present research.

In the vibrational relaxation study of symmetrical modes in polar liquids by means of spontaneous Raman spectroscopic technique, considerable attention has been paid to the non-coincidence effect [16-18,42-55].

In most liquids, the existence of some average orientational structure assists the intermolecular coupling between identical vibrations in nearby molecules and induces the transfer of vibrational energy between them. The phenomenology associated with this process is observed in the Raman bands of these vibrations through non-coincidence effect (NCE), which is the phenomenon arising due to the difference in the peak wave numbers of anisotropic and isotropic profiles of a Raman band.

The NCE can unambiguously provide information about the molecular coupling mechanisms of short-range orientational order, which arises from the inter- and intra- molecular interactions in dense fluid phase. The phenomenon of NCE is closely related with the occurrence of resonant vibrational interaction, which due to its intermolecular nature can be suppressed by any dilution of the active

oscillator. For some polar molecules, the anisotropy shift may be as large as 14 cm^{-1} [16]. Concentration studies have shown that the magnitude of the splitting decreases with increasing concentration of the solvent.

The NCE in solutions have been studied theoretically [42-49]. However there have been limited experimental studies on the dependence of NCE on solvent concentration [50-53]. A few studies have been devoted to the temperature and pressure dependence of NCE in pure liquids [8,10,54-55].

Isotopic dilution experiments [56-58] allow us to isolate the effect of resonant intermolecular vibrational coupling in vibrational bands, when the molar fraction of active molecule is decreased, the RET is gradually eliminated, but the non-resonant interactions are not influenced. It has been experimentally verified [27-34,52-65] that for vibrational modes involving RET, the position of peak frequencies are different for anisotropic and isotropic Raman band component and the corresponding infrared absorption. Wang and McHale [3-4] concluded that local short-range order is not of fundamental importance for NCE, even if its existence can modify the shift between the isotropic and anisotropic maxima. The essential condition for a RET process is the angular dependence of interaction potential. McHale proposed that $S = \epsilon^{-2}$ while Mirone corrected the screening factor as $S= [(n^2 + 2)/(2\epsilon+n^2)]^2\epsilon$

. The NCE is assumed to be the result of resonant excitonic transfer of vibrational excitation between the same normal modes of different solute molecules.

Mirone and Fini [43] showed that the separation between the isotropic and the anisotropic maxima of the Raman band of the polar molecule varies with the concentration of the active substance in a manner with a characteristic of the ratio of the static dielectric constant of the solute and the solvent. The data were found to fit in an empirical equation [43]. This behavior suggested that the NCE is related, at least in a first approximation to the interaction between the permanent dipole of the dissolved molecule. Starting from this hypothesis and making the supplementary assumption of a coupling mechanism through the transition dipole McHale derived theoretically the expression for δν

$$\delta\nu = \frac{2\mu^2\left(\frac{\delta\mu}{\delta Q}\right)^2}{25\pi^2 c^2 \nu_0 kTd^3}\frac{N_0}{V_M}\phi\ S$$

where N_0 is Avogadro's number, φ is the volume fraction of the solute, ν_0 is the vibrational frequency of the isolated molecule, d is the maximum intermolecular distance, V_M is the molar volume of the solute, kT is the thermal energy, μ is the dipole moment, Q is the normal coordinate of vibrational mode under consideration and $\frac{\delta\mu}{\delta Q}$ is

the transition moment. S is the screening factor which comprises of two factors S_p and S_t related to the interaction of permanent and transition dipoles respectively and are given by the Onsager-Fröhlich model as $S_p = [(n^2 + 2)/(2\epsilon+n^2)]^2\epsilon$ and $S_t = ([(n^2 + 2) / (2 \epsilon_\infty + n^2)]^2 \epsilon_\infty$ where n is the refractive index of the solute, ϵ is the static dielectric constant of the medium and ϵ_∞ is the dielectric constant at infinite frequency.

Giorgini et al [46] studied the effect of composition on the non-coincidence of the isotropic and anisotropic Raman frequencies of the C=O stretching bands of several molecules .The change in anisotropy shift was explained making the assumption that the interaction energy of the dissolved dipoles is described by the above dielectric model. They inferred that even though several approximations were involved in the Onsager-Fröhlich model, the success in interpreting their data of $\delta\nu$ over the whole composition range justified the hypothesis that $\delta\nu$ has the same functional dependence on the dielectric constant of the medium at all concentrations [46].

It was pointed out by Giorgini et al. [46] that this may be due to fortuitous cancellation of errors caused by the different approximation made while deriving the equation. Later Purkayastha and Kumar [16] while studying N,N-dimethylacetamide observed that there is kink around 50% solute concentration and suggested that this may be because the theory is valid for high dilution and different behavior at

lower dilution may be expected. Das and Kumar [18,33] showed that for the p-methyl acetophenone and benzaldehyde molecules the data points fit rather well in two straight lines with a sharp discontinuity around 50% concentration. They inferred that it might be due to the reason that below 50% dilution interactions were expected to occur more among solute molecules than between solute and solvents. Further, it was pointed out that to explain the NCE in case of complex molecular systems where the effects of dispersion, induction, multipolar interaction etc are likely to vary from solvent to solvent, the screening effect may not be as effective as envisaged by the Onsager-Fröhlich model. In case of benzaldehyde molecule it was suggested that the structure breaking effects and local fluctuations may also be playing role for the discontinuity observed. Das and Kumar [18,33] have also suggested that repulsive forces are playing role in such molecular systems. However, further work is required in the complex molecular systems to establish the discontinuity and the role of repulsive forces.

The experimental work on Resonance Energy Transfer (RET) assumes that the coupling mechanism is mainly due to transition dipole – transition dipole (TD-TD) interaction [1-5,52-55,59-65].

Owing to the strong interactions between permanent dipoles, this order permits a vibrational coupling through the neighbouring transition dipoles. The phenomenon of NCE is exhibited by liquids to a

large extent for the vibrations of molecular groups like C=O which are strongly infrared active. It has been shown [62] that the vibrational exciton approach developed under the assumption of transition dipole coupling mechanism, predicts how the orientational structure of the molecular liquid determines the magnitude and sign of NCE. Giorgini [62] cited that the NCE is large and positive for molecular liquids structured by dipolar forces whereas negative NCE may arise when the liquid structures are dominated by non-dipolar forces. For ring breathing aromatic systems [59] the negative sign of the splitting between anisotropic and isotropic profiles has been attributed to a balance of repulsive and attractive forces. The magnitude of NCE also depends on the thermodynamical state, because it is related to the local structural order in the liquid [63]. Higher absolute NCE values are obtained for molecules with higher steric effects [60]. Torii [61,63] observed anomalous vibrational frequency shift (negative NCE) in some usually used solvents that has a large dipole derivative. He also studied [65] the role of atomic quadrupoles in intermolecular electrostatic interactions and observed that large atomic quadrupolar effect is important for electrostatic interactions around covalent bonded atoms. Thus the phenomenon of non-coincidence can be examined from different point of view.

In order to understand the nature of intermolecular interactions and microenvironment, there is a definite need for additional systematic studies on vibrational relaxation and frequency shifts in various liquids. The study of the influence of solvents on the band shape parameters is of paramount importance not only in connection with molecular structure and liquid dynamics but also in connection with solution kinetics. In the present work, the Raman band shapes of Methyl Ethyl Ketone, Acetophenone and Methyl Acetate molecules were chosen for vibrational relaxation studies as these molecules contain C=O bond which is highly polar in nature. These molecules have been studied in different solvents of varying polarity. These solvents were found suitable after considerable screening taking into consideration, no overlapping bands, avoiding strong hydrogen bonding effects. These molecules are of considerable biophysical significance. The solvent dependent studies of Raman band shape parameters may also serve as a model for the environmental effects on the vibrational modes. These studies are therefore expected to throw light on the nature of intermolecular forces playing key role in the interactions of great biophysical significance. The study of the spectral properties of Raman bands has contributed in a major way to our understanding of the various processes involved in liquids. In this work, the potential function, which incorporates the repulsive and dispersion forces found in regular fluids and the

contributions of multipolar moments, specifically dipole and /or quadrupole moments have been investigated. The C=O stretching mode of vibration have been chosen for the present study because its normal mode presents particular characteristics that makes its study of great importance:

(1) It lies at high frequencies, so the condition $\hbar\omega >> k_BT$ is always true.

(2) Usually it is little mixed and /or coupled with other vibrations, which means that its normal coordinate may be considered as a pure one.

(3) It is a well separated mode for all molecules under study. Therefore, it is particularly suitable for probing the molecular environment and is expected to give detailed information regarding the complex molecular systems.

In case of polar Raman bands such as C=O stretching vibration, it is possible to separate the vibrational relaxation from rotational effects, hence the studies have been limited to the C=O stretching mode of vibration. The choice of solvents was such that solvent molecules were of varying size and shape, different multipolar moments and electrical properties because of which they are important in the study of intermolecular forces in the solute-solvent systems. The benzene and substituted benzene molecules ($C_6H_5CH_3$ and C_6H_5Cl) have significant effects in solute-solvent interactions from the point of view of

quadrupole moment and plate like structure. The CH_3CN and CCl_4 molecules have dipole moment and octupole moment respectively. They are also having different shapes. The $CHCl_3$ molecule provides the possibility of hydrogen bonding through C-H bond as hydrogen is slightly acidic. The chloroform molecule also has symmetric top structure. Out of these six solvents, three (CH_3CN, $CHCl_3$ and C_6H_5Cl) solvents belong to the category of dipolar molecules and three (CCl_4, C_6H_6 and $C_6H_5CH_3$) are non-dipolar in nature. The dipolar effects may be studied using CH_3CN, $CHCl_3$ and C_6H_5Cl solvents and they are therefore quite effective in reducing the interactions between the solute molecules. Besides the dipolar interactions, the induction and dispersion forces are also operative and play a significant role in liquid structure. In case of polar molecules all the three types of interactions may be effective. The screening effect due to dielectric constant of the medium may also be investigated using these six solvents, as their dielectric constants are quite different from each other.

REFERENCES:

1) G. Fini, P. Mirone, J. Chem. Soc. Faraday Trans.2, **70**, 1776 (1974).

2) G. Fini, P. Mirone, Spectrochim. Acta Part A, **32**, 625 (1976).

3) C.H. Wang, J. McHale, J. Chem. Phys. **72**, 4039 (1980) and reference therein.

4) J. McHale, J. Chem. Phys. **75**, 30 (1981).

5) W. Schindler, P.T. Sharko, J.Jonas, J.Chem. Phys. **76**, 3493 (1982).

6) J. Schroeder, J. Jonas, J. Chem. Phys. **34**, 11(1978).

7) W. Schindler, J. Jonas, J. Chem. Phys. **72**, 5019 (1980).

8) T.W. Zerda, S. Perry, J. Jonas, Chem. Phys. Lett. **83**, 600 (1981).

9) B. Hegemann, J. Jonas, J. Chem. phys. **79**, 4683 (1983).

10) W. Schindler, T.W. Zerda, J.Jonas, J.Chem.Phys. **81**,4306 (1984).

11) J. Schroeder, V.H. Schiemann, P.T. Sharko, J. Jonas, J. Chem. Phys. **66**, 3215 (1977) and references therein.

12) G.Seiferet, R.Zuerl, H.Graener, J.Phys.Chem.A,**103**,10749 (1999).

13) D.Biengmenn,A.M.King, F.F.Crim, J.Chem.Phys.**113**,5018 (2000).

14) A Charvat, J. Aβmann, D. Scwarzer, B. Abel, J. Phys. Chem. A, **105**, 5071 (2001).

15) A Charvat, J. Aβmann, B. Abel, D. Scwarzer, K. Henning, K. Luther, J. Troe, Phys. Chem. Chem. Phys, **3**, 2230 (2001).

16) A. Purkayastha, K. Kumar, J. Raman Spectrosc. **22**, 721 (1991).

17) A.Purkayastha,R.Das,K.Kumar,Spectrochim.Acta **47A**,525 (1991).

18) A. Das, K. Kumar, J. Raman Spectrosc. **30**, 563 (1999).

19) A. Morresi, L. Mariani, M.R. Distefano, M.G. Giorgini, J. Raman Spectrosc. **26**,179 (1995).

20) D.W. Oxtoby, Adv. Chem. Phys, **40**, 1 (1979).

21) D.W. Oxtoby, Ann. Rev. Phys. Chem. **32**, 77 (1981).

22) D.W. Oxtoby, J. Phys. Chem. **87**, 3028 (1983).

23) S.F.Fischer, A.Laubereau, Chem. Phys. Lett. **55**, 189 (1978).

24) S.F. Fischer, A. Laubereau, Chem. Phys. Lett. **36**, 6, (1975).

25) G. Döge, R. Arndt, J. Yarwood, J. Mol. Phys. **52**, 399 (1984).

26) R.M. Lynden-Bell, Mol. Phys. **33**, 907 (1977).

27) A. Purkayastha, K. Kumar, Spectrochim. Acta **43A**, 1269 (1987).

28) A. Purkayastha, K. Kumar, J. Raman Spectrosc. **19**, 249 (1988).

29) D. Bhattacharjee, A. Ghosh, T.N. Mishra, Bull. Chem. Soc. Jpn. **67**, 1221 (1994).

30) D. Bhattacharjee, A. Ghosh, T.N. Mishra, Bull. Chem. Soc. Jpn. **68**, 1269 (1995).

31) D. Bhattacharjee, A. Ghosh, T.N. Mishra, S.K. Nandy, J. Raman Spectrosc. **27**, 457 (1996).

32) A. Purkayastha, K. Kumar, Spectrochim. Acta **46A**, 1545 (1990).

33) A. Das, K. Kumar, Spectrochim. Acta **54A**, 793 (1998).

34) Th.G. Devi, K. Kumar, J. Raman. Spectrosc. **35**, 835 (2004).

35) T. Elsaesser, W. Kaiser, Annu. Rev. Phys. Chem. **42**, 83 (1991).

36) D.W. Miller, S.A. Adelman, Int. Rev. Phys. Chem. **42**, 83 (1991).

37) J.C. Owrutsky, D. Raferty, R.M. Hochstrasser, Annu. Rev. Phys. Chem. **45**, 519 (1994).

38) R.M. Stratt, M. Maroncelli, J. Phys. Chem. **100**, 12981 (1996).

39) E.J. Hutchinson, D. Ben-Amotz, J. Phys. Chem. B **102**, 3354 (1998).

40) J. Chesnoy, G.M. Gale, Adv. Chem. Phys. **70**, 297 (1998).

41) F. Seifert, K.L. Oehme, G. Rudakoff, W. Hölzer, W. Carius, O. Schrötter, Chem. Phys. Lett. **105**, 635 (1984).

42) G. Fini, P. Mirone, B. Fortunato, J. Chem. Soc. Faraday Trans. 2, **69**, 1243 (1973).

43) P. Mirone, G. Fini, J. Chem. Phys. **71**, 2241 (1979).

44) P. Mirone, J. Chem. Phys. **77**, 2704 (1982).

45) J. McHale, J. Chem. Phys. **77**, 2705 (1982).

46) M.G. Giorgini, G. Fini, P. Mirone, J. Chem. Phys. **79**, 639 (1983).

47) D.E. Logan, Chem. Phys. **103**, 215 (1986).

48) D.E. Logan, Mol. Phys. **58**, 97 (1986).

49) D.E. Logan, Chem. Phys. **131**, 199 (1989).

50) M. Kamoun, P. Mirone, Chem. Phys. Lett. **75**, 287 (1980).

51) D. Scheibe, J. Raman Spectrosc. **13**, 103 (1982).

52) V.M. Shelly, A. Talintyre, J. Yarwood, R. Buchner, Farady Discuss. Chem. Soc. **85**, 211 (1988).

53) V.M. Shelly, J. Yarwood, Chem. Phys. **137**, 277 (1989).

54) H.D. Thomas, J. Jonas, J. Chem. Phys. **90**, 4144, 4632, (1989).

55) T.F. Sun, J.B. Chan, S.L. Wallen, J. Jonas, J. Chem. Phys. **94**, 7486 (1991).

56) G. Döge, Z. Naturforsch, Teil A. **28**, 919 (1973).

57) P.C.M. Van Woerkom, J. de Bleyser, M. de Zwart, J.C. Leyle, Chem. Phys. **4**, 236 (1974).

58) W.G. Rothschild, J. Chem. Phys. **62**, 1253 (1975).

59) G. Döge, D. Schneider, A. Morresi, Mol. Phys. **80**, 525 (1993).

60) A. Morresi, M. Paolantoni, P. Sassi, R.S. Cataliotti, G. Paliani, J. Phys.: Condens. Matter **12**, 3631 (2000).

61) H. Torii, J. Chem. Phys. **119**, 2192 (2003).

62) M.G. Giorgini, Pure and Applied Chemistry **76**, 261 (2004).

63) H. Torii, J. Phys. Chem. A **108**, 2103 (2004).

64) M.G. Giorgini, M. Musso, H. Torri, J. Phys. Chem. A, **109**, 5846 (2005).

65) H. Torri, M. Musso, M.G. Giorgini, J. Phys. Chem. A, **109**, 7797 (2005).

CHAPTER 2

CHAPTER 2

THEORETICAL ASPECTS

2.1. VIBRATIONAL RELAXATION IN LIQUIDS:

Vibrations are sensitive probes of molecules in liquid phase because in liquids, vibrational energy levels are quantized whereas rotations and translations are not quantized since the molecules in liquid phase are in random motion and undergo successive collisions before it can rotate freely.

Vibrational relaxation occurs through the coupling of a quantum vibrational system to a classical "heat bath" of rotational and translational degrees of freedom [1-3]. Considering an isolated active oscillator, we can characterize its vibrational wave function by a quantum state and a phase. On introducing a solvent to a liquid reference system, the isolated active oscillator for any normal mode shall be perturbed. When the oscillator is perturbed by the external environment, its wave function can be modified in both these contributions. We have a vibrational energy relaxation (also named population relaxation) when the quantum state changes. In this case,

the energy difference between the vibrational excited and the ground state is dissipated to the bath. However, the perturbation may conserve the vibrational energy of the oscillator and may cause only a change in its phase leading to phase relaxation, which is also termed as vibrational dephasing [1]. In the liquid phase, population relaxation events usually need relatively long lifetimes in comparison with phase relaxation events [2]. It can be stated that in most cases vibrational line shapes are determined by dephasing process. Sometimes, both processes can contribute to the whole vibrational relaxation. The vibrational relaxation process responsible for the line broadening of the isotropic component of the Raman band can be explained on the basis of dephasing mechanisms. The vibrational relaxation process is generated by a large variety of inter-molecular forces including dipole-dipole, dipole-induced dipole, dispersion and short range repulsion [4].

The vibrational relaxation may be explained on the basis of the following processes:

1. **Life-time broadening** – This arises because of the finite lifetime of the quantum state due to uncertainty principle. In liquids where population relaxation times have been measured, this uncertainty principle may be estimated. It generally makes a rather small contribution to the line width.

2. **Environmental broadening** – It is also called "pure dephasing". It arises due to the fact that the vibrational frequency of the molecule is perturbed due to interaction with other molecules. Therefore, it has a component fluctuating with time and is responsible for the modulation of vibrational frequency.
3. **Resonant energy transfer** – It is also called "excitonic broadening". This contribution to the vibrational line broadening appears in pure liquid and decreases when solute is dissolved in solvent. When two molecules are brought together, the two energy levels, which are earlier same, may split with one moving higher and the other lower. If a large number of molecules are brought together, this splitting is continuous until a broad excitonic band is formed.

When dipole-dipole interactions and dispersion forces are included, there are three contributions to line broadening [5]. The first 'Self term', the second 'exchange term' and the third is 'cross self exchange term', respectively. The exchange term is due to the transfer of vibrational quantum between two identical molecules through corresponding normal modes. This mechanism is normally referred as resonant energy transfer. It is possible to single out this particular kind of dephasing by performing dilution measurements.

The microscopic Hamiltonian of a dephasing system can be generally written as

$$H = H_{osc} + H_B + H_{coupl} \quad (2.1)$$

Where H_{osc} is the Hamiltonian for the isolated active oscillator, H_B includes the translational and rotational degrees of freedom of the bath and H_{coupl} describes the coupling of the vibrations to the bath.

The phase of the molecule changes due to changes in the orientation of the colliding molecules. As the collisions of molecules are considered in dephasing process, the collision time is taken to be identical with correlation time (time taken to correlate with the collision).

There are three different relaxation times [4] associated with each vibrational normal mode, T_1, T_2, T_2^*. Here T_1^{-1} is the rate at which energy is dissipated from the vibrational to the surroundings, T_2^{-1} is decorrelation rate of the vibrations, which is sometimes known as the total dephasing rate. It is related to the half width of the vibrational spectra line by

$$\Delta_{1/2} = 1/2\pi T_2.$$

The decorrelation rate can be written as

$$T_2^{-1} = \tfrac{1}{2} [T_1^{-1} + (T_2^*)^{-1}] \quad (2.2)$$

which defines the pure dephasing rate, $(T_2^*)^{-1}$. In many situations the decorrelation is dominated by the pure dephasing term.

2.1.1Resonant Energy Transfer and Non-coincidence effect:

The resonant energy transfer (RET) process occurs due to the interaction between the identical molecules [3]. In this process, the microscopic local order in liquid phase permits the coupling between the vibrational states of the molecule through neighbouring transition dipoles and leads to non-coincidence effect.

The coupling potential V can be expanded [6-8] in a Taylor series as a function of normal co-ordinate Q

$$V_i = V_o^i + \left(\frac{\delta V}{\delta Q_i}\right)_0 Q_i + \frac{1}{2}\left(\frac{\delta^2 V}{\delta Q_i^2}\right)_0 Q_i^2 + \frac{1}{2}\sum_{ij}\left(\frac{\delta^2 V}{\delta Q_i \delta Q_j}\right)_0 Q_i Q_j + \cdots\cdots \quad (2.3)$$

The first three terms are similar to the potential of a harmonic oscillator corresponding to a normal coordinate Q_i. By choosing the energy of the equilibrium configuration to be zero, V_o may be eliminated. The last term is responsible for resonant energy transfer from one oscillator to another and leads to non-coincidence effect.

Since $V \leq H_o$, the first order perturbation calculation for the frequency difference between the ground and first excited states can be performed leading to the expression

$$\Delta E = \left(\frac{\delta V}{\delta Q_i}\right)_0 \left(\langle 1|Q|1\rangle - \langle 0|Q|0\rangle\right) + \frac{1}{2}\left(\frac{\delta^2 V}{\delta Q_i^2}\right)_0 \left(\langle 1|Q^2|1\rangle - \langle 0|Q^2|0\rangle\right) + \left(\frac{\delta^2 V}{\delta Q_i \delta Q_j}\right)_0 \left(\langle 1|Q|0\rangle\right)^2 \quad (2.4)$$

where Q is the normal coordinnate of the molecule and $<1|Q|0>$ is the expectation value of the normal coordinate in the transition state which is same for molecules i and j as we are considering similar vibrational modes of both molecules. In the above equation, the first term corresponds to memechanical anharmonicity, the second term to electrical anharmonicity and the last term to resonance interaction. $\langle 1|Q|1\rangle - \langle 0|Q|0\rangle$ vanishes for a harmonic oscillator, but in real molecules we deal with anharmonic oscillators. Mechanical anharmonicity is one factor that might give them intensity through violating the $\Delta v = \pm 1$ selection rule.

Another possible cause, which might operate even when the oscillator is harmonic is the electrical anharmonicity. The electrical anharmonicity is the nonlinear part of the variation of the dipole moment with normal coordinates. It can give intensity to overtones and

combination tones. The dipole moment μ varies during the vibration and it can be expressed in a Taylor series

$$\mu = \mu_0 + \left(\frac{\delta \mu}{\delta Q}\right)_0 + \left(\frac{\delta^2 \mu}{\delta Q^2}\right)_0 Q^2 + \cdots\cdots \qquad (2.5)$$

where μ_0 is the permanent dipole moment of the molecule and the sum of the terms higher than linear terms is called electrical anharmonicity. The third term in equation (2.4) is the resonance interaction term given by

$$\Delta E_{res} = \left(\frac{\delta^2 V}{\delta Q_i \delta Q_j}\right)_0 \left(< 1|Q|0 >\right)^2 \qquad (2.6)$$

The most common source of resonant transfer relevant to the non-coincidence effect is due to the transition dipole-transition dipole coupling [9]. Consider the interaction potential between two identical molecules

$$V = \left(\frac{\mu_i \mu_j}{R_{ij}^3}\right) K_{ij} \qquad (2.7)$$

where μ is the dipole moment of the molecule, R_{ij} is the distance between the two dipoles and K_{ij} is the geometric factor describing the relative orientation of the two dipoles having dipole moments μ_i and μ_j. For point dipoles,

$$K_{ij} = 2\cos\theta_i \cos\theta_j + \sin\theta_i \sin\theta_j \cos\Phi_{ij} \qquad (2.8)$$

where θ_i is the angle between the dipole moment vector of molecules i and the ij vector which connects molecules i and j, Φ_{ij} is the angle between the perpendicular components of the dipole moments of the molecules i and j.

The equation (2.6) can therefore be written as

$$\Delta E_{TD\text{-}TD} = \left(\frac{\delta\mu}{\delta Q}\right)^2 \left\langle \frac{K_{ij}}{R_{ij}^3} \right\rangle \left(< 1|Q|0 > \right)^2 \qquad (2.9)$$

For the dipole-dipole coupling, the splitting factor is given by

$$\delta\nu = \nu \text{ (out of phase)} - \nu \text{ (in phase)}$$

$$\propto \left\langle \frac{K_{ij}}{R_{ij}^3} \right\rangle \left(\frac{\delta\mu}{\delta Q}\right)^2 \qquad (2.10)$$

The brackets indicate an ensemble average for different relative orientations where the anisotropic component of the band is shifted in various degrees depending on the magnitude of the orientational factor K_{ij}.

At infinite dilution, the splitting factor reduces to zero i.e. the isotropic and anisotropic Raman components tend to coincide. The quantity $\left\langle \frac{K_{ij}}{R_{ij}^3} \right\rangle$ is difficult to calculate hence only proportionality factor may be considered here

$$\delta \nu \infty \left(\frac{\delta \mu}{\delta Q} \right)^2 \qquad (2.11)$$

The quantity $\left(\frac{\delta \mu}{\delta Q} \right)^2$ is proportional to the infrared absorption coefficient for a given vibration, hence, the Raman bands studied corresponding to the strong IR absorption exhibit the non-coincidence effect.

Logan [9] presented a theory for the non-coincidence effect and according to it, the non-coincidence effect has been attributed to resonant transfer of vibrational excitation in the presence of local order due to strong interaction between permanent dipoles. In resonant excitonic transfer process, the main interaction is due to transition dipole-transition dipole coupling. Thus Logan's theory satisfied the resonant energy transfer [RET] process; however it does not always give good approximation for the dispersion effect. Logan's approach assumes only point dipoles whereas it is necessary to account for the dipoles of finite length. Besides repulsive interactions should also be considered. According to Wang and Mchale [10], the non-coincidence effect can be explained by the induced dipole-induced dipole interaction mechanism. Giorgini et al [11] used the Logan's theory and found valuable information regarding the non-coincidence effect based on thermodynamic state.

2.1.2. Isolated binary collision (IBC) model:

A simple model based on IBC has been developed by Fischer and Laubereau [12]. It was based on semi-classical theory to describe the dephasing of vibrationally excited molecules in a liquid. In this model, phase shifts and therefore bandshapes are obtained using a repulsive potential surface. This concept was subsequently modified by Oxtoby et al. [6] with the introduction of anharmonicity and by Tanabe and Jonas [13] for use in binary mixtures.

In this model, both the energy dissipated and the pure dephasing are considered to be independent processes. Therefore, assuming that collisions are not correlated, it is possible to describe the general expression of vibrational relaxation rate or the dephasing time as the sum of two contributions as given in equation (2.2) where the dephasing term $(T_2^*)^{-1}$ is due to pure dephasing caused only by quasi-elastic collisions.

However, this model does not reflect the whole complexity of the liquid environment because of difficulties in estimating some parameters for complex molecules. For complex systems, the values of anharmonicity constants and the reduced mass of the molecules are not always available and were hence neglected in this model, which has been rectified by the hydrodynamic model proposed by Oxtoby [1].

2.1.3. The hydrodynamic model:

A hydrodynamic model calculation was also presented by Oxtoby [14], which also included the effect of vibrational anharmonicity. It was essentially an opposite approach to that of Fischer and Laubereau. The hydrodynamic model can provide a good qualitative and semi-quantitative description of dephasing in molecular liquids. In this approach, a vibrating molecule is modeled as a macroscopic body embedded in a visco-elastic medium. This model has correctly predicted the shortcomings of the hydrodynamic model [15] including the sphere in a viscose continuum with slip boundary condition and the negative minimum in the velocity auto-correlation function. In the limit of weak coupling of vibration to the bath, collective effects are involved producing a viscosity dependent collision frequency. The expression for vibrational dephasing rate for polyatomic systems is given by

$$\tau_v^{-1} = \eta T \qquad (2.12)$$

showing the dependence on viscosity η and temperature T. It has been found that the pure dephasing is playing a major contribution in the isotropic bandwidth study. This model however does not reflect the whole complexity of the liquid environment, and it seems more appropriate for gas-like systems.

The model proposed by Schweizer and Chandler [16] illustrates the importance of a detailed description of the liquid state structure in determining the dephasing process. It shows the effect of repulsive and slowly varying attractive forces on the vibrational frequency and dephasing of polyatomic molecular liquids. This model simultaneously examines both the broadening mechanism and frequency shifts. Refinement of the Schweizer and Chandler theory were proposed by Ben Amotz et al. [17]. Competitive short range repulsive and long range attractive forces were invoked to reproduce solute and solvent induced frequency shifts. A cavity distribution function was introduced to describe the repulsive frequency shift, while a van der Waals' mean field approximation was used for attractive contribution.

2.1.4. Kubo model of correlation function

A general theory of relaxation mechanism as developed by Kubo [18] has also been adapted by several workers to explain the vibrational relaxation. This theory has been applied to vibrational dephasing via resonant energy transfer due to modulation of long range dipolar potentials and to other dephasing mechanisms involving short range potentials [19].

It is possible to adopt a stochastic model to the dephasing process, treating the molecule as an oscillator perturbed by random

forces. Its original spectrum $I(\omega)$, centered on the frequency ω_o will be broadened around the center by a random modulation $\omega(t)$, giving a distribution of frequency $(\omega-\omega_o)$ with the hypothesis that

(1) $\omega(t)$ is a Gaussian process, that is, the frequency fluctuations are due to weak but persistent perturbations.

(2) The correlation function $\psi(t)$ for $\omega(t)$ is an exponential

$$\psi(t) = e^{-\tau/\tau_c} \tag{2.13}$$

where τ_c is the correlation time.

(3) Dephasing due to different process is statistically independent and applying the algebra of commutants, the Fourier transform of an isotropic profile is represented [20] by the function, relative to one dephasing process

$$\Phi(t) = \exp[-M_2\{\tau_c^2(e^{-t/\tau_c} - 1) + t\tau_c\}] \tag{2.14}$$

where τ_c is the modulation or correlation time related to the time scale of the molecular fluctuations in the medium. It can be identified with the average time taken between perturbation events. M_2 is the second moment of frequency and is given as

$$M_2 = [<\Delta\omega_i^2>]^{1/2}$$

which is the root mean square frequency displacement of the instantaneous transition frequency. It measures the magnitude of the random frequency modulation, that is, the range of frequency

distribution due to various molecular interactions. It is obtained from the frequency domain with

$$\left\langle \Delta\omega_i^{\,2} \right\rangle = \frac{\int_{band} I_{iso}(\omega)\omega^2 \, d\omega}{\int_{band} I_{iso} \, d\omega} \qquad (2.15)$$

The τ_c and $<\Delta\dot{\omega}_i^2>$ contain valuable information about the nature of the intermolecular potential.

Different speeds of $\psi(t)$ leads to slow fast processes of molecular fluctuations in the medium. We can have a modulation regime depending on the value of $<\Delta\omega_i^2>\tau_c$

If $<\Delta\omega_i^2>\tau_c^{-1}>>1$,we are in the slow modulation limit. The active molecule undergoes perturbation for a long time and the phase memory of the oscillator is rapidly lost. If $\tau_c \rightarrow \infty$, the function $\Phi(t)$ decays rapidly and assumes a Gaussian form with a small long time exponential tail and its Fourier transform $I_{iso}(\omega)$, is also a Gaussian function.

If $<\Delta\omega_i^2>\tau_c^{-1}<<1$, we are in the fast modulation limit. There is a perturbation on the active molecule due to fluctuations in the intermolecular potential which rapidly decays and therefore memory of the oscillator is retained for longer times. $\Phi(t)$ therefore decays more slowly and hence band profile significantly narrows and for time $t>\tau_c$ an

exponential decay is observed and the corresponding $I_{iso}(\omega)$ is a Lorentzian curve.[21]

However at short times (high frequency displacements from the band center), $\Phi(t)$ the function will eventually reflect a Gaussian distribution of intensity. It is necessary to retain the correct behaviour of band moments (because there is no definite second or higher moment for Lorentzian profile of the band)

Since τ_c represents a modulation time, it is related to the time scale of the modulation fluctuations in the medium. The second measures the range of frequency distribution due to various molecular interactions.

Expression (2.14) can be modified into two extreme cases of short and long times [22]. For $\tau < \tau_c$ (short time approximation), $\Phi(t)$ is Gaussian. When $\tau > \tau_c$ (long time approximation), $\Phi(t)$ is described by an exponential. Following Fourier transform algebra, the corresponding lineshape equation (2.14) will be Lorentzian around the center and Gaussian in the wings.

The vibrational relaxation time can be defined as

$$\tau_v = \int_0^\infty \phi_{pp}(t)dt \qquad (2.16)$$

In the case of long time approximation or fast modulation, we require

$$\tau_v = [\pi c(FWHM)]^{-1} \quad (2.17)$$

Where FWHM= full width at half maximum and c is the velocity of light.

The FWHM is measured for the isotropic component for the calculation of the vibrational relaxation time.

In the case of short time approximation or slow modulation, we require

$$\tau_v^{-1} = \langle \Delta\omega_i^2 \rangle \tau_c$$

$$\tau_v = (\langle \Delta\omega_i^2 \rangle \tau_c)^{-1} \quad (2.18)$$

where τ_v and τ_c have a time scale in picosecond. Therefore depending upon the rate of modulation process, one may predict the band profile.

It is important to emphasize that this model does not give us additional information with respect to the analytical study of band shape. The best advantage of the Kubo lineshape theory is the temporal picture of vibrational dephasing, that is, it permits us to confront to the problem as to how is the vibrational dephasing determined. In case of long-range dipolar interaction, τ_c is directly proportional to dynamic viscosity [20] and hence the vibrational relaxation rate is expected to depend on the viscosity of the medium. So far the band shapes considered are for simple, well-separated transitions. If other transitions are overlapping; there can be further contributions to phase relaxation and spectral broadening [23-24]

Although considerable progress has been made towards the understanding of the vibrational relaxation processes, further theoretical work and experimental studies are certainly required in this direction.

2.1.5. Diffusion properties of molecular liquids and solvent cage effect:

The molecular motions in a liquid are difficult to visualize as the molecules of a liquid are almost as close as in the crystalline solid. There is approximately 10% expansion on melting which leads to some looseness and randomness in the liquid structure [25].

To get a better picture of the solute-solvent system, one may consider the so-called solvent cage effect where the molecules of a solute are confined in a potential well, created by the solvent molecules. The molecule is considered to be vibrating against its immediate neighbours, with an occasional escape to its adjacent position. The cage exerts forces directed against the expansion of the solute molecule. If the cage is tight enough to prevent the molecules from escape, this is called cage effect. In solution phase, the lingering of a molecule near another because of the hindering presence of the solvent molecules is the solvent cage effect. The solvent cage effect is depicted in figure 2.1(a), where the molecules are shown to be roughly spherical in shape.

The cage model is supported by the successful treatment of diffusion in liquids. According to this model, the random diffusional motion of molecules in the liquid is taken to occur as a sequence of jumps from one molecular position to the next, so that collision with identical molecules are involved. With dilute solution, the solute molecule may be assumed to be in a cage of solvent molecules.

The elementary jump distance 'λ' is about $2r_0$ where r_0 is the radius of the molecule. The diffusion coefficient is given as

$$D = \frac{\lambda^2}{6\tau} \qquad (2.19)$$

where τ is the average time between jumps

If we treat the liquid as having a quasi-crystalline structure, with more or less definite sites, it turns out that a somewhat more accurate treatment should be given to the equations (2.19). For the small molecules, a reasonable value of λ which is taken as $2r_0$ is about 4Å. The solvent cage is sufficiently loose one and the average vibrational energy is kT. Vibrations against the wall of the cage occurs at intervals of h/kT or about $1.5X10^{-13}$ sec at 25^0C. We may therefore conclude that the molecule in a solution vibrate about $2.5X10^{-11}$ / $1.5X10^{-13}$ or approximately 200 times against its immediate neighbours before escaping to a new position and new neighbours.

This picture is also applicable to solute molecules. The frequency with which two solute molecules will, by the process of diffusion, accidently become neighbours may be obtained from figure 2.1(b) where the size of the solvent and solute molecules are comparable. This process is known as encounter and the estimation of encounter frequencies is central to much of solution kinetics. However, the complicated structure of two liquids makes the problem quite difficult. Therefore one may make the approximation that the molecules of the solvent and solute are of same size and are also spherical in shape which then leads to about 12 nearest neighbours. On each jump, the solute molecule finds 6 new molecules. These considerations are of great value in studying the solute-solvent interactions.

2.1.6. Vibrational Relaxation Rate:

The vibrational relaxation rate for a Lorentzian line profile is given by the relationship [26]

$$\tau_v^{-1} = \pi c \Gamma_{iso} \qquad (2.20)$$

where Γ_{iso} is the bandwidth (Full Width at Half Maximum of intensity, (FWHM)) of the isotropic component of the Raman band and c is the velocity of light.

The electrical and electronic properties of solvent induced environment also play a significant role in determining the vibrational relaxation rate [22]. Considering a simple model [22] for the vibrational relaxation based on the electrical properties of solvent induced disordered systems, the steady state conductivity (σ) for the disordered system is given by

$$\sigma = Nq\mu \tag{2.21}$$

where N is the density of a moving charge q and μ is the mobility. The charge q may be taken as a partial charge generated on solute molecules by the solvent molecules.

The average relaxation time τ for a system [22] may be given as

$$\tau = \tau_0 \exp\left(\frac{\Delta W}{KT}\right) \tag{2.22}$$

where the symbols have their usual meanings.

This process is also associated with an activation energy, since the energy of a given localized position is different from that of another position. The conductivity due to such a process may depend on the hopping probability between two adjacent molecular positions. This probability on the other hand, will depend on the distance between the solute molecules. The conductivity may be calculated by taking the average over jumps between molecular position i and j. The equation for such a current flow may be equivalent to Kirchoff's law for a three-

dimensional resistive network. The transition between two molecular position may be linked with the resistance in the network. The electrical conductivity tensor [27], for example, may be expressed abstractly by the Kubo equation

$$\sigma_{\mu\nu} = \frac{1}{KT}\int_0^{\infty} < j_\mu(t) j_\nu(0) > dt \qquad (2.23)$$

The conductivity therefore depends on the time co-relation between a component of the current operator j_ν (θ) at time zero and the component j_μ (t) at some later time t, integrated from all times and evaluated as the average of the expectation value of the product over the equilibrium ensemble. The conductivity (σ) may be expressed in terms of λ and τ using the equation

$$\sigma = Nq\mu$$

and the relationship

$$\frac{\lambda}{\tau} = v = \mu E,$$

Thus we have

$$\sigma = Nq\ \mu = \frac{Nq\ \lambda}{\tau\ E} \qquad (2.24)$$

Here E is the electric field, which is the reaction field of the solvent molecules and may be taken as due to the dispersion forces at high frequencies (ca 10^{14} Hz) given by

$$E = \frac{2\mu}{a^3}\left(\frac{n^2-1}{2n^2+1}\right) \tag{2.25}$$

Where μ is the dipole moment of the solute molecule and 'a' is the radius of the spherical cavity in which the solute molecule is sitting.

The conductivity is also related to the dynamic viscosity (η). Using the stokes' law [28] for the motion of a sphere of radius r moving with velocity v in a viscous medium under the action of a constant force, we have

$$\sigma = \frac{Nq^2}{6\pi r\eta} \tag{2.26}$$

Eliminating the value of σ from equations (2.24) and (2.26), and then substituting the value of E from (2.25), the average relaxation time τ can be written as

$$\tau = \frac{6\pi\eta r^2 a^3}{q\mu}\left(\frac{n^2-1}{2n^2+1}\right)^{-1} \tag{2.27}$$

If the radius of the spherical cavity is small enough, **a** can be taken approximately equal to the radius of the molecules r. The quantity qμ can be taken as the dipole moment of the solute molecule.

Then equation (2.27) can be written as

$$\tau = \frac{6\pi\eta r^6}{\mu^2}\left(\frac{n^2-1}{2n^2+1}\right)^{-1} \tag{2.28}$$

This collision time τ may be considered as the correlation time τ_c. Hence, equation (2.18) can be written as

$$\tau_v^{-1} = (M_2)_v \tau_c$$

$$= (M_2)_v \frac{6\pi\eta r^6}{\mu^2}\left(\frac{n^2-1}{2n^2+1}\right)^{-1} \quad (2.29)$$

The vibrational second moment $(M_2)_v = [<\Delta\omega_i^2>]^{1/2}$ is related to the density ρ of the liquid [20] as

$$(M_2)_v = A\rho \quad (2.30)$$

where A is a constant depending mainly on the solute properties.

Hence, equation (2.29) can be written as

$$\tau_v^{-1} = A\rho \frac{6\pi\eta r^6}{\mu^2}\left(\frac{n^2-1}{2n^2+1}\right)^{-1} \quad (2.31)$$

$$= C_m f(\rho,\eta, n) \quad (2.32)$$

where $C_m = A\frac{6\pi r^6}{\mu^2}$ is a solute dependent constant and

$$f(\rho,\eta, n) = \rho\eta\left(\frac{n^2-1}{2n^2+1}\right)^{-1} \quad (2.33)$$

Hence, the vibrational relaxation rate is dependent on the parameter $f(\rho,\eta,n)$.

2.1.7. Theory Of Microviscosity:

The theory of microviscosity takes into account the discreteness of the medium, starting from the view that it is impossible to have various liquid layers separated by a distance less than the molecular size [29]. This is where lies the difference between the microviscosity theory and the Stokes theory in which infinitesimally close layers moving with different velocities are assumed. Introduction of the finite limiting distance of closeness between molecular layers in Stokes formalism leads to expression for coefficient of friction in the theory of microviscosity [30] as:

$$\beta = 6\pi a\eta\gamma = 6\pi\eta a\,[(3b/2a) + (1+ b/a)^{-1}]^{-1}$$

$$\approx 6\pi\eta a\,(0.19 + 0.31a/b) \qquad (2.34)$$

Here γ is the so-called microfriction factor for translational molecular motion which has the form

$$\gamma = [0.16+0.4(a/b)]$$

'b' is the radius of the molecule surrounding the molecule of radius 'a' considered. The notion of microviscosity was introduced by Gierer, Spernol and Wirtz for establishing relations between Debye's correlation time τ_1 and the coefficient of diffusion, on one hand and viscosity on the other hand. They simultaneously carried out experimental verification

of the relation (2.34) for dilute solutions, in which in place of relation (2.34) the empirical formula for the microviscosity was obtained [29] as follows

$$\eta_m = \eta\left[0.16 + 0.4\left(\frac{a}{b}\right)\right] \qquad (2.35)$$

In the experimental verification, the molecular sizes were determined from the assumption of the closest packing of molecular spheres in the liquid (space factor 0.74).

While using the theory of microviscosity for solutions, the specificity of the solvent is taken into consideration, though in a very one-sided manner, by the fact that the microfriction factor depends on the ratio of the sizes of the molecules of the dissolved substance and the solvent. However, as in Stoke's theory, the same kind of interaction is assumed between the solvent and the dissolved substance and among the molecules of the solvent themselves.

2.2. RAMAN SCATTERING:

When light is scattered from a molecule most photons are elastically scattered. The scattered photons have the same energy and, therefore, same frequency, as the incident photons. However, a small fraction of light (approximately 1 in 10^7 photons) is scattered at optical frequencies different from, and usually lower than, the frequency of the incident

photons. The process leading to this inelastic scattering is termed as Raman effect. Raman scattering can occur with a change in vibrational, rotational or electronic energy of a molecule. For Vibrational Raman scattering the difference in energy between the incident photon and the Raman scattered photon is equal to the energy of a vibration of the scattering molecule.

The Raman scattering from totally symmetric vibrations will be strongly polarized parallel to the plane of polarization of the incident light. The scattered intensity from non-totally symmetric vibrations is 3/4 as strong in the plane perpendicular to the plane of polarization of the incident light as in the plane parallel to it.

Raman scattering study is generally carried out in the visible and near-UV range of excitation frequencies. The theory of Raman Effect shows that the amount of Raman scattering from a sample is directly proportional to the intensity of the incident radiation at the sample, to the fourth power of the incident frequency and to the concentration of the scattering species. Furthermore, the Raman scattered radiation is incoherent since the phase of Raman scattering varies arbitrarily from molecule to molecule. Thus, the intensity of Raman scattering is proportional to the number of scattering species i.e. to the concentration of the sample.

When the electric field of the incident radiation is very large, the non-linear contributions to the molecular polarizability become significant. Due to non-linear interaction of a molecular system with an intense laser radiation, many new phenomena arise which changes the wave number of the laser exciting line. The effects reflecting these phenomena are namely, the hyper-Raman Effect, the stimulated Raman effect, the inverse Raman effect and coherent Anti-Stokes Raman Scattering (CARS) respectively. The CARS is an important tool for the study in chemical physics, biological samples and in analyzing the molecular structure. This technique has the advantage of spectral and spatial discrimination against fluorescence and does not require a spectrometer.

The phenomenon of the Raman Effect arises because molecular vibrations modulate the frequency of the induced dipole in a molecule by an incident field. The induced electric dipole moment by the electric field E can be expanded [31] as

$$\mu = \alpha_1 E + \alpha_2 E^2 + \alpha_3 E^3 \qquad (2.36)$$

where the E and μ are the electric field and induced dipole moment of the molecule respectively. α_1 is the polarizability tensor of rank 2 while α_2 and α_3 are the hyperpolarizabilities of rank 3 and 4 etc.

The linear term in the equation (2.36) represents the Spontaneous Raman Scattering.

Although a quantum mechanical treatment necessary for a complete explanation of Raman scattering phenomenon, still many aspects of the phenomenon can be described reasonably well by the classical electromagnetic of the induced dipole and the molecular vibration. The variation of the polarizability with vibrations of the molecule can be expressed by expanding each component α_{ij} of the polarizability tensor in a Taylor series with respect to the normal coordinates of vibration [32] as

$$\alpha_{ij} = (\alpha_{ij})_0 + \sum_k \left(\frac{\partial \alpha_{ij}}{\partial Q_k}\right)_0 Q_k + \frac{1}{2}\sum_k \left(\frac{\partial^2 \alpha_{ij}}{\partial Q_k \partial Q_\lambda}\right)_0 Q_k Q_\lambda + \cdots\cdots \quad (2.37)$$

where Q is the vibrational normal co-ordinate, $(\alpha_{ij})_0$ is the polarizability tensor of the molecule in its equilibrium position. The subscript 'o' indicates that the expansion is centered at the equilibrium molecular configuration. The summations are over all normal co-ordinates.

For normal linear Raman Effect, the polarizability of the molecule is related to the normal coordinate Q_k by the equation

$$(\alpha_{ij})_k = (\alpha_{ij})_0 + \left(\frac{\partial \alpha_{ij}}{\partial Q_k}\right)_0 Q_k \quad (2.38)$$

neglecting the higher terms

This equation holds for each of the six polarizability components. Raman transitions invariably arise from the ground vibrational state,

which belongs to a totally symmetric representation. Furthermore, the induced dipoles responsible for Raman scattering associated with the molecular frequency ωk will be zero unless one of the components of the derived polarizability tensor $\left(\frac{\partial \alpha_{ij}}{\partial Q_k}\right)_0$ is non-zero. Hence, for a particular vibrational mode to be Raman active, at least one component of the polarizability tensor, a plot of that component against the normal coordinate must have a non-zero gradient at the equilibrium position. Both in the infrared and Raman spectrum [31], we have the selection rule $\Delta v_i = \pm 1$ for each normal vibration v_i.

Only those vibrations that are connected with a change in dipole moment can have $\Delta v_i = \pm 1$ for an infrared transition and only those vibrations that are connected with a change of polarizability can have $\Delta v_i = \pm 1$ for a Raman transition.

2.2.1. Isotropic and anisotropic Raman bands:

The isotropic and anisotropic components can be obtained by recording the $I_{VV}(\nu)$ and $I_{VH}(\nu)$components. The isotropic component of the Raman band can be used to get information about vibrational relaxation [33] .If ϵ_I and ϵ_S are the polarization directions of the

incident and scattered beam, two different measurements of vibrational bands I(ν) can be performed:

(i) $I_{VV}(\nu)$: with ϵ_I and ϵ_S in a parallel configuration, and

(ii) $I_{VH}(\nu)$: with ϵ_I and ϵ_S in a perpendicular configuration.

As far as vibrational modes belonging to a totally symmetric representations are concerned, we can define the isotropic profile $I_{iso}(\nu)$ and the anisotropic profile $I_{anso}(\nu)$ as:

$$I_{iso}(\nu) = I_{VV}(\nu) - \frac{4}{3} I_{VH}(\nu) \tag{2.39}$$

$$I_{aniso}(\nu) = I_{VH}(\nu) \tag{2.40}$$

Following Gordon [34], it is possible to demonstrate that

$$I_{iso}(\nu) \propto \int_{-\infty}^{\infty} \langle \alpha(t)\, \alpha(0) \rangle\ e^{i\omega t}\, dt$$

$$\propto \int_{-\infty}^{\infty} \langle Q_i(t)\, Q_i(0) \rangle\ e^{i\omega t} \tag{2.41}$$

$$I_{aniso}(\nu) \propto \int_{-\infty}^{\infty} \langle Tr[\beta(t)\, \beta(0)]\, Q_i(t)\, Q_i(0) \rangle\ e^{i\omega t}\, dt \tag{2.42}$$

Where α is the mean polarizability derivative, β is the traceless polarizability anisotropy derivative and Q_i is the vibrational coordinate of the i^{th} molecule. The expression $\langle Q_i(t)\ Q_i(0) \rangle$ is an example of correlation function, generally this is a physical quantity that describes

how long a property of a system is maintained, until it is averaged out by the microscopic motion of the system.

From equation 2.41, we can see that $I_{iso}(\nu)$ is Fourier transform of the auto correlation function $\langle Q_i(t)\, Q_i(0)\rangle$, usually indicated as vibratonal correlation function. This function contains all the non-reorientational contributions to the decay of the total correlation function. This will include the various possible ways of vibrational relaxation and collision induced effects.

In the anisotropic profile (equation 2.42), both orientational and vibrational information is present. It can be assumed that these two processes are not correlated, that is, if they have a very different time scale,

$$I_{aniso}(\nu) \propto \int_{-\infty}^{\infty} \langle Tr[\beta_i(t)\, \beta_i(0)]\rangle\langle Q_i(t)\, Q_i(0)\rangle\ e^{i\omega t}\, dt \qquad (2.43)$$

Although there may be some complicated factors that lead to problems in separating vibrational relaxation and the reorientational correlation function, it has been shown that in case of polar Raman bands arising due to totally symmetric vibration, the vibrational and reorientational contributions may be separated and the bands for which the value of depolarization ratio, $\rho=0$, there is no contribution from the anisotropic part of the scattering tensor.

The intermolecular forces modulate the vibration of a symmetrical mode, change the oscillator force constant of this mode, and causes a splitting of vibration into an isotropic and anisotropic vibration. The isotropic vibration is governed by the angular dependent inter-molecular forces. The isotropic and anisotropic components differ not only in the band shapes but also in most cases in the peak frequencies of these two bands.

2.3. LINE SHAPE FUNCTION

An atom can interact with radiation over a range of frequencies, strength of the interaction is a function of the frequency. This function is known as the line shape function [35]

The lineshape function depends on the various types of broadening mechanism, explained by different models.[7,12-13]. There are mainly two types of line broadening and consequently two types of line profile functions.

2.3.1. Lorentzian line profile:

A line broadening mechanism will be called homogenous when it broadens the line of each individual atom and therefore broaden the whole system. This mechanism gives a Lorentzian line shape function

whose width depends on the average collision time. The line profile is given by [35]

$$g(\omega - \omega_o) = \frac{1}{2\pi}\left[\frac{\tau_c}{1+(\omega-\omega_o)^2\tau_c^2} + \frac{\tau_c}{1+(\omega+\omega_o)^2\tau_c^2}\right] \tag{2.44}$$

Where, ω= frequency at any point on the line

ω_o= frequency at the peak

τ_c= collision time

The half width at half maximum (HWHM) is given by

$$\Delta\omega_o = 1/\tau_c \tag{2.45}$$

Considering only the positive value of ω, as the Lorentzian line shape is symmetric about the peak position, we have

$$g(\omega-\omega_o)=(1/\pi\Delta\omega_o)(1/1+(\omega-\omega_o)^2/\Delta\omega_o)) \tag{2.46}$$

The peak value is given by

$$g(0)=(1/\pi\Delta\omega_o) = 0.318/\Delta\omega_o \tag{2.47}$$

2.3.2. Gaussian line profile:

A line broadening mechanism will be called inhomogenous when it distributes the resonance frequencies of the atoms over a given band and therefore broaden the line of individual atoms. The line shape function in this case is Gassian. The profile is given by

$$g^*(\omega - \omega_o) = \frac{c}{\omega_o}\left[\frac{M_2}{2\pi kT}\right] exp\left[-\frac{Mc^2(\omega - \omega_o)^2}{2kT\omega_o^2}\right]$$

(2.48)

Where M = mass of an atom

c = velocity of light

ω = frequency at any point on the line

ω_o= frequency at the peak

T = temperature in degree Kelvin

k = Boltzmann constant.

The half width at half maximum (HWHM) is

$$\Delta\omega_o^* = \omega_o\left[\frac{2kT}{Mc^2}\ln(2)\right]^{\frac{1}{2}}$$

(2.49)

Applying equation (2.48) and (2.49), the line profile function becomes

$$g(\omega - \omega_o) = \frac{1}{\Delta\omega_o}\left[\frac{\ln(2)}{\pi}\right]^{\frac{1}{2}} exp\left[\left[\frac{\omega - \omega_o}{\Delta\omega_o}\right]^2 \ln(2)\right]$$

(2.50)

The peak value is given by

$$g(o) = \frac{1}{\Delta\omega_o}\left[\frac{\ln(2)}{\pi}\right]^{\frac{1}{2}} = \frac{0.47}{\Delta\omega_o}$$

(2.51)

2.3.3. Voigt profile:

In most of the situation the actual line profile involves a convolution of the above two types of broadening mechanisms. This convolution is known as the voigt profile function. Thus the actual profile function can be written in the form of convolution as [36]

$$\xi(\omega) = \int_{-\infty}^{+\infty} G(\omega^*)\, D(\omega, \omega^*) d\omega^* \tag{2.52}$$

where, $D(\omega, \omega^*)$ represents the Lorentzian probability of emission at ω for an emitter having a line center frequency ω^*.$G(\omega^*)\, d\omega^*$ represents the Gaussian probability of an emitter having the line center frequency in the interval $(\omega^*, \omega^* + d\omega^*)$ due to its thermal motion. When there is a relative motion between the emitter and an observer, the relative homogenous line profile is Doppler shifted, i.e, the rest-frame line center frequency ω_0 is Doppler shifted to ω^*.

$$\omega^* = \omega \left[1 \pm \frac{U_x}{c}\right] \tag{2.53}$$

From equation (2.44)and (2.50), we can write

$$G(\omega^*) = \left[\frac{1}{\beta\pi^{\frac{1}{2}}}\right] exp\left[-\frac{(\omega_o - \omega^*)^2}{\beta}\right]$$

(2.54)

and

$$D(\omega, \omega^*) = \left[\frac{1}{\pi}\right] \left[\frac{\frac{1}{\tau}}{(\omega^* - \omega)^2 + \left(\frac{1}{\tau}\right)^2}\right]$$

(2.55)

where β represents the Gaussian HWHM (Half Width at Half Maximum) divided by $(\ln 2)^{1/2}$ and $1/\tau$ represents the Lorentzian HWHM. Consequently,

$$\xi(\omega) = \left[\frac{1}{\beta\tau\pi(\pi)^{\frac{1}{2}}}\right] \int_{-\infty}^{+\infty} \frac{exp\left[\frac{-(\omega_o - \omega^*)^2}{\beta^2}\right]}{(\omega^* - \omega)^2 + \left(\frac{1}{\tau}\right)^2} d\omega^*$$

(2.56)

Introducing

$$y = \left[\frac{(\omega^* - \omega_o)}{\beta}\right], \quad u = \left[\frac{(\omega - \omega_o)}{\beta}\right], \quad a = \frac{1}{\beta c}$$

Equation (2.56) becomes

$$\xi(u) = \frac{a}{\beta\pi(\pi)^{\frac{1}{2}}} \int_{-\infty}^{+\infty} \frac{e^{-y^2}}{(u - y)^2 + a^2} dy$$

(2.57)

This equation represents Voigt line function. In general at core frequency ($u \approx 0$), $\xi(u)$ is close to Gaussian and in the wings of the profile ($u >> 1$), $\xi(u)$ is essentially Lorentzian.

2.4. INTERMOLECULAR INTERACTIONS IN LIQUIDS:

All intermolecular attractions are known collectively as van der Waals' forces. Consider the interacting system of the molecules, which are located in such a way that the separation is large enough to avoid the overlapping of electronic orbital. Depending on the nature of molecules which are interacting, the various type of interactions present among the interacting molecules may be categorized as follows:

2.4.1. Keesom forces or dipole-dipole effect:

These forces are heavily related to the electronegativity of an atom and arises due to the interaction between the permanent dipole moments of the molecules. The strength of a dipole-dipole interaction depends on both the dipole centers separation and their relative orientation [37]. These forces are dependent on temperatures.

The interaction potential between two molecules of dipole moments μ_i and μ_j at positions r_i and r_j which tend to align both molecules [38] is

$$V_{or}(r_{ij}) = \mu_i \nabla_i \nabla_j \left| r_i - r_j \right|^{-1} \mu_j \qquad (2.58)$$

The orientation giving the lowest energy is the parallel alignment of the two molecules along the joining vector $r_{ij} = r_i - r_j$.

The interaction energy [39] for such system can be written as

$$V_{or} = -\frac{2\mu_i \mu_j}{r_{ij}^3} \text{ for } k_B T << \frac{\mu_i \mu_j}{r_{ij}^3}$$

$$= -\frac{2\mu_i^2 \mu_j^2}{3k_B T\, r_{ij}^6} \text{ for } k_B T >> \frac{\mu_i \mu_j}{r_{ij}^3} \qquad (2.59)$$

where the orientation effect of both the dipoles have been considered leading to the doubling of interaction energy. This orientation effect is for the molecule, which possesses permanent dipoles. However, at high temperature, any alignment vanishes due to the thermal motion. The dipole-dipole interaction is relatively weak over the large distances of separation because of the $1/r^6$ distance dependence. However, over short distances of separation, dipole-dipole interaction is quite important.

2.4.2. Debye forces or the dipole induced-dipole effect:

Forces which result from the interaction of a permanent dipole and induced dipoles are known as Debye forces. Debye pointed out that

molecules having permanent dipole moments not only align but also polarize each other. An induced dipole rotates simultaneously with the inducing dipole, so that a temperature independent energy gains results.

If a molecule i exhibits a permanent dipole μ_i, then the dipole induced at molecule j is $\mu_i \nabla_i \nabla_j r_{ij}^{-1} \alpha_j$

The interaction potential of two dipoles [38] is given by

$$V_{ind}(r_{ij}) = \left(-\frac{1}{2}\right)\mu_i \nabla_i \nabla_j r_{ij}^{-1} \alpha_j \nabla_i \nabla_j r_{ij}^{-1} \mu_j \qquad (2.60)$$

The factor (1/2) arises due to dipole μ_j induced by μ_i and α_j is the polarizability of molecule j.

At high temperature, all orientations contribute according to Boltzmann statistics,

$$\Delta E_{ind} = -\frac{\left(\alpha_j \mu_i^2 + \alpha_i \mu_j^2\right)}{r_{ij}^6} \qquad (2.61)$$

This induction effect yields an attraction proportional to r_{ij}^{-6}. With the increase in temperature, the induction effect decreases but does not vanish its value. The dipole-induced dipole interaction exists only when the distance of separation is very small and therefore the energy involved for large distance of separation is extremely low.

2.4.3. London forces or dispersion effect:

The interaction of electric moments arising from fluctuations in the charge distributions of the molecules at large separations leads to the well-known London dispersion energy, which is present even if the molecules do not possess permanent moments. The London forces or the dispersion effects are based on the quantum mechanics [38]. According to it, photons are moving randomly in space and these photons are constantly scattered by any particles, which are present so that instantaneous induced dipoles are able to produce rapidly fluctuating fields. This in turns polarized the other molecules, thereby lowers the energy of the instantaneous dipole.

Suppose each instantaneous dipole P_i^{inst} of molecule i induces a dipole P_j^{ind} of molecule j, then the interaction potential of both molecules has the form

$$V_{dis}(r_{ij}) = \left(-\frac{1}{2}\right) < P_i^{inst} \nabla_i \nabla_j r_{ij}^{-1} X_j \nabla_j \nabla_i r_{ij}^{-1} P_i^{inst} >_{av} \qquad (2.62)$$

where, X_j is the molecular polarizability, the coupling parameter between photons and molecules.

The average polarization $< P_i^{inst} P_i^{inst} >_{av}$ of molecule i is proportional to the number of photons which is obtained from Planck's distribution.

The dispersion energy expression derived by London is

$$\Delta U(r)_{dis} = -\frac{3}{2}\frac{h\nu_i h\nu_j}{h(\nu_i+\nu_j)}\frac{\alpha_i\alpha_j}{r_{ij}^6} \qquad (2.63)$$

which is in the form of $\Delta U(r)_{dis} = -\frac{C_6}{r^6}$, where C_6 is called the van der Waals' coefficient.

The dispersion energy occurs between any two molecules and it increases with the increase in temperature. At long range the interaction energy can be classified as multipolar (electrostatic), dispersion and induction energy and at short range as overlap (electrostatic and exchange) energy. The dispersion type of interaction can explain the general additive attraction between arbitrary atoms or molecules. The orientation effect and the induction effect require an alignment of permanent dipoles along the vector r_{ij} joining the interacting molecules. The orientation effect is not necessarily added between three molecules and in many cases repulsion of the third molecule rather than attraction is to be expected. Similarly, the induction effect is greatly reduced if many molecules superimpose their polarizing field from different sides. Hence, the dispersion type of interaction is more applicable in explaining the van der Waals' interaction comparing the other two effects.

2.4.4. Intermolecular Potential:

Now let us consider two molecules or atoms, which are of rigid and perfectly elastic sphere interacting to each other. These molecules follow the gas laws and hence they attract to each other at longer distances and repel each other at shorter distances. When two molecules or atoms are sufficiently close to each other then, the two nuclei and the two electron clouds tend to vibrate together thereby leading to attraction between different molecules. The functional form of the intermolecular potential [40-42] is given by

$$V = 4\varepsilon\left[\left(\frac{\sigma}{r}\right)^{12} - \left(\frac{\sigma}{r}\right)^{6}\right] \tag{2.64}$$

where ε is the well depth, σ is the distance between atoms or molecules. This is called the Leonard-Jones potential.

In general terms,

$$V = 4\varepsilon\left[\left(\frac{\sigma}{r}\right)^{m} - \left(\frac{\sigma}{r}\right)^{n}\right], m > n \tag{2.65}$$

where m and n are the integers.

The potentials are zero at r = ∝ and r = σ and have a minimum at

$$\sigma_{min} = r\left(\frac{n}{m}\right)^{1/m-n} \tag{2.66}$$

For larger values of r, the Leonard-Jone potential is asymptotic to an r^{-6} curve and therefore it has correct form to reproduce the long-range dispersion energy between closed shell atoms and molecules.

Another expression for intermolecular potential combined with the exponential repulsion $Ae^{-\alpha r}$ is given by

$$\dot{V} = Ae^{-\alpha r} - \frac{B}{r^6} \tag{2.67}$$

where A, B and α are constants.

2.4.5. Multipolar Interactions:

In space-fixed axes, the dipole-dipole term V_{11} is given by

$$V_{11} = -\frac{\mu_1 \mu_2}{r^3}(3C_1C_2 - C_{12}) \tag{2.68}$$

where C_i is the cosine angle between μ_i and r, C_{12} is the cosine of the angle between μ_1 and μ_2. The direction of r is chosen from molecule 1 and 2 in the intermolecular frame with polar axes along r.

For axially symmetric molecules [39] is

$$V_{12} = \frac{3}{2}\left(\frac{\mu_1 Q_2}{r^4}\right)\left[C_1(5C_2^2 - 1) - 2C_{12}C_2\right] \tag{2.69}$$

The quadrupole-quadrupole term V_{22} in the space fixed axes as

$$V_{22} = \frac{3}{4}\left(\frac{Q_1Q_2}{r^5}\right)\left(1 - 5C_1^2 - 5C_2^2 + 2C_{12}^2 + 35C_1^2C_2^2 - 20C_1C_2C_{12}\right) \quad (2.70)$$

The minimum energy orientations for the three orientations V_{11}, V_{12} and V_{22} are shown in figure 2.2.

The two linear quadrupoles prefer a T configuration which can be understood using a point charge model such as + = +. These minimum energy configurations are of importance for orientational structures of gas dimers, liquids and solids.

2.4.6. Dielectric Theory:

When an electric field is applied to a dielectric, the material is polarized through the alignment of permanent dipoles or the induction of molecular dipoles. For large field, the permanent dipoles are aligned better. The polarization **P** and the macroscopic field **E** are related [43-44] as

$$\mathbf{P} = \varepsilon_0 \chi \mathbf{E} \quad (2.71)$$

where χ is the dielectric susceptibility.

The relation showing the dependence of polarization [43-44] on electric field strength is given by

$$\mathbf{D} = \varepsilon \mathbf{E} = 4\pi \mathbf{P} + \mathbf{E}$$

i.e.
$$P = \left[\frac{\varepsilon - 1}{4\pi}\right] E \quad (2.72)$$

where **D** is the electric displacement.

If the material consists of non-polar molecules, the induced dipole moment **P** in a molecule of the dielectric is given by

$$\mathbf{p} = \alpha \mathbf{E}_i \tag{2.73}$$

where $\mathbf{E}_i$ is called the internal field, which is equal to the total electric field at the position of the molecule minus the field due to the molecule itself.

If the material contains N dipoles per unit volume, using equation (2.73)

$$\mathbf{P} = N\mathbf{p} = N\alpha \mathbf{E}_i \tag{2.74}$$

From equation (2.71) and (2.74), the dielectric susceptibility is

$$\chi = \left(\frac{N\alpha E_i}{\varepsilon_0 E} \right) \tag{2.75}$$

Equation (2.72) is valid for liquids and gases in static or low frequency fields of moderate intensity. The electric field at moderate intensity gives rise to dipole density by translation (deformation) and rotation (reorientation) effect. In the translation effect, two types of phenomena are encountered. First, the electrons are shifted relative to the positive charge, which is known as electric polarization. The second one is the atomic polarization where atoms or atom groups are displaced relative to each other.

In the rotation effect, the electric field tends to direct the permanent dipoles. This effect is strongly dependent on temperature due to counter action by the thermal motion of the molecules. On the contrary, the translation effects being intra-molecular phenomena are slightly dependent on the temperature.

At higher field intensities, the field tends to direct an isotropic particle to an orientation such that its axis of highest polarizability coincides with the direction of the external field. The electric field shifts the chemical equilibrium between components with different permanent dipole moments in favour of the component with high permanent dipole moments.

The polarization **P** is assumed to be divided into two parts as

$$\mathbf{P} = \mathbf{P}_{\alpha} + \mathbf{P}_{\mu} \tag{2.76}$$

where $\mathbf{P}_{\alpha}$ is the induced polarization caused by the translation effects and $\mathbf{P}_{\mu}$ is the dipole polarization caused by the orientation of the permanent dipoles.

The equation (2.72) can be written as

$$\mathbf{P}_{\alpha} + \mathbf{P}_{\mu} = \left[\frac{\varepsilon - 1}{4\pi}\right]\mathrm{E} \tag{2.77}$$

Consider the electric field acting on a single molecule where the environment of the molecule is considered a continuum with the macroscopic properties of the dielectric.

The induced [45] polarization (P_α) may be written as

$$\mathbf{P}_\alpha = \sum_k N_k \alpha_k (E_i)_k \qquad (2.78)$$

where N is the number of particle per cm^3, α is the scalar polarizability of a particle and E_i is the average field strength acting upon that particle. The index k refers to the k^{th} kind of particle.

The orientation polarization $\mathbf{P}_\mu$ can be written as

$$P_\mu = \sum_k N_k \bar{\mu}_k \qquad (2.79)$$

where $\bar{\mu}_k$ is the value of the permanent dipole vector arranged over all orientations. The value of $\bar{\mu}_k$ can be computed from the energy of the permanent dipole, which depends on the part of the electric field $\mathbf{E}_d$ tending to direct the permanent dipoles.

The average moment per dipole in the direction of the applied field is given by

$$\bar{\mu} = \left(\frac{\mu^2}{3k_B T} \right) E_d \qquad (2.80)$$

Equation (2.79) can be written as

$$P_\mu = \sum_k N_k \frac{\mu_k^2 (E_d)_k}{3k_B T} \qquad (2.81)$$

Using equations (2.78) and (2.81) in equation (2.77), we get

$$\sum_k N_k \left[\alpha_k (E_i)_k + \frac{\mu_k^2 (E_d)_k}{3k_B T} \right] = \frac{(\varepsilon - 1)E}{4\pi} \qquad (2.82)$$

This equation is the fundamental equation for the dielectric constant for various polar and non-polar dielectrics.

When a molecule with permanent dipole strength μ is surrounded by the other particles, the inhomogeneous field of the permanent dipole polarizes its environment. In the surrounding particles, moments proportional to the polarizability are induced. If these particles have a permanent dipole moment, their orientation is influenced. Bell [45] introduced a better model for the dipole in a molecule, which is an ideal dipole in the centre of a spherical cavity to calculate the consequences of the effects cited above. The field of the dipole in such a cavity polarizes the surrounding matter, and the resulting inhomogeneous polarization of the environment will give rise to a field **R** at the dipole, which is called the reaction field. **R** will have the same direction as the dipole vector μ due to symmetry and **R** will be proportional to μ as long as no saturation effects occur [45]. Hence

$$\mathbf{R} = f\boldsymbol{\mu} \qquad (2.83)$$

where the factor f is called the factor of the reaction field.

Using Onsager approximation

$$\frac{4}{3}\pi N a^3 = 1 \qquad (2.84)$$

where N is the number of particles per cm^3, **a** is the radius of the spherical cavity where the ideal dipole moment μ is placed. The value of **a** is generally considered to be approximately equal to the molecular radius.

The reaction field of a non-polarizable point dipole is given by

$$R = \frac{1}{a^3}\frac{2(\varepsilon-1)}{2\varepsilon+1}\mu \qquad (2.85)$$

Comparing this equation with (2.83), we conclude that the factor of the reaction field is given by

$$f = \frac{1}{a^3}\frac{2(\varepsilon-1)}{2\varepsilon+1} \qquad (2.86)$$

The field in the dielectric can be described as the field of a virtual dipole μ_e at the centre of the cavity, which was called by Onsager as the external moment of the immersed dipole and is given by

$$\mu_e = \frac{3\varepsilon}{2\varepsilon+1}\mu \qquad (2.87)$$

For the case of polarizable permanent dipole, the reaction field induces a dipole $\alpha\mathbf{R}$ and hence satisfies the equation

$$R = f(\mu + \alpha R) \qquad (2.88)$$

where μ is the permanent dipole moment.

α is the average polarizability

Therefore,
$$R = \frac{f}{1 - f\alpha}\mu \tag{2.89}$$

Eliminating the value of **f** from equation (2.86), we get

$$R = \frac{1}{\left[\frac{2\varepsilon+1}{2(\varepsilon-1)} - \frac{\alpha}{a^3}\right]}\frac{1}{a^3}\mu \tag{2.90}$$

In order to find the value of **R** in the case of liquids containing one kind of particle, we use the Onsager's approximation (2.84) and the equation

$$\frac{\alpha}{a^3} = \frac{n_D^2 - 1}{n_D^2 + 2} \tag{2.91}$$

where n_D is the refractive index.

Now equation (2.90) becomes

$$R = \frac{4\pi}{3} N \frac{2(\varepsilon-1)}{2\varepsilon + n_D^2}\frac{n_D^2 + 2}{3}\mu \tag{2.92}$$

N is the number of particles per cm^3 and can be computed from

$$N = \left(\frac{d}{M}\right)N_A$$

where M is the molecular weight of the substance

d is the density and N_A is the Avogadro's number.

Under the influence of the reaction field **R**, the dipole moment is increased considerably and the increased moment [45-46] is given by

$$\mu^* = \mu + \alpha\mathbf{R} \tag{2.93}$$

Substituting the value of R from (2.89) to (2.93), we get

$$\mu^* = \left(\frac{\mu}{1 - f\alpha} \right) \tag{2.94}$$

Using the value of **f** from (2.86) to the above equation, we have

$$\mu^* = \frac{\mu}{1 - \frac{\alpha}{a^3} \frac{2(\varepsilon - 1)}{2\varepsilon + 1}} \tag{2.95}$$

Again substituting the value of $\frac{\alpha}{a^3}$ from equation (2.91) to equation (2.95), we have

$$\frac{\mu^*}{\mu} = \frac{2\varepsilon + 1}{2\varepsilon + n_D^2} \frac{n_D^2 + 2}{3} \tag{2.96}$$

When the dipole is not surrounded by molecules of the same kind, the reaction field and the ratio $\frac{\mu^*}{\mu}$ are changed. From equation (2.92), N and n_D refer to the pure dipole compound, whereas ε is the dielectric constant of the mixture. Thus the changes in **R** and $\frac{\mu^*}{\mu}$, when the environment of the dipole is changed, result in a change of the factor $\frac{2(\varepsilon - 1)}{2\varepsilon + n_D^2}$ in equation (2.92) and a change of the factor in $\frac{2\varepsilon + 1}{2\varepsilon + n_D^2}$ equation (2.95) respectively.

2.4.7. The onsager equation for polar and non-polar dielectrics in internal and directing fields

For a non-polar system, the fundamental equation [45] for the dielectric constant eq.(2.82) simplifies to

$$\frac{\varepsilon - 1}{4\pi} E = \sum_k N_k \alpha_k (E_i)_k \qquad (2.97)$$

The internal field $\mathbf{E}_i$ is also influenced by the cavity field $\mathbf{E}_c$ and the reaction field R of the induced dipole and hence considering both the effects of the fields, $\mathbf{E}_i$ can be written as

$$E_i = E_c + R \qquad (2.98)$$

where the cavity field $\mathbf{E}_c$ is given by

$$E_c = \left[\frac{3\varepsilon}{2\varepsilon + 1}\right] E \qquad (2.99)$$

The internal field for the case of polar molecules can also be built up from the cavity field and the reaction field. In this case, the reaction field is taken as field of the total dipole moment of the molecule. In the spherical cavity, the permanent dipole moment and the reaction field caused by it will have the same direction, as the angle between them will be constant during the movement of the molecule. Therefore, the reaction field **R** does not influence the direction of the dipole moment of the molecule and does not contribute to the directing field $\mathbf{E}_d$. On the

other hand, the reaction field polarizes the molecule, contributes to the internal field $\mathbf{E}_i$. As a result, there is a difference between the internal field $\mathbf{E}_i$ and the directing field $\mathbf{E}_d$ and this difference gives the value of the reaction field averaged over all orientations of the polar molecule

$$E_i - E_d = \bar{R} \qquad (2.100)$$

where $\bar{\mathbf{R}}$ is the total reaction field connected with the permanent part of the dipole moment.

For finding the value of $\mathbf{E}_d$, the polarizability of the molecule must be taken into account. The directing field $\mathbf{E}_d$ can be obtained by removing the permanent dipole of a molecule without changing its polarizability. In this case, we have eliminated the contribution of r to $\mathbf{E}_i$. The field $\mathbf{E}_d$ causes a dipole $\alpha\mathbf{E}_d$ with reaction field $f\alpha\mathbf{E}_d$, where f is the reaction field given by equation (2.86). Thus, $\mathbf{E}_d$ is given by the equation

$$\mathbf{E}_d = \mathbf{E}_c + f\alpha\, \mathbf{E}_d$$

Therefore,
$$E_d = \left[\frac{1}{1-f\alpha}\right] E_c \qquad (2.101)$$

where $\mathbf{E}_c$ is the cavity field given by equation (2.99)

f is the reaction field factor and α is the polarizability.

Substituting the value of $\mathbf{E}_c$ from (2.99) to equation (2.101), we get

$$E_d = \frac{1}{1-f\alpha}\frac{3\varepsilon}{2\varepsilon+1}E \qquad (2.102)$$

If the dielectric consists of different kinds of molecules, then the directing

field for each kind of molecule must be calculated separately.

For the k^{th} kind of molecule, the directing field is given by

$$(E_d)_k = \frac{1}{1-f_k\alpha_k}\frac{3\varepsilon}{2\varepsilon+1}E \qquad (2.103)$$

with $$f_k = \frac{1}{a_k^3}\frac{2(\varepsilon-1)}{2\varepsilon+1} \qquad (2.104)$$

where ε is the dielectric constant of the mixture and a_k is the radius of the cavity belonging to the particle of the k^{th} kind.

Then from equation (2.100), the internal field can be written as

$$\mathbf{E}_i = \mathbf{E}_d + \bar{R}$$

From equation (2.89),we have $\bar{R} = \frac{f}{1-f\alpha}\bar{\mu}$

where $\bar{\mu}$ is the value of the μ averaged over all orientations and is given

as $$\bar{\mu} = \frac{\mu^2}{3k_BT}E_d$$

Hence $$E_i = \left(1+\frac{f}{1-f\alpha}\frac{\mu^2}{3k_BT}\right)\frac{1}{1-f\alpha}\frac{3\varepsilon}{2\varepsilon+1}E \qquad (2.105)$$

For a mixture of different kinds of molecules, the internal field at the k^{th} kind of molecule is

$$(E_i)_k = \left(1+\frac{f_k}{1-f_k\alpha_k}\frac{\mu_k{}^2}{3k_BT}\right)\frac{1}{1-f_k\alpha_k}\frac{3\varepsilon}{2\varepsilon+1}E \qquad (2.106)$$

Now substituting equations (2.103) and (2.106) in the fundamental equation (2.82), we have

$$\frac{(\varepsilon-1)(2\varepsilon+1)}{12\pi\varepsilon} = \sum_k N_k \frac{1}{1-f_k\alpha_k}\left[\alpha_k + \frac{1}{3k_BT}\frac{\mu_k^2}{1-f_k\alpha_k}\right] \qquad (2.107)$$

Taking Onsager's approximation for the radius of cavity

$$\frac{4}{3}N_k a_k^3 = 1 \qquad (2.108)$$

and the polarizability is given by

$$\frac{(\varepsilon_\infty)_k - 1}{(\varepsilon_\infty)_k + 2} = \frac{4}{3}\pi N_k \alpha_k \qquad (2.109)$$

where ε_∞ is the dielectric constant characteristic for the induced polarization, we obtained for the ratio $\frac{\alpha_k}{a_k^3}$ as

$$\frac{\alpha_k}{a_k^3} = \frac{(\varepsilon_\infty)_k - 1}{(\varepsilon_\infty)_k + 2} \qquad (2.110)$$

Using equations (2.104) and (2.110), we get

$$\frac{1}{1-f_k\alpha_k} = \frac{((\varepsilon_\infty)_k + 2)(2\varepsilon+1)}{3(2\varepsilon + (\varepsilon_\infty)_k)} \qquad (2.111)$$

Hence equation (2.107) can be written as

$$\frac{\varepsilon-1}{4\pi\varepsilon}=\sum_{k}N_{k}\frac{(\varepsilon_{\infty})_{k}+2}{2\varepsilon+(\varepsilon_{\infty})_{k}}\left[\alpha_{k}+\frac{((\varepsilon_{\infty})_{k}+2)(2\varepsilon+1)}{3(2\varepsilon+(\varepsilon_{\infty})_{k})}\frac{\mu_{k}^{2}}{3k_{B}T}\right] \tag{2.112}$$

For pure dipolar liquids, we find

$$\frac{\varepsilon-1}{4\pi}=\frac{3\varepsilon}{4\pi}\frac{\varepsilon_{\infty}-1}{2\varepsilon+\varepsilon_{\infty}}+\frac{(\varepsilon_{\infty}+2)^{2}(2\varepsilon+1)\varepsilon}{(2\varepsilon+\varepsilon_{\infty})^{2}}\frac{N\mu^{2}}{9k_{B}T} \tag{2.113}$$

after substituting α_k and using equations (2.108) and (2.110)

Hence,
$$\mu^{2}=\frac{9k_{B}T}{4\pi N}\frac{(\varepsilon-\varepsilon_{\infty})(2\varepsilon+\varepsilon_{\infty})}{\varepsilon(\varepsilon_{\infty}+2)^{2}} \tag{2.114}$$

Equation (2.114) is called the Onsager equation. The permanent dipole moment of a molecule can be computed from the dielectric constant of the pure dipole liquid if the density and ε_∞ are known. Moreover, for most dielectrics the dielectric constant ε_∞ is equal to the square of the index of refraction n, as followed from Maxwell's relation.

$$\varepsilon_{\infty} = n^{2} \tag{2.115}$$

In Onsager equation, the particles are assumed spherical and it takes into account the local field due to molecules within distances large compared to molecular dimensions but small compared to the thickness of the material. However, it neglects the local directional forces on the molecules due to their neighbours [46]. For the case of dilute solutions of a dipolar solute in a nonpolar solvent, the polar molecules are far apart so that the interactions between them can be neglected. However,

there will be an interaction between the polar molecules and the solvent molecules and this interaction can be taken into account approximately by using the form of Lorentz local field.

2.4.8. Theories of Kirkwood and Fröhlich:

Fröhlich [45] developed a model which represents a dielectric with dielectric constant ε, consisting of polarizable molecules with a permanent dipole moment. In this model, he introduced a continuum with dielectric constant ε_∞ in which point dipoles with a moment μ_d are embedded. Each molecule is replaced by a point dipole μ_d having the same non-electrostatic interactions with the other point dipoles, while the polarizability of the molecule can be assumed to form a continuum with dielectric constant ε_∞.

The polarization P can be divided into two parts as

$$\mathbf{P} = \mathbf{P}_{in} + \mathbf{P}_{or} \qquad (2.116)$$

where $\mathbf{P}_{in}$ is the induced polarization and $\mathbf{P}_{or}$ is the orientation polarization.

The induced polarization is equal to the polarization of the continuum with dielectric constant ε_∞, hence we can write

$$P_{in} = \left[\frac{\varepsilon_\infty - 1}{4\pi}\right] E \qquad (2.117)$$

The orientation polarization is given by the dipole density, which is due to dipoles μ_d. Consider a sphere with volume V containing N dipoles, then

$$P_{or} = \frac{1}{V} < M_d.e > \tag{2.118}$$

where
$$M_d = \sum_{i=1}^{N} (\mu_d)_i \tag{2.119}$$

$<\mathbf{M}_d.\mathbf{e}>$ is the average component of the moment due to dipoles in the sphere, in the direction of the field and is expressed as

$$< M_d.e >= \frac{\int dx^N M_d.e \exp\left(-\frac{U}{k_B T}\right)}{\int dx^N \exp\left(-\frac{U}{k_B T}\right)} \tag{2.120}$$

where U is the energy of the dipoles in the sphere and consists of three parts namely the energy of the dipoles in the external field, the electrostatic interaction energy of the dipoles and the non-electrostatic interaction energy between the molecules. The third kind of energy is responsible for the short-range correlation between orientations and positions of the molecules.

The external field in this model is equal to the field situated in a spherical cavity which is filled with a continuum with dielectric constant ε_∞, and this field is called the Fröhlich field $\mathbf{E}_F$. In this case the

spherical cavity is situated in a dielectric with dielectric constant ε. The Fröhlich field [45] is given by

$$E_F = \frac{3\varepsilon}{2\varepsilon + \varepsilon_\infty} E \tag{2.121}$$

The general expression for the dielectric constant can be written as

$$\frac{\varepsilon - 1}{4\pi} = \left(\frac{\partial}{\partial E} (P_{in} + P_{or}) \right)_{E=O} \tag{2.122}$$

After substituting equations (2.117) and (2.118) in eq. (2.122), we get

$$\varepsilon - \varepsilon_\infty = \frac{4\pi}{V} \left(\frac{\partial}{\partial E} < M_d.e > \right)_{E=O} \tag{2.123}$$

Now rewriting E_F instead of E as the independent variable, we have

$$\varepsilon - \varepsilon_\infty = \frac{4\pi}{V} \left(\frac{\partial E_F}{\partial E} \right)_{E=O} \left(\frac{\partial}{\partial E_F} < M_d.e > \right)_{E_F=O} \tag{2.124}$$

Since in this case, $$\frac{\partial U}{\partial E_F} = -M_d.e$$

We obtain,

$$\varepsilon - \varepsilon_\infty = \frac{4\pi}{V} \left(\frac{\partial E_F}{\partial E} \right)_{E=O} \frac{< M_d^2 >_o}{3k_B T} \tag{2.125}$$

which is the expression for the dielectric constant in Fröhlich's model.

Using the value of E_F from (2.121) to the above equation, we can write

$$\varepsilon - \varepsilon_\infty = \frac{4\pi}{V}\frac{3\varepsilon}{2\varepsilon+\varepsilon_\infty}\frac{< M_d^2 >_o}{3k_BT} \tag{2.126}$$

i.e. $$< M_d^2 >_0 = \frac{k_BTV}{4\varepsilon}\frac{(\varepsilon-\varepsilon_\infty)(2\varepsilon+\varepsilon_\infty)}{\varepsilon} \tag{2.127}$$

Evaluating the average $< M_d^2 > 0$ which is equal to $N'\mu_d^2\sum_{j=1}^{N'} < \cos\theta_{ij} >$,

we get

$$\frac{(\varepsilon-\varepsilon_\infty)(2\varepsilon+\varepsilon_\infty)}{12\pi\varepsilon} = \frac{N}{3k_BT}g\mu_d^2 \tag{2.128}$$

where $N = \frac{N'}{V}$ and the correlation factor $\mathbf{g} = \sum_{j=1}^{N'} < \cos\theta_{ij} >$

This correlation factor takes into account the correlation between the orientations due to the short-range order.

The permanent dipole moment μ_d in the centre is given by

$$\mu_d = \frac{\varepsilon_\infty + 2}{3}\mu \tag{2.129}$$

where μ is the dipole moment of the molecules in the gas phase.

Substituting the value of μ_d from (2.128) to (2.129), we have

$$g\mu^2 = \frac{9k_B T}{4\pi N} \frac{(\varepsilon - \varepsilon_\infty)(2\varepsilon + \varepsilon_\infty)}{\varepsilon(\varepsilon_\infty + 2)^2} \qquad (2.130)$$

This equation (2.130) is called the Kirkwood–Fröhlich equation. Equations (2.88) and (2.130) are compared and it is clear that Kirkwood –Fröhlich equation is the generalization of the Onsager equation. The Kirkwood –Fröhlich equation gives the relation between the dielectric constant ε, the dielectric constant of induced polarization ε_∞, the temperature, the density and the permanent dipole moment.

The correlation factor g is a measure of the local ordering in the material. Positive deviation of **g** from unity results when short range hindering torques favour parallel orientation of the dipoles of neighbouring molecules, while negative deviations result from antiparallel orientation. If g is unity, it means that fixing the position of one dipole does not influence the positions of the others except through the long-range electrostatic forces.

For the evaluation of the undetermined parameters in the model, it is useful to determine **g** as a function of the concentration when the compound is dissolved in a non-polar solvent. However the equation (2.130) is valid only for pure dipolar liquids.

The equation, which is valid for solutions of polar compounds in non-polar solvents is given by

$$g\mu^2 = \frac{9k_BT}{4\pi N_A x_P}\frac{(2\varepsilon+\varepsilon_\infty)^2}{(\varepsilon_\infty+2)^2(2\varepsilon+1)}\left[\frac{\phi(\varepsilon-1)}{\varepsilon}-\frac{3x_0M_0(\varepsilon_0-1)}{(2\varepsilon+\varepsilon_0)d_0}-\frac{3x_PM_1(\varepsilon_\infty-1)}{(2\varepsilon+\varepsilon_\infty)d_1}\right] \quad (2.131)$$

where d_1 and d_0 are the densities of the polar and non-polar compounds in the pure state. x_0 and x_p are the molar fractions for the non-polar and the polar component respectively. M_o and M_1 are the molecular weight of the non-polar solvent and the polar solvent. $\phi = \frac{x_0M_0 + x_PM_1}{d}$ is the molar volume of the mixture and N_A is the Avogadro's number.

Equation (2.131) helps in calculation of the Kirkwood correlation function **g** from experimental data for solutions of associating compounds in non-polar solvents.

REFERENCE:

1. D.W.Oxtoby, J.Phys. Chem. **87**, 3028 (1983).
2. W.G.Rothschild "Dynamics of Molecular Liquids" p 53, Wiley, New York (1984).
3. J. Jones, Acc. Chem. Rev. **17**, 74 (1983) and reference cited there in.
4. S.F.Fischer, A.Laubereau, Chem. Phys. Lett. **55**, 189 (1978).
5. D. Schiebe, G. Döge, Ber. Bunsenges. Phys. Chem. **85**, 520 (1981).
6. D. W. Oxtoby, D. Levesque, J.J. Weis, J. Chem. Phys. **68**, 528 (1978).
7. G. Döge, R. Arndt, J. Yarwood, Mol. Phys. **52**, 399 (1984).
8. W. Schindler, T. W. Zerda, J. Jonas, J. Chem. Phys. **81**, 4306 (1984).
9. D. E. Logan, Chem. Phys. **103**, 215 (1986).
10. C. H. Wang, J. Mchale, J. Chem. Phys. **72**, 4039 (1980).
11. M. G. Giorgini, M. Musso, A. Asenbaum, G. Döge, Mol. Phys. **98**, 783 (2000).
12. S.F. Fischer, A. Laubereau, Chem. Phys. Lett. **35**, 6 (1975).
13. K. Tanabe, J. Jonas, Chem. Phys. Lett. **53**, 278 (1978).
14. D.W. Oxtoby, J. Chem. Phys **70**, 2605 (1979).
15. R. Zwanzig, M. Bixon, Phys. Rev. **2A**, 2005 (1970).

16. K. S. Schweizer, D. Chandler, J. Chem. Phys. **76**, 2296 (1982).

17. D. Ben Amotz, M.R. Lee, S.Y. Cho, D.J. List, J. Chem. Phys. **96**, 8781 (1992).

18. R. Kubo in "Fluctuations, Relaxation and Resonance in Magnetic systems", edited by D. ter Haar, p 23, Oliver and Boyd, Edinburgh (1962).

19. R. Arndt, R.E.D. McClung, J. Chem. Phys. **69**, 4280 (1978).

20. J. Yarwood, R. Arndt, in "Molecular Association", edited by R.Foster, Vol.**2**, pp.287, 297-300, Academic Press, London (1979).

21. G.J. Remar, R.A. Macphail, J. Chem. Phys. **103**, 4388 (1995).

22. A. Purkayastha, K. Kumar, J. Raman Spectrosc. **19**, 249 (1988).

23. C.B. Harris, R.M. Shelby, P.A. Cornelus, Chem Phys Lett. **57**, 8, (1978).

24. R.M. Shelby, C.B. Harris, P.A. Cornelus, J. Chem. Phys. **70**, 34, (1979).

25. A.W. Adamson, "A text book of Physical Chemistry" p 691, Academic Press, New York, (1973).

26. K. Fukushi, M. Kimura, J. Raman Spectrosc. **13**, 9 (1982).

27. J. M. Ziman, "Principles of Theory of Solids", p 214, Cambridge University Press, Cambridge (1972).

28. B. Tareev, "Physics of Dielectric materials", p 49, Mir publishers, Moscow (1975).

29. V.V. Frolov in "Nuclear Magnetic Resonance" Edited by P.M. Borodin, p 13, Amerind, New Delhi (1975).

30. A. Gierer, K. Wirtz, Zs. Naturforschung. **8a**, 522 (1953).

31. G. Herzberg "Molecular spectra and Molecular structure" II- *Infrared and Raman spectra of polyatomic molecules*, p 249, D. Van Nostrand Company Inc., New York (1945).

32. D. A. Long, Raman Spectroscopy, Mcgraw-Hill International Book Company, London (1977).

33. L.a. Nafie, W.L. Pelicolas, J. Chem. Phys. **57**, 3145 (1972).

34. R.G.Gordon, Adv. Magn. Reson. **3**, 1 (1968).

35. O. Svelto "Principles of Lasers" p 49, Plenum Press, New York (1992)

36. T. Sundius, J. Raman Spectrosc. **1**, 471 (1973).

37. R. Gabler "Electrical Interactions in Molecular Biophysics" p 157, Academic Press Inc., New York (1978).

38. D. Langbein in "Springer Tracts in Modern Physics: Van der Waals attraction" Vol. **72**, Edited by G.Höhler, p 4, Springer-Verlag, Berlin (1974).

39. C. G. Gray and K. E. Gubbins "Theory of Molecular fluids: Vol **1**: Fundamentals", International Series of Monographs on Chemistry, Clarendon Press, Oxford (1984).

40. M. Karplus and R. N. Porter "Atoms and Molecules: An Introduction for students of Physical Chemistry", pp 262-267, The Benzamin/Cummings Publishing Co., California (1970).

41. H. Margenau and N. R. Kestner "Theory of Intermolecular Forces", Pergamom Press, Oxford (1971).

42. C. Kittel "Introduction to Solid State Physics", pp 56-63, John Wiley and Sons, Inc., Singapore (1995).

43. David J. Griffiths "Introduction to Electrodynamics", Prentice Hall of India Pvt. Ltd., New Delhi (1997).

44. S. Bone, J. Eden, P.R.C. Gasloyne, R. Pethig, J. Chem. Soc. Faraday Trans. 1, **77**, 1729 (1981).

45. C.J.F. Bottcher "Theory of electric polarization" Vol **1** Elsevier, Amsterdam (1973).

46. P. Smyth in "Molecular interaction" Vol **2**, edited by H. Ratajczak and W. J. Orville-Thomas, John Wiley and Sons, Chichester (1981).

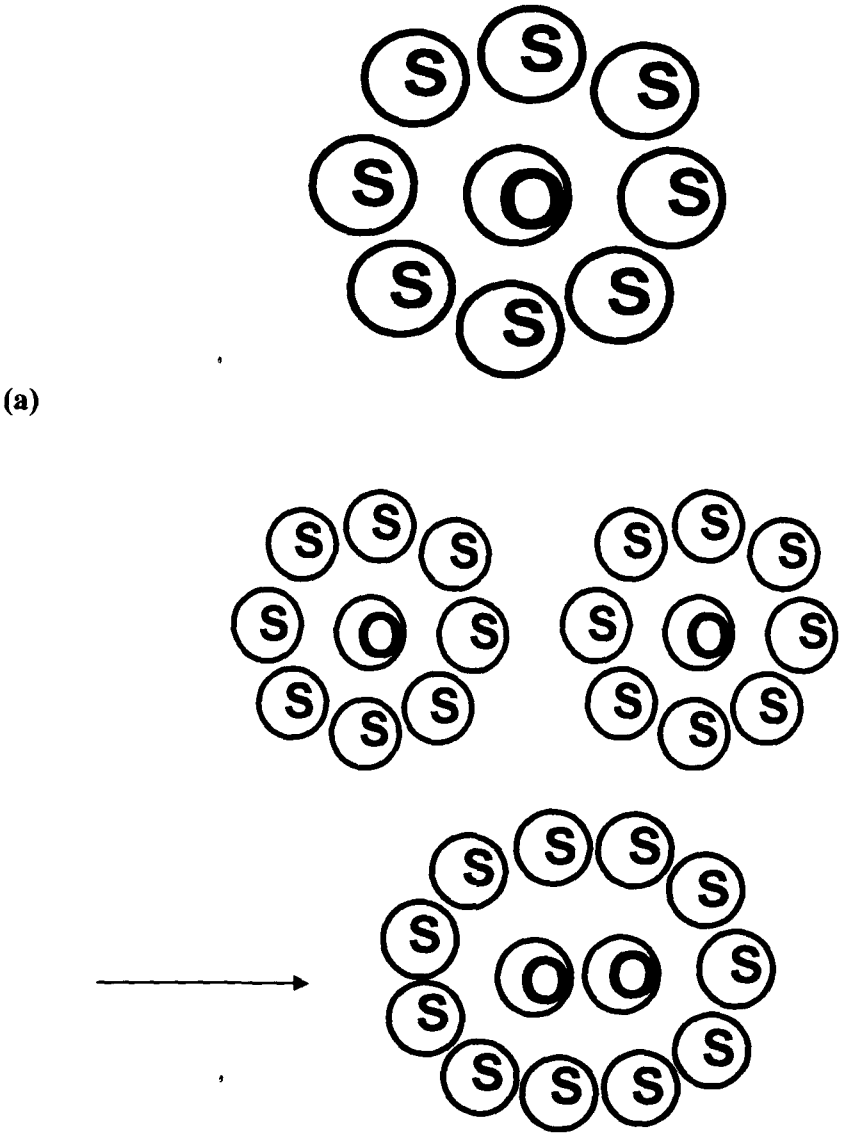

Fig. 2.1: (a) The solvent cage effect where O - solute and S – solvent molecules.
(b) Interaction of the solvation layers of the solutes with solvents, where the size of solvent and solute molecules are comparable.

(a)

(b)

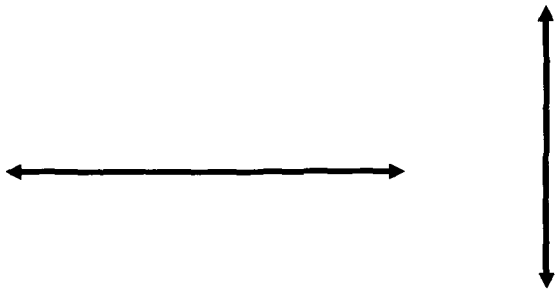

(c)

Fig. 2.2: Minimum energy orientation for
(a) dipole-dipole interactions.
(b) dipole-quadrupole interactions.
(c) quadrupole-quadrupole interactions.

CHAPTER 3

CHAPTER 3

EXPERIMENTAL ASPECTS

3.1. INTRODUCTION

The experimental methodology adopted for our studies is mainly the laser Raman scattering experiment. In this chapter, the present state of experimental techniques is described, including a concise description of the instrumentation . The kind of spectrometer used and the importance of slit width etc. on Raman band have been detailed. The various aspects which have to be taken into consideration for the accurate measurement of Raman band for the present study is also cited in the later part of this chapter.

The Raman scattering phenomenon is very weak compared to Rayleigh scattering, in which only a small fraction of photons are scattered by Raman scattering. So Raman lines are usually very weak (~ 10^{-6} of the Rayleigh scattering intensity). The majority of the scattered light is similar to the original incident light in terms of photon energy. The ratio of incident light to Raman scattered light sometimes exceeds 10^{9}.

A modern Raman spectrometer consists of a laser, a sample compartment, a double monochromator and a photoelectric detection system. In a standard Raman experiment, the intense monochromatic radiation (usually a laser) is focused on the sample. The scattered light is then gathered by the collecting optics and is directed towards a dispersive system (usually a double monochromator), which does the job of selecting the scattered light of particular frequency range. At the exit port of the double monochromator, the Raman spectrum displays in the form of a series of faint lines. The signals are detected by a photomultiplier tube and recorded by a DATAMATE using a DM-3000 software. The block diagram of the Raman instrument is shown in figure 3.1.

The various sections of the experimental setup are described as follows:

3.2. EXCITATION SOURCE: SPECTRA PHYSICS MODEL 165 Ar^+ LASER

The small cross-section of Raman scattering demands a strong excitation source, preferably a laser. Also the theory of Raman effect shows that the amount of Raman scattering from a sample is directly proportional to the intensity of incident radiation at the sample, to the fourth power of frequency of the exciting line and the concentration of

the scattered species. This means that a blue or a green laser will be more efficient for excitation than a red laser. Hence an argon ion laser operating at 4880Å (= 20,487cm^{-1}) is suitable to cause a greater Raman scattering. Also in order to study the solvent dependence at very dilute concentrations, high powers are required. Since high powers are available with the 4880 Å laser line from Ar^+ laser, the Spectra Physics Model 165 Ar^+ laser as used for recording the Raman spectra.

The specification of Spectra Physics model 165 Ar^+ laser is presented below:

Noise, light control RMS, 10Hz-20MHz	0.2%
Noise, Current control RMS, 10Hz-2MHz	1%
Frequency stability	60MHz/°C
Beam Diameter	1.25mm
Beam Divergence (full angle)	0.69mrad
Cavity configuration	long radius, output flat, high reflector
Cavity length w/o prism	1+0.003 meter
w/ prism	1.05+0.003 meter
Folded cavity	N/A
Polarization	Vertical

The Spectra Physics Model Ar^+ is a continuous wave (CW), which essentially consists of a laser head and the Spectra Physics Model 265

exciter. The laser head consists of a rugged trouble free Beryllium Oxide plasma tube closed at each end by the Brewster angle window, a solenoid and an optical resonator. The optical resonator is formed by a spherical reflector at the output end, together with a prism assisted by a flat reflecting mirror at the back end. The prism is placed in the optical path of the resonator in such a way that it selects the correct wavelength. The plasma tube is positioned exactly along the central line of the mirror. External thumb wheel controls are provided for the selection of wavelength of the emitted radiation and for changing the intra-cavity aperture. The emitted light from this laser source is polarized and the plane of polarization can be changed to any desired plane by using the $\lambda/2$ plate.

The Spectra Physics Model 265 exciter contains the necessary electric and electronic circuits in order to create, sustain and monitor the ionic discharge in the plasma tube. It also monitors and controls the output power and regulates the solenoid current of the 165 Ar^+ laser head. The 265 exciter operates on a 230 volts three phase power line which is provided by a power transformer supplied with a three phase 400 volts stabilized power from the main line. The input stabilization was achieved with the help of three single 8.3 KVA (each) Nelco voltage stabilizers connected in the star (Y) configuration. Cooling of both 165 Ar^+ laser head and the 265 exciter are provided by a NESLAB model

HX-500 air cooled water chilled plant which continuously circulates chilled de-ionized distilled water at a constant temperature of 15° C and at a pressure of 40 PSIG.

3.3. OPTICS AROUND THE SAMPLE

A laser filter or the laser mate is kept in the path of the light before it enters the focusing system. The laser filter is a small grating monochromator, which allows the excitation wavelength to pass through but blocks the weaker non-lasing lines from the laser plasma. It is therefore able to provide a clean Raman spectrum uncluttered by the laser plasma lines, especially for a strong scattering sample [1].

The filtered laser beam is deflected upward by 90° using a mirror and is focused onto the sample to a spot of diameter of about 10 μm by the fused silicon-condensing lens. Scattered radiation from the sample passes through a polarization analyzer, a device based on birefringence and total reflection or on dichorism. The polarization analyzer transmits light of a particular polarization depending on the orientation of the polarizer. Use of polarization analyzer therefore provides direct information regarding the state of polarization of the observed plasma band. The scattered radiation is collected by an elliptical, which ascertains a large solid angle about the focal volume and hence collects

the optimum amount of scattered light. The optical diagram of the light scattering systems is shown in figure 3.2.

3.4. COLLECTING OPTICS FOR SCATTERED RADIATION

A standard sampling platform is supplied with the spex 1459 illuminator. The 1431 B liquid cell of 1 ml capacity with 1431M holder was used for holding the sample. The sample is illuminated with laser radiation and then the laser focus control is adjusted until the brightest image is observed at the sample. The collection system geometry for the Raman scattered radiation is depicted in figure 3.2. The image of the sample scattered radiation is deflected on the target. The imaging of the scattered radiation on the entrance slit of the spectrometer is done by an elliptical collection mirror (f/1.4). The image is centered on the cross hairs with the lateral adjustments and focus adjustment is turned until the sharpest image is achieved. By rotating the swing away mirror counter-clockwise, the sample scattered radiation is allowed to pass into the spectrometer. The signal is now peaked photoelectrically between the focus and the lateral adjustment until the signal from the detector is maximum. In order to increase the scattering and collection efficiency, spherical mirrors may be mounted above and behind the sample in the 1459 illuminator. Both mirrors increase the amount of

scattered radiation that reaches the spectrometer entrance slit and therefore also increases the signal from the detector.

Two optical elements may be interposed in the beam, an analyzer and a scambler, before it reaches the entrance slit. The analyzer is based on birefringence and total reflection or dichorism. The scambler is a wedge of birefringence material. The two components of polarized light passing through it will be thrown out of phase as with a $\lambda/2$ plate. The retardation will vary from place to place and is not exactly $\lambda/2$; hence the emerging radiation will be depolarized. It cancels variations in spectrometer response that results from polarization dependent efficiencies.

The laser output is polarized perpendicularly whereas the Raman radiation from the sample is depolarized. The analyzer interposed in the path may transmit the light either perpendicularly polarized or parallel polarized, depending on the orientation of the analyzer. In both the cases, the same scrambler is employed in front of the entrance slit of the monochromator to depolarize the radiation.

3.5. THE SPECTROMETER: SPEX RAMALOG 1403 DOUBLE MONOCHROMATOR

Since the high spectral purity is required to unveil the weak Raman spectra, a double monochromator with high stray light rejection

capability, good resolution and sensitive detection system with very low inherent noise is therefore required for the collection of Raman data.

The function of the spectrometer is to separate the spatially scattered photons from the sample on the basis of their frequency. The light dispersing process is repeated by linking two single monochromator to form a double monochromator. The double monochromator also separates the Raman photons from the overwhelming number of Rayleigh photons.

The 1403 Spex Ramalog has a 0.85m focal length double monochromator with an aperture f / 7.8 that selectively passes radiation on the basis of their frequency. This instrument has a spectral coverage from 3.1 x 10^4 cm^{-1} to 1.1 x 10^4 cm^{-1}. An accuracy of ± 1 cm^{-1} in the 10,000 cm^{-1} range, a resolution of 0.15 cm^{-1} and a spectral repeatability of ± 0.2 cm^{-1} can be achieved by this instrument. The 1800 grooves / mm holographic grating blazed at 5000 Å are used in this instrument and there are four slits on it to pass the radiation. The entrance and exit slits primarily functions to control resolution, while the two central slits are responsible for blocking stray light from entering the second half of the monochromator. The optical diagram of the Spex Ramalog 1403 model double monochromator is shown in figure 3.1.

The holographic gratings are mounted on a modified Czerny – Turner mount as shown in figure 3.3. The fundamental grating equation [2] as applied to Czerny – Turner mount is

$$d (\sin \alpha + \sin \beta) = m \lambda \qquad (3.1)$$

where m = grating order,

λ = wavelength of incident light,

d = grating spacing,

α = angle of incidence,

β = angle of diffraction.

In the case of 1403 instrument, equation (3.1) may be expressed as

$$2d \sin \theta \cos \varphi = m \lambda \qquad (3.2)$$

so that $\alpha = \theta + \varphi$ and $\beta = \theta - \varphi$.

where $\varphi = 10^{o}$ and hence $\cos \varphi = 0.984$.

Here θ denotes the angle of rotation of the grating form zero as illustrated in figure 3.3 and φ represents the constant angle, which depends on the design of the instrument.

The 1800 grooves / mm holographic grating disperse the scattered radiation focussed onto the entrance slit of the spectrometer. Nearly monochromatic radiation of frequency ν for a particular tuning of the spectrometer reaches the exit slit of the double monochromator by the grating mirror combination.

The theoretical resolving power R_T of the grating is given by

$$R_T = \frac{\lambda}{\Delta\lambda} = \frac{\nu}{\Delta\nu} = 2\sin\theta\cos\phi\frac{W}{\lambda} = mN \qquad (3.3)$$

where λ = wavelength,

ν = wavenumber,

N = total number of grating grooves,

W = width of the grating ruting,

m = order of diffraction.

3.6. PHOTON COUNTING AND DETECTION: SCANNING OF RAMAN SPECTRA

The photon counting detection system consists of a RCA C31034-02, II stage QUANTACON type photomultiplier tube (PMT) with S-20 response in the photon counting mode. The C31034-02 is designed specifically for use at reduced temperature, e.g. -30° C. Cooling reduces the dark current caused by the thermionic emission to ~10 cps. The supply voltage is adjusted to provide a current amplification of ~10^6. Both Spex DATAMATE - DM1 and DM-3000 software were used for scanning the spectrometer and also for acquisition of the data. The central processing unit (CPU) of the DATAMATE is 8-bit microprocessor ROM. The data can be processed in real time to subtract away background, take ratio, integrate or convert logarithm from absorbed states. DATAMATE photon counting results

are expressed as and normalized to counts/sec. The DATAMATE also supplies HV (0-2000volts D.C –ve) to the PMT. The HV is CPU selectable in 10volts increment. The output current is variable from 0 to 2 mA. The linearity is better than 0.01% over full range. The noise level is 0.015% peak to peak at full load. The input in photon counting – DAM mode is negative giving pulse 0.1 mV amplitude or greater. The gain of the amplifier is 400 and the rise time is 10 nsec. he pulse pair resolution is < 25 nsec. The discriminator is initially adjustable from 5 mV to 200 mV. The maximum count rate for photon counting is 25 x 10^6 Hz. The linearity and accuracy of the output data (Y axis) is 0.3% full scale and resolution is one part in 4000.

3.7. THE PHOTOMULTIPLIER TUBE

RCA C31034-02 photomultiplier tube cooled to –30°C by a thermoelectric cooling device was used for obtaining the Raman spectral data. The photomultiplier tube having an almost linear responsivity,3000 Å wavelength range was operated for a current gain of ~10^6 with a maximum dark pulse summation of 12 cps. The RCA C31034-02 photomultiplier tube consists of a gallium arsenide chip placed at its photocathode, an ultra violet transmitting glass window and an inline copper beryllium dynode structure consisting of eleven dynodes.

The raw data is obtained from the output of the preamplifier (pc DAM) of gain 400. The anode of the PMT is the input of the pc DAM. The high voltage of 1450 volts requited for operating the PMT is supplied by the DATAMATE with a stability of +0.002% after 30 minutes of warm up.

3.8. THE POLARIZED AND DEPOLARIZED COMPONENTS OF SCATTERED LIGHT

In order to measure the depolarization ratio accurately, the polarization of the exciting laser beam is kept constant and the analyzer is placed after the sample [3]. Suppose the polarization of the laser beam is parallel to the Z- axis (fig.3.4) and the direct transmission of the analyzer is turned from Y to Z direction to measure I_{VH} and I_{VV} respectively. The intensity of the I_{VH} component is proportional to

$$I_{VH} \propto 3\gamma'^2$$

and that of I_{VV} component is proportional to

$$I_{VV} \propto (45\alpha'^2 + 4\gamma'^2)$$

where the factors α'^2 and γ'^2 are defined by the derivatives of the polarizabilities as,

$$\alpha' = \frac{1}{3}(\alpha'_{XX} + \alpha'_{YY} + \alpha'_{ZZ})$$

$$\gamma'^2 = \frac{1}{2}[(\alpha'_{XX} - \alpha'_{YY})^2 + (\alpha'_{YY} - \alpha'_{ZZ})^2 + (\alpha'_{ZZ} - \alpha'_{XX})^2]$$

$$+ 6(\alpha'^2_{XY} + \alpha'^2_{YZ} + \alpha'^2_{ZX})$$

Since the constant factor is same for the fixed experimental conditions, the depolarization ratio is

$$\rho = \frac{I_{VH}}{I_{VV}} = \frac{3\gamma'^2}{45\alpha'^2 + 4\gamma'^2} \qquad (3.4)$$

If the Raman scatter is known for the directions X and Y, its intensity in any direction ϕ of the X-Z plane may be calculated from

$$I(\phi) = I_X \cos^2\phi + I_Z \sin^2\phi \qquad (3.5)$$

The angle dependent intensities after the analyzer are

$$I_{VH}(\phi) \propto 3\gamma'^2$$

$$I_{VV}(\phi) \propto (45\alpha'^2 + 4\gamma'^2)\cos^2\phi + 3\gamma'^2\sin^2\phi$$

$$= (45\alpha'^2 + \gamma'^2)\cos^2\phi + 3\gamma'^2$$

The observed depolarization ratio is

$$\rho_{obs} = \rho + \rho(1 - \rho)\frac{\phi^2}{3} \qquad (3.6)$$

For $\rho << 0.75$, $\rho(1-\rho)\frac{\phi^2}{3}$ is of the order of magnitude of ϕ.

Thus the measured depolarization ratio ρ_{obs} will be larger than the true depolarization ratio, ρ.

If an angle ϕ = 10^0 (= 0.175 rad) is needed to measure a depolarization ratio of ρ = 0.01, in the case of highly polarized band, this method will produce a systematic error of

$$\left(1-\rho^2\right)\frac{\phi^2}{3} \approx 10^{-4} \text{ or } 1\%$$

However, if a completely depolarized band is to be measured for which the depolarization ratio is ρ = 0.75, the systematic error by using the same collecting angle ϕ = 10^0 will be

$$0.19 \text{ X } 10^{-2} \text{ or } 0.3\%$$

Therefore, we see that measured depolarization ratio is always larger than the theoretically expected value.

The intensity of the isotropic and anisotropic components of Raman band can be calculated using the standard relationship:

$$I_{iso}(\nu) = I_{VV}(\nu) - \frac{4}{3} I_{VH}(\nu) \tag{3.7}$$

$$I_{aniso}(\nu) = I_{VH}(\nu) \tag{3.8}$$

where $I_{VV}(\nu)$ and $I_{VH}(\nu)$ represent the polarized and depolarized Raman Spectra [4-7] respectively ν is the wavenumber in cm^{-1}.

In order to accurately determine the full width at half maximum (FWHM) of the isotropic component Γ_{iso} one must record the band profile with as high spectral resolution as possible.

The effect of finite slit width on Raman line width can be corrected by using [8] the equation

$$\Gamma_t = \Gamma_a [\, 1 - (S/\Gamma_a)^2] \qquad (3.9)$$

Where Γ_t and Γ_a are the true and apparent Raman line width (FWHM) respectively, and S is the spectral slit width in cm^{-1}.

3.9. FACTORS INFLUENCING THE RESOLUTION

There are two factors which mainly influence the resolution. They are:

(1) **Source of radiation**: From equation (3.1), since d (sin α + sin β) = m λ. This implies that the resolution depends linearly on the grating width (i.e optical path difference). Resolution deteriorates if the source illuminates less than the full width of the grating mirror. As a result, the source or condensing lens should fully illuminate the collimating mirror. This can usually be checked visually by opening the spectrometer, or in the case of energy outside the visible spectrum, by making certain that throughput is reached when the edges of the collimating mirrors are obstructed.

(2) **Slit width and slit height**: The slit is the most important part of the spectrometer. The mechanical slit dimension is however to be taken into account, instead one should think in terms of spectral band pass.

(a) **Slit width**: The spectral bans pass (spectral slit width is a function of reciprocal linear dispersion, which in turn depends on the wavelength, the grating constant, the focal length of the instrument and the spectral order. The spectral slit width S is given by

$$S = W D^{-1} = W (f \, d\theta/d\lambda)^{-1} \qquad (3.10)$$

Where D^{-1} is the reciprocal linear dispersion, W is the mechanical slit width, f is the focal length of the collimator and $d\theta/d\lambda$ is the angular dispersion.

(b) **Slit height**: The increase of height of a straight slit decreases the instrumental resolution. As the height of the slit is increased, the ends of the exit slits begin to pass portions of adjoining wavelengths. The effect of resolution is analogous to the increasing the slit width. Therefore, the height of the straight slit should be limited when maximum resolution is required.

The maximum throughput is attained whenever the source subtends at least a large solid angle at the slit as does the collimating mirror in the spectrometer. In case of photoelectric detection, the detectors integrate energy over the entire irradiated area and as a consequence, the total flux can be increased simply by increasing the slit height or width. The slit setting should be varied from scan to scan until the optimum balance of throughput and resolution are achieved.

3.10. SAMPLE HANDLING TECHNIQUES AND PRECAUTIONS TO MINIMIZE ERRORS

In order to record the spectra with good signal to noise ratio, the cell should be clean and free from grease and fingerprints, as these can cause a considerable increase in florescent background of the spectrum and from air bubbles which increases the scatter of laser beam, thereby reducing the excitation efficiency and increasing the amount of laser radiation reaching the monochromator. The outside of the cell should be wiped with a tissue moistened with chloroform or acetone to remove as much dirt as possible before use.

The best signal to noise ratio (S/N) in the spectrum of a liquid is obtained when it is contained in a capillary cell. The cell relies for its high efficiency on the multiple reflection of Raman light from the walls, thus bringing a large proportion of it to the collector lens. A 1 cm path length sample cell used in absorption spectroscopy is adequate for Raman experiments for liquid samples, provided the cell bottom is transparent. In order to minimize the amount of scattered light from the interface reaching the spectrometer, the cell should be topped around the meniscus. Due to the low intensity of Raman light, it is essential that the stray light is as low as possible.

REFERENCE:

1. Operation and maintenance instrumental manual for SPEX Model 1403 Spectrometer (1982).
2. H. A. Strobel "Chemical Instrumentation", pp. 320-327, Addision-Wesley, Mass (1973).
3. C. D. Allemand, Applied Spectrsc., **24**, 348 (1970).
4. M. A. Ricci, G. Signorelli and V. Mazzacurati, J. Phys.Condens. Matter, **2**, 183 (1990).
5. A. Das and K. Kumar, Spectrochim. Acta, **54A**, 793 (1998).
6. Y. J. Kim, H-Chou Chang, V. S. Sullivan and J. Jonas, J. Chem. Phys. **111**, 9658 (1999).
7. C. J. Fecko, J. D. Eaves and A. Tokmakott, J. Chem. Phys. **117**, 1139 (2002).
8. K. Tanabe ,Spectrochim. Acta, **40A**, 437(1984).

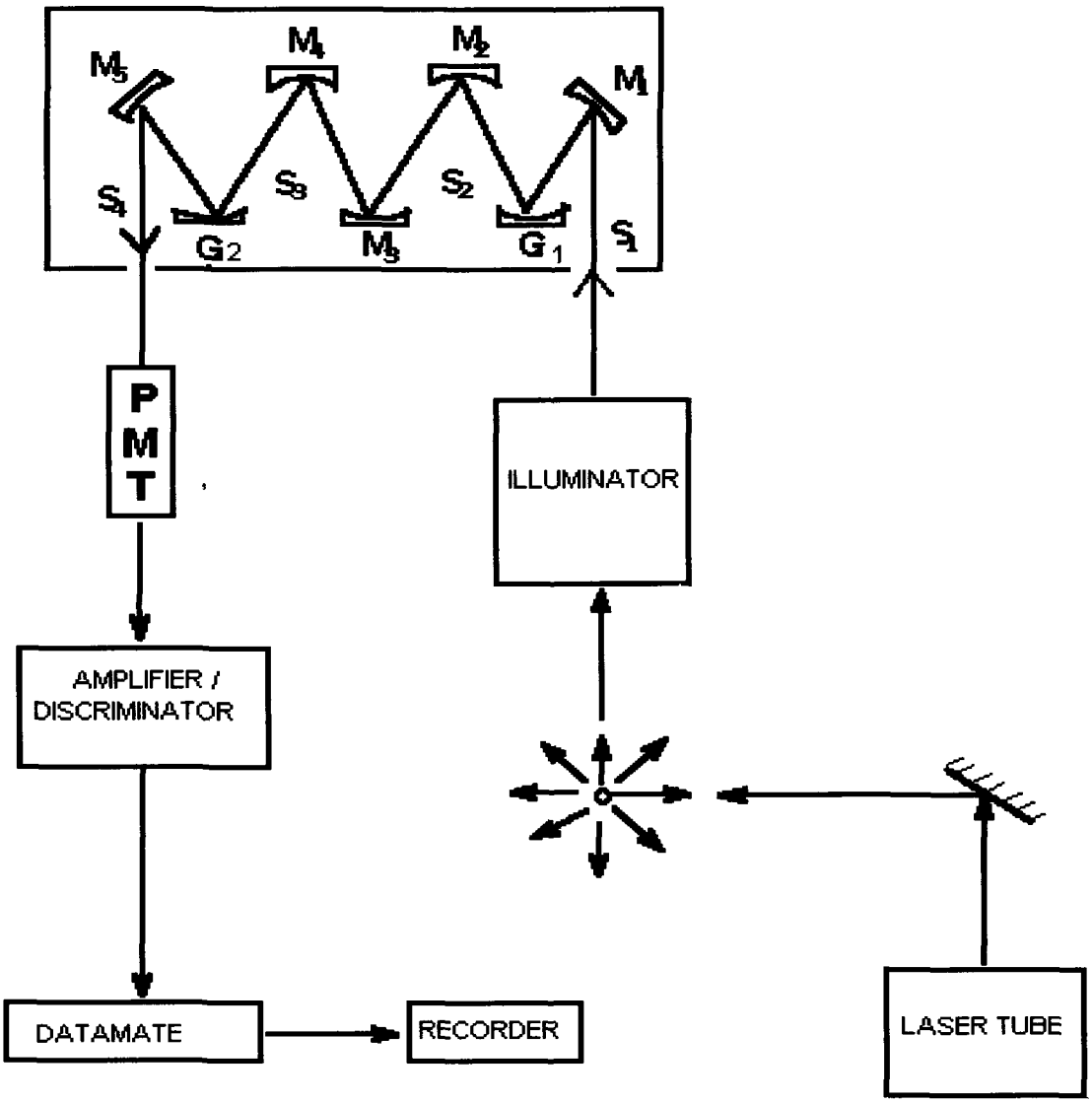

Fig. 3.1: Block diagram of a Raman instrument used in recording spectra

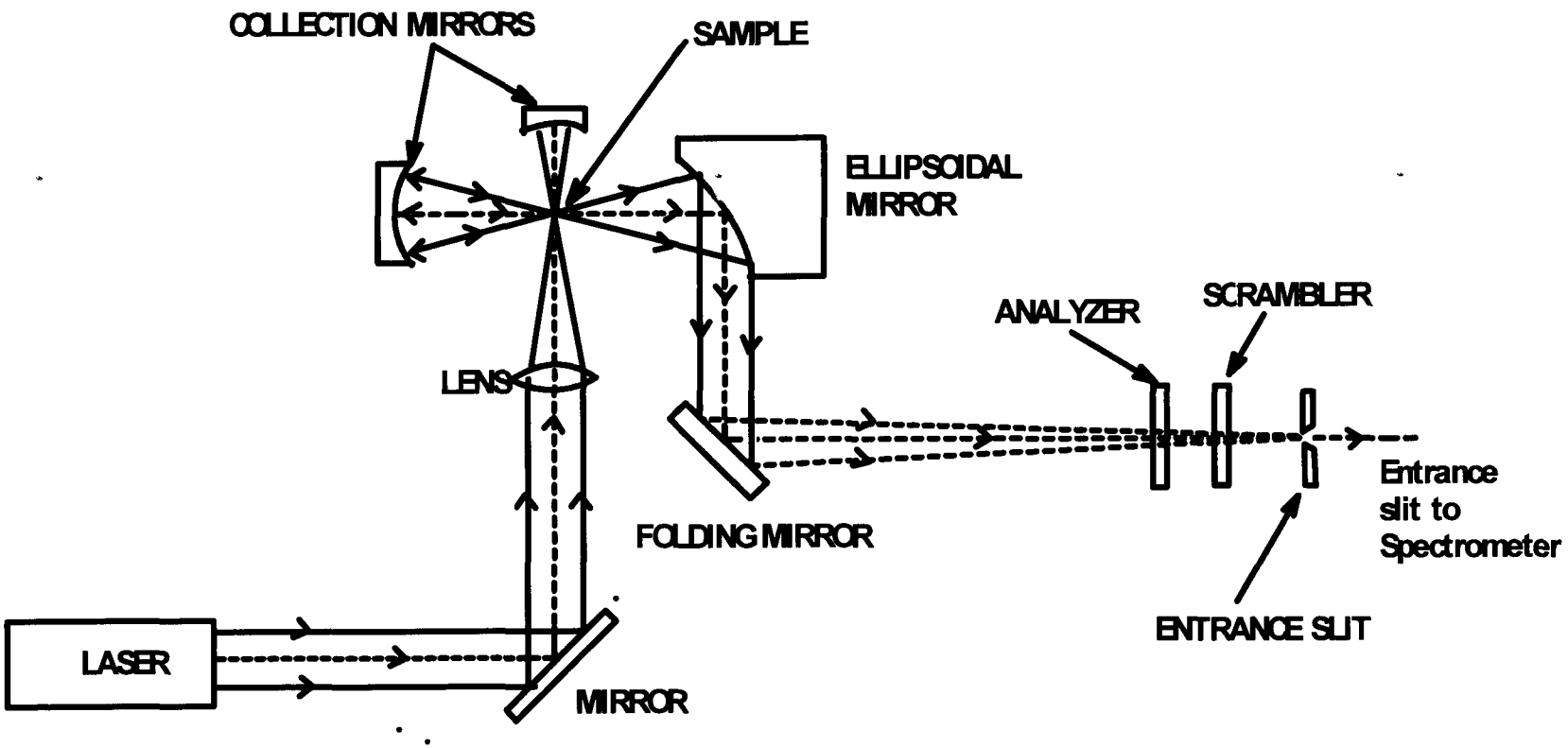

Fig. 3.2: Optical diagram of the light-collecting system of a Raman instrument

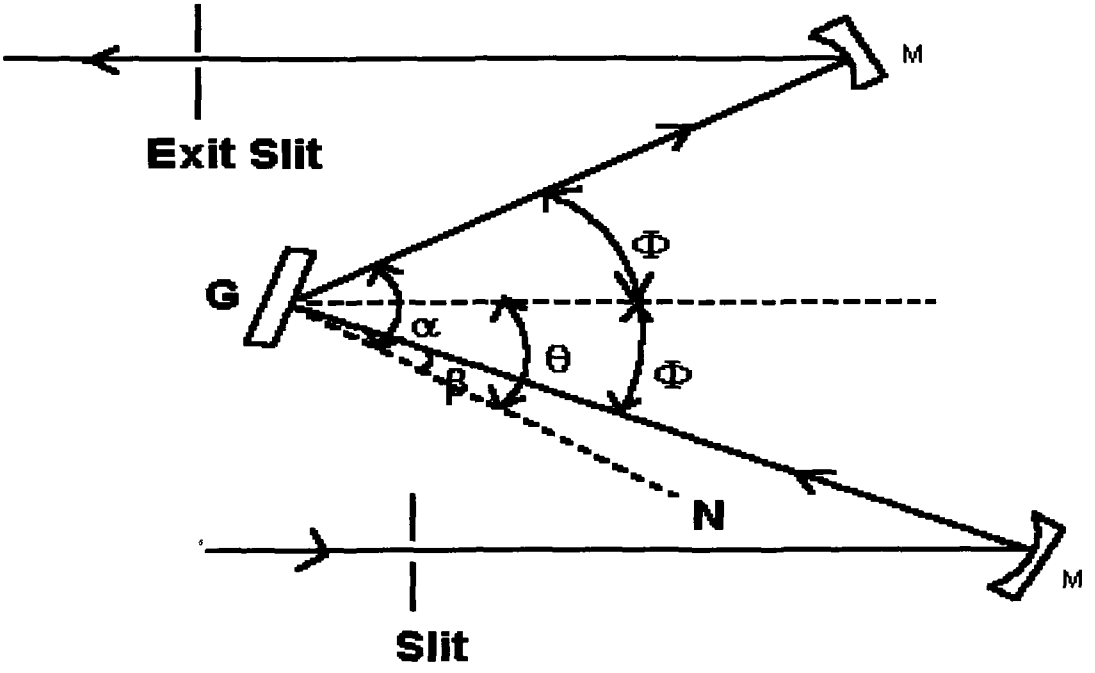

Fig. 3.3: Diagram showing the Czerny-Turner mount of gratings.

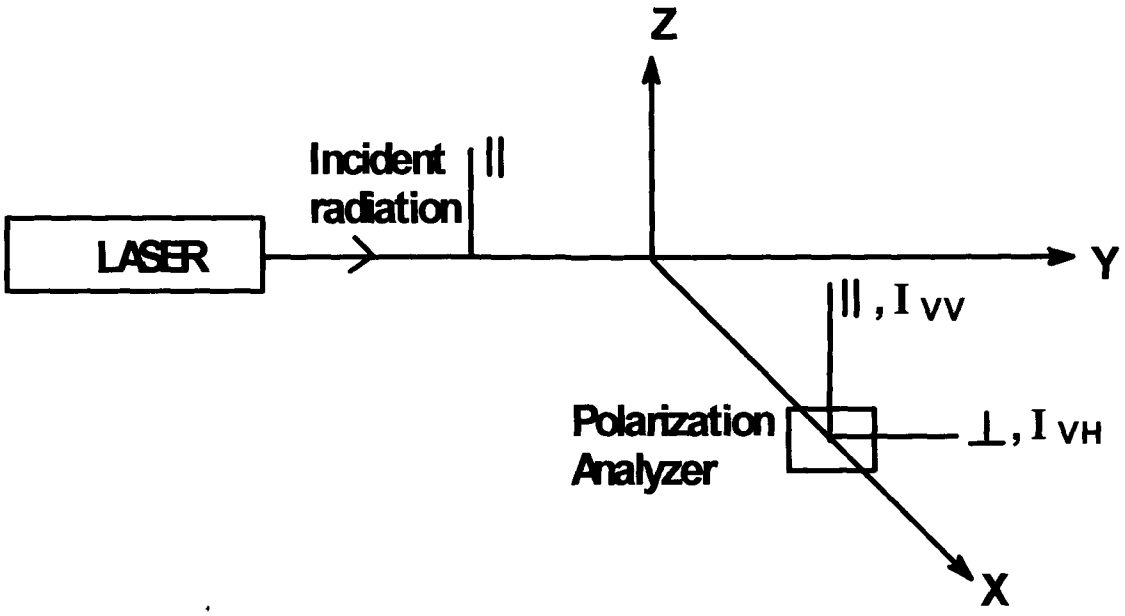

Fig. 3.4: Optical diagram showing the two Raman components I_{VV} and I_{VH} of scattered intensity.

CHAPTER 4

CHAPTER 4

NON-COINCIDENCE EFFECT IN METHYL ETHYL KETONE: A SOLVENT DEPENDENT RAMAN STUDY

4.1. INTRODUCTION

The analysis of the isotropic and anisotropic profiles of a Raman band can provide much information on the molecular dynamics and vibrational relaxation of molecular liquids [1–8]. The frequency difference observed between the isotropic and anisotropic components of a Raman band is due to the non-coincidence effect (NCE) and is known as anisotropy shift [9-11]. The spherically symmetric and asymmetric forces play significant role in determining the band shape of isotropic and anisotropic components respectively. The non-coincidence between the peak wavenumbers of isotropic and anisotropic components has always been considered an efficacious probe of the structure and dynamics of liquid systems. The dependence of NCE on local environment in liquids or solutions has allowed improved

understanding of microscopic structural order of the system under investigation.

The origin of NCE in liquids is mainly due to orientationally dependent intermolecular forces. The intermolecular forces change the oscillator force constant and hence modulate the vibration of a symmetric mode. The NCE is commonly associated with the Raman bands of polar molecules that are strongly infrared (IR) active [12-13], although this phenomenon has been observed in IR inactive [3,14] and in collision induced IR activated modes [15] of non-polar molecules as well. For IR active modes possessing transition dipole moment such as C=O stretching mode of carbonyl containing molecules, the NCE is attributed to a resonant transfer of vibrational energy via transition dipole coupling (TDC) occurring in the presence of short-range orientational order [9-11]. Several theoretical models have been proposed for the explanation of NCE, notably by Fini and co-workers [9-11,16], Wang and McHale [17-18], Döge et al [2,3] and Logan [19-21]. The theory proposed by Wang and McHale takes into account several mechanisms such as hydrogen bonding, quadrupole-quadrupole coupling, dipole-dipole coupling and transition dipole - transition dipole interactions. Logan's approach assumes NCE to be the result of resonant excitonic transfer of vibrational excitation between the same normal modes of different solute molecules. Fini and co-workers [9-

11,16] hypothesized that the NCE is the result of microscopic local ordering of the liquid phase, owing to the strong interaction between permanent dipoles which permits vibrational coupling through neighboring transition dipoles. The neighboring molecules are oriented and form aggregates with a lifetime longer than the vibrational period. Torii and Tasumi [22-24] performed model calculations on the NCE, based on microscopic liquid structures obtained by Monte Carlo simulations and the TDC mechanism. The good agreement of the simulation with the experimental results showed not only that the TDC is a dominant mechanism responsible for the non-coincidence of the isotropic and anisotropic components of Raman bands with a transition dipole moment, but also the short-range order in a liquid induced by the molecular interactions is important in determining the sign and magnitude of the non-coincidence. The effect of intramolecular coupling can be separated from intermolecular contributions of the coupling between the C=O modes of neighbouring molecules by dilution with suitable solvents [25].

The NCE can unambiguously provide valuable information about coupling mechanisms of short-range orientational order in liquids which arise from the inter- and intramolecular interactions in dense fluid phase. In many cases the vibrational coupling that gives rise to the NCE is determined by the transition dipole coupling mechanism and

hence sensitive to distance and relative orientation of the interacting molecules [26]. The NCE varies with the concentration of active substance in a manner, which depends upon the static dielectric constant of the solute and solvent. Although few studies have been carried out in ketones exhibiting NCE ,this important class of molecular liquids with strong interactions has not been subjected to investigation from the point of view of vibrational relaxation in a detailed manner. The present study deals with the study of the solute-solvent interactions with Methyl Ethyl Ketone (MEK) as a solute in various solvents of varying dielectric constants, dipole moments etc. The NCE for C=O stretching vibrational mode of MEK was first reported by Scheibe [8]. However ,a detailed analysis is required on this interesting molecule therefore the present study was undertaken .We present a quantitative analysis of the anisotropy shift and interpret the experimental results on NCE in terms of coupling between vibrations of neighboring molecules having strongly polar bonds. It is reported by Das and Kumar [27] that the repulsive type of intermolecular forces play a vital role in determining the band shape of the molecular systems undergoing intermolecular interactions.

MEK is a molecule with wide range of industrial applications. This molecule is free from hydrogen bonding in neat liquid and has a high dielectric constant and dipole moment. The C=O stretching mode of

MEK molecule is chosen for study as the intramolecular coupling of this mode of vibration to other internal vibrations is less probable since it is well isolated from other vibrational transitions .Further, the dipole moment of MEK is expected to be totally concentrated on the C=O bond of the molecule.

4.2. EXPERIMENTAL

Raman spectral measurements for the totally symmetric C=O stretching band were made for MEK in various solvents (CH_3CN, CCl_4, $CHCl_3$, C_6H_6, $CH_3C_6H_5$ and C_6H_5Cl) as a function of solvent concentration (v/v). The spectra were recorded in the frequency region 1600-1800 cm^{-1} approximately for each Raman band. All the compounds were either of spectroscopic grade or extra-pure analytical reagents and were used without further purification. The experiments were performed using a SPEX Ramalog 1403 double monochromator and a photon counting arrangement. The spectrometer control and data processing were achieved with the help of a datamate using DM-3000 software. Laser radiation of 4880 Å from the Spectra Physics Model 165 Ar^+ Laser was used as the excitation source. The experiments were carried out with a maximum power of about 300 mW and the spectral slit width was maintained at ~3 cm^{-1}. The spectra were recorded at 0.5 cm^{-1}/ s scanning rate.

The accuracy of the measurements is believed to be ± 0.5 cm^{-1}. At least five measurements were made for each sample.

To register the I_{VV} and I_{VH} components of the scattered Raman radiations, an analyzer was placed in the path of scattered radiation. A polarization scrambler located just in front of the spectrometer entrance slit was used in all experiments to correct the polarization bias of the double monochromator (grating).

The isotropic and anisotropic components were obtained using the standard formula as described in Chapter 2:

$$I_{iso}(\nu) = I_{VV}(\nu) - \frac{4}{3} I_{VH}(\nu) \qquad (4.1)$$

$$I_{aniso}(\nu) = I_{VH}(\nu) \qquad (4.2)$$

where $I_{VV}(\nu)$ and $I_{VH}(\nu)$ are the polarized and depolarized Raman spectra respectively and ν is the wave number in cm^{-1}.

4.3. RESULTS AND DISCUSSION

If a vibrational mode of an active oscillator interacts with the same mode of the identical molecule, this is called resonant intermolecular vibrational coupling.

The isotropic profile of Raman band reflects the spherically symmetric average of the interaction potential whereas the anisotropic profile reflects the angular dependence of the interaction potential. The different dependencies of the isotropic and anisotropic profiles will lead to different line shapes and also shifts to different extents leading to a splitting given by:

$$\delta \nu = \nu_{aniso} - \nu_{iso} \qquad (4.3)$$

The magnitude of splitting in equation (4.3) depends on the liquid structure and on the relative orientation of the neighboring molecules. The NCE is generally small compared to the isotropic and anisotropic band widths. The MEK molecule shows an anisotropy shift, $\delta\nu$, of about 7 cm^{-1} in neat liquid (Fig. 4.1). The Raman spectra of MEK in various solvents at 10%, 50% and 90% solvent concentration is shown in figure 4.2. The anisotropy shift decreases as the solvent concentration increases irrespective of the nature of the solvent (Fig. 4.3). The anisotropy shift is a result of resonant energy transfer mechanism through transition dipole coupling where the microscopic local order in liquid phase permits the coupling between the vibrational states of the solute molecules through neighbouring transition dipoles. The pair interaction between the solute molecules is considered to lead to the local ordering in liquids, which gives rise to in-phase (isotropic) and out-of-phase (anisotropic) type of vibrations. Therefore, anisotropy shift

is pronounced in neat liquid and is suppressed by dilution of the active oscillator.

According to Logan's hypothesis of a resonant coupling interaction [19-21], the separation between isotropic and anisotropic maxima in different solvents also varies with concentration of the active substance and NCE values in all molecules decreases with isotopic dilution. It has been shown by Logan that the presence of NCE and its general vanishing on isotopic dilution indicates the presence of a resonant coupling due to transition dipole – transition dipole (TD-TD) interactions [21].

Let us consider the dipole-dipole coupling to be responsible for the interaction leading to orientational order between the molecules of MEK. The coupling potential V, which arises due to TD-TD interaction of two adjacent molecules can be expanded in Taylor series as a function of normal co-ordinate Q

$$V_i = V_o^1 + \left(\frac{\delta V_i}{\delta Q_i}\right)_0 Q_i + \frac{1}{2}\left(\frac{\delta^2 V}{\delta Q_i^2}\right)_0 Q_i^2 + \frac{1}{2}\sum_{ij}\left(\frac{\delta^2 V}{\delta Q_i \delta Q_j}\right)_0 Q_i Q_j + \cdots\cdots \quad (4.4)$$

The first three terms are similar to the potential of a harmonic oscillator corresponding to a normal coordinate Q_i.

If the coupling potential V is given by

$$V = \left(\frac{\mu_i \mu_j}{R_{ij}^3} \right) K_{ij} \qquad (4.5)$$

where R_{ij} is the distance between the two dipoles and K_{ij} is the geometric factor describing the relative orientation of the two dipole moments μ_i and μ_j.

The first order perturbation calculation between the ground state and first excited state leads to the following expression for the transition dipole-transition dipole (TD-TD)interactions :

$$\Delta E_{TD-TD} = \left(\frac{\delta \mu}{\delta Q} \right)^2 \left\langle \frac{K_{ij}}{R_{ij}^3} \right\rangle \left(< 1 | Q | 0 > \right)^2 \qquad (4.6)$$

The brackets indicate an ensemble average for different relative orientations where the anisotropic component of the band is shifted in various degrees depending on the magnitude of the orientational factor K_{ij}.

At infinite dilution, the splitting factor reduces to zero i.e. the isotropic and anisotropic Raman components tend to coincide.

The quantity $\left\langle \frac{K_{ij}}{R_{ij}^3} \right\rangle$ is difficult to calculate hence only proportionality factor may be considered here

$$\delta \nu \infty \left(\frac{\delta \mu}{\delta Q} \right)^2 \qquad (4.7)$$

The quantity $\left(\frac{\delta \mu}{\delta Q}\right)^2$ is proportional to the infrared absorption coefficient for a given vibration, hence, the Raman bands corresponding to the strong IR absorption exhibit the non-coincidence effect.

The assumption that the anisotropy shift is an effect due to resonance coupling can be confirmed experimentally by the fact that in all solutions, this effect vanishes at high dilution, whatever the solvent. The maximum shift decreases with decreasing polarity of the solvent, and so may be a measure of the strength of the potential field perturbing the vibration, when there are only solvent molecules in the neighborhood. Besides polarity, this potential field is dependent on other properties of the solvent, as for example, bond polarities or formation of hydrogen bond.

While the value of the anisotropy shift in high dilution seems to be mainly a function of the molecular and liquid properties of the solvents, the concentration dependence is likely to be determined by the properties of the mixture. The results of the variations of the peak frequencies of the C=O stretching mode of MEK are shown as a function of concentration of CH_3CN, CCl_4, $CHCl_3$, C_6H_6, $CH_3C_6H_5$ and C_6H_5Cl solvents (Fig. 4.3). The anisotropy shift decreases as the solvent concentration increases irrespective of the nature of the solvent. The

experimental results for the mixtures studied can be summarized as follows:

MEK - CH_3CN system:

In CH_3CN, the maximum frequency of isotropic component increases linearly compared to the pure liquid, whereas the anisotropic maximum decreases linearly. The NCE in this case vanishes at 80% concentration of CH_3CN as the pair interaction among the solute weakens due to relatively high dipole moment of CH_3CN and subsequently pair breaking occurs. CH_3CN being a polar solvent is able to almost substitute for the MEK molecule.

MEK - $CHCl_3$ system:

On dilution with $CHCl_3$, the isotropic maximum is almost constant with tendency to shift towards higher wavenumber. The anisotropic maximum frequency on the other hand decreases with dilution. In $CHCl_3$ there is a possibility of formation of hydrogen bonding with the C=O group of MEK. This leads to a very large shift relative to gas frequency and compared with the pure liquid even to a shift into the direction of lower wavenumber, through the effect of decoupling would lead to a shift in the opposite direction [8]. The NCE in $CHCl_3$ decreases very slowly which shows that the effect of resonant transfer of

vibrational energy due to TD-TD interaction on the band shape is removed only at very high solvent concentration (beyond 90% $CHCl_3$). The properties of the mixture MEK/$CHCl_3$ indicate strong interaction between solvent and solute molecule [8].

MEK - CCl_4 system:

In this system, the shift of the maxima of isotropic and anisotropic components compared with pure liquid is rather strong from the beginning of dilution. But the curve of the concentration dependent maximum shift is not linear. The isotropic maximum frequency shifts to higher wavenumber whereas the anisotropic maximum remains constant upto ~ 60% of CCl_4 and thereafter increases slowly. This is perhaps due to the resonant decoupling. The properties of mixture indicate strong interaction with each other . The NCE is found to vanish at ~90% concentration of CCl_4.

MEK - C_6H_6, $C_6H_5CH_3$ and C_6H_5Cl systems:

The peak frequency behavior of C=O stretching band in these three aromatic solvents is very similar. There is an increase of isotropic maximum frequency towards the higher wavenumbers whereas the anisotropic maximum remains almost same throughout the range of solvent concentration.

Starting from the hypothesis that the NCE is related, atleast to a first approximation, to the interaction between permanent dipoles of the dissolved molecules and making the supplementary assumption of a coupling mechanism through transition dipoles, McHale [17] derived theoretically the following expression:

$$\delta\nu = \frac{2\mu^2\left(\frac{\delta\mu}{\delta Q}\right)^2}{25\pi^2 c^2 \nu_0 kTd^3}\frac{N_0}{V_M}\phi\ S \qquad (4.8)$$

where N_0 is Avogadro's number , φ is the volume fraction of the solute, ν_0 is the vibrational frequency of the isolated molecule, d is the maximum intermolecular distance, V_M is the molar volume of the solute, kT is the thermal energy, μ is the dipole moment, Q is the normal coordinate of vibrational mode under consideration and $\frac{\delta\mu}{\delta Q}$ is the transition moment. S is the screening factor which comprises of two factors S_p and S_t related to the interaction of permanent and transition dipoles respectively and is given by the Onsager-Fröhlich model as

$$S_P = \left(\frac{n^2+2}{2\varepsilon+n^2}\right)^2 \varepsilon$$

and

$$S_t = ([(n^2 + 2) / (2\ \epsilon_\infty + n^2)]^2\ \epsilon_\infty$$

where n is the refractive index of the solute, ϵ is the static dielectric constant of the medium and ϵ_∞ is the dielectric constant at infinite frequency. In pure liquids S_t takes the form

$$S_t = \frac{\left(n^2+2\right)^2}{9n^2}$$

which has a almost constant value 0.89 for $1.30 < n < 1.50$.

Following the Onsager-Fröhlich model, which treats the dielectric as continuum, equation (4.8) takes the form

$$\delta\nu\left(2\varepsilon+n^2\right)^2\varepsilon^{-1} = \frac{2\mu^2\left(\frac{\delta\mu}{\delta Q}\right)^2\left[n^2+2\right]^2 N_0}{25\pi^2c^2\nu_0 kTd^3V_M}\phi \qquad (4.9)$$

In order to understand the dependence of NCE on the molecular properties and solution dynamics, the function $F = \delta\nu\,(2\epsilon + n^2)^2\,\epsilon^{-1}$ was plotted against volume fraction (φ) of the solute (Fig. 4.4). The dielectric constants of the solution was calculated using the relationship

$$\epsilon_{solution} = \varphi\,\epsilon_{solute} + (1-\varphi)\,\epsilon_{solvent} \qquad (4.10)$$

The dielectric constants of all the compounds were obtained from literature [28]. The molecular parameters for the solute and solvents are shown in table 4.1.

The plots of F vs. φ are shown in Fig 4.4. A close examination of the plots reveals that the data points cannot be fitted in a line. They would rather fit well in two straight lines. There is clear discontinuity

between 50% to 60% of solute concentration for all solvents except CH_3CN. Owing to several approximations involved in the Onsager-Fröhlich model, it is expected that the validity of equation (4.9) may be limited only to dilute solutions. Below 50% solvent concentration, the interactions were expected to occur more among solute molecules than among solute and solvent molecules. This study indicates that in these solvents, the discreteness of the medium exists where the effects of dispersion interaction, multipolar interaction, etc. are likely to vary from solvent to solvent and the screening factor may not be as effective as sighted by the Onsager-Fröhlich model. The dielectric continuum theory may explain the MEK-CH_3CN system. For all other solvents under study, the observation reveals that the Onsager-Fröhlich dielectric continuum model based upon the transition dipole coupling mechanism does not hold good. At the most it may be expected to be valid only for dilute solutions. The theories which use the continuum approach for the environment of molecules may not be applicable as such. However, the change observed in anisotropy shift with composition is in agreement with the assumption that the interaction energy of the permanent dipoles of the dissolved molecules is described quantitatively by the dielectric model of Onsager-Fröhlich. The observations of discontinuity in MEK is similar to that found in p-methyl acetophenone and benzaldehyde molecules [27,29]. The

discontinuity may be attributed to as being due to structure breaking effects and local fluctuations [30,31] in liquid solutions. The competitive short-range repulsive forces and the long-range attractions among the molecules invoke chaos in this region when the solute and solvent concentrations become comparable. The variation of chemical composition of the solvation shell surrounding the active molecule gives rise to local fluctuations. The pair interaction gives rise to local orientational order because of dipole-dipole interactions in identical molecules. On dilution with solvents, this order tends to break. This reduction in the structural order due to the effect of solvent is the structure breaking effect [31].

The plot of F vs. φ is linear without any break in case of CH_3CN solvent and it may be explained for CH_3CN solvent on the basis of dipole-dipole interactions. The interactions are expected to be stronger among solute-solvent molecules due to the high dipole moment of CH_3CN. Therefore, at relatively low CH_3CN concentration the pair interaction among the solute molecules weakens and subsequently the pair breaking occurs. As a resulting of breaking of the pair the NCE vanishes, thus leading to a dielectric continuum.

For all other solvents showing a discontinuity in the plot of F vs. φ (Fig. 4.4) the graphs may be described by the non-linear relationship [29] as

$$F(\varphi) = x\,(\varphi - \varphi_o)\,F_1(\varphi) + F_2(\varphi)\,x\,(\varphi - \varphi_o) \qquad (4.11)$$

where φ_o is the concentration of solute at which F vs. φ shows a discontinuity.

The concentration dependence of shift may be due to several interactions such as dipole-dipole, dipole-quadrupole, quadrupole-quadrupole and higher multipole interactions in the solute-solvent systems. In these systems, discreteness of the medium also exists. The effect of dispersion force and various multipolar interactions are likely to vary from solvent to solvent. Hence it is clear that the dielectric screening may not be as effective as envisaged by the Onsager-Fröhlich model in such systems.

A quantity *ln* F has been shown to be useful [27,29] for plotting the data points. We have plotted *ln* F against solute concentration (φ) and it is a clear linear plot (Fig. 4.5). Thus, it further supports the earlier findings [27,29] that *ln* F is a better parameter than F for explaining the variation of $\delta\nu$ against φ.

The data points for F may thus be fitted into an exponential curve as shown in figure 4.6. The fitting of the data to exponential curves indicates that an exponential factor is coming into play, which may be due to the presence of repulsive forces. By considering the molecular interactions as hard sphere interaction model, it may be inferred that the repulsive potential function of the type $e^{-\alpha R}$ (where R is the

appropriate distance of closest approach and α is a constant) from an exponential-6 van der Waals' potential [32] is playing a dominant role, in most of the solute-solvent systems. Fluctuations of dipole moments and polarizabilities may arise as a result of concentration fluctuations. The different multipolar interactions which are repulsive in nature may be playing a significant role in such complex molecular systems. This supports earlier observations [27,29] where aromatic molecules were found to exhibit the repulsive type of potential among the molecules. Further, it may be inferred that the same holds for aliphatic molecules as well. In uniform liquids, the net force on a given molecule arising from the long ranged and more slowly varying attractive interaction essentially cancels in most typical configurations leaving only the repulsive correlations. The repulsive potential has been sighted by Morresi *et al.* [33] as due to a steric hindrance, which varies with the number and position of the substituent in the aromatic ring. Similarly, in case of MEK it is possible that due to the presence of CH_3 and C_2H_5 groups the molecules are unable to come closer and form a layered structure. Thus steric effects may also be playing a significant role in contributing towards the repulsive potential in case of aliphatic molecules. The anomalous vibrational frequency shift observed in some solvents for the C=O stretching mode, which has large dipole derivative, the atomic quadrupoles may play role in intermolecular electrostatic

interaction for chlorine containing molecules. It has been seen that large atomic quadrupoles are obtained from chlorine suggesting that atomic quadrupole effects are important for electrostatic interactions around covalently bonded atoms [34]. The C-Cl bond of CCl_4 molecule points to the carbonyl oxygen producing a strong electric field on C=O bond in the direction that the chlorine atoms look as if they had large positive charges. The electron densities inside the chlorine atoms in CCl_4 are found to be highly anisotropic. This anisotropy is considered to be the electronic structural origin of large atomic quadrupoles [34]. It may therefore be inferred that atomic quadrupole effects may also be giving rise to the repulsive forces in these solute-solvent systems besides other intermolecular forces. The dipole-quadrupole interactions, in the benzene and benzene substituted solvents, which are repulsive in nature [27], may not allow the close proximity of solute-solvent molecules. The multipolar interactions may start playing a significant role.

Table 4.1: Molecular parameters for solute and solvents

Molecules	Dielectric constant (ε)	Refractive index (n)
Methyl Ethyl Ketone	18.4	1.379
CH_3CN	37.5	1.341
$CHCl_3$	4.806	1.45
CCl_4	2.24	1.457
C_6H_6	2.28	1.498
$C_6H_5CH_3$	5.708	1.49
C_6H_5Cl	2.379	1.523

REFERENCES

1. Th.G. Devi, A.Das, K.Kumar, Spectrochim. Acta. **60A**, 211 (2004).
2. G. Döge, R. Arndt, J. Yarwood, Mol. Phys. **52**, 399 (1984).
3. G. Döge, D. Schneider, A. Morresi, Mol. Phys. **80**, 525 (1993).
4. E.W. Knapp, S.F. Fischer, J. Chem. Phys. **76**, 4730 (1982).
5. A. Das, R. Das, K. Kumar, Spectrochim. Acta. **58A**, 1583 (2002).
6. V.R. Kalasinsky, T.S. Little, J. Raman Spectrosc. **14**, 253 (1983).
7. T. Bien, G. Döge, J. Raman Spectrosc. **12**, 82 (1982).
8. D. Scheibe, J. Raman Spectrosc. **13**, 103 (1982).
9. G. Fini, P. Mirone, S. Fortunato, J. Chem. Soc., Faraday Trans. 2, **69**, 1243 (1973).
10. G.Fini, P.Mirone, J.Chem.Soc., Faraday Trans. 2,**70**, 1776 (1974).
11. M.G. Giorgini, G. Fini, P. Mirone, J. Chem. Phys. **79**, 639 (1983).
12. T.F. Sun, J.B. Chan, S.N. Wallen, J. Jonas, J. Chem. Phys. **94**, 7486 (1991).
13. V.M. Shelly, J. Yarwood, Chem. Phys. **137**, 277 (1989).
14. D.R. Jones, C.H. Wang, D.H. Christensen, O.F. Nielson, J. Chem. Phys. **64**, 4475 (1976).
15. S.L.Wallen,L.Nikiel,J.Yi,J.Jonas, Chem.Phys.Lett. **229**, 82 (1994).
16. P. Mirone, G. Fini, J. Chem. Phys. **71**, 2241 (1979).
17. J.L. McHale, J. Chem. Phys. **75**, 30 (1981).
18. C.H. Wang and J. McHale, J. Chem. Phys. **72**, 4039 (1980).

19. D.E. Logan, Chem. Phys. **103**, 215 (1986).

20. D.E. Logan Chem. Phys. **131**, 199 (1989).

21. D.E. Logan, Mol. Phys. **58**, 97 (1986).

22. H. Torii, M. Tasumi, J. Chem. Phys. **99**, 8459 (1993).

23. H. Torii, J. Mol. Struct. : THEOCHEM **311**, 199 (1994).

24. H. Torii, J. Phys. Chem. A **103**, 2843 (1999).

25. Y.J. Kim, H.C. Chan, V.S. Sullivan, J. Jonas, J. Chem. Phys, **111**, 9658 (1999).

26. H. Torii, J. Phys Chem. A, **108**, 2103 (2004).

27. A. Das, K. Kumar, J. Raman Spectrosc. **30**, 563 (1999).

28. "Handbook of Chemistry and Physics" Edited by R.C. Weast, **56**th Edition. CRC PRESS, 18901, Cranwood Parkway, Cleveland, Ohio; pp E55-E56 (1975-1976).

29. A. Das, K. Kumar, Spectrochim. Acta. **54A**, 793 (1998).

30. G. Tarjus, S. Bratos, Mol. Phys. **42**, 307 (1981).

31. S. Bratos, G. Tarjus, Phys. Rev. A. **24**, 1591 (1981).

32. M.Karplus and R.N.Porter "Atoms and Molecules: An introduction for Students of Physical Chemistry" Benjamin/Cummings, Mento Park, CA; pp 262-267 (1970).

33. A. Morresi, M. Paolantoni, P. Sassi, R.S. Cataliotti, G. Paliani, J. Phys.: Condens. Matter. **12**, 3631 (2000).

34. H. Torii, J. Chem. Phys. **119**, 2192 (2003).

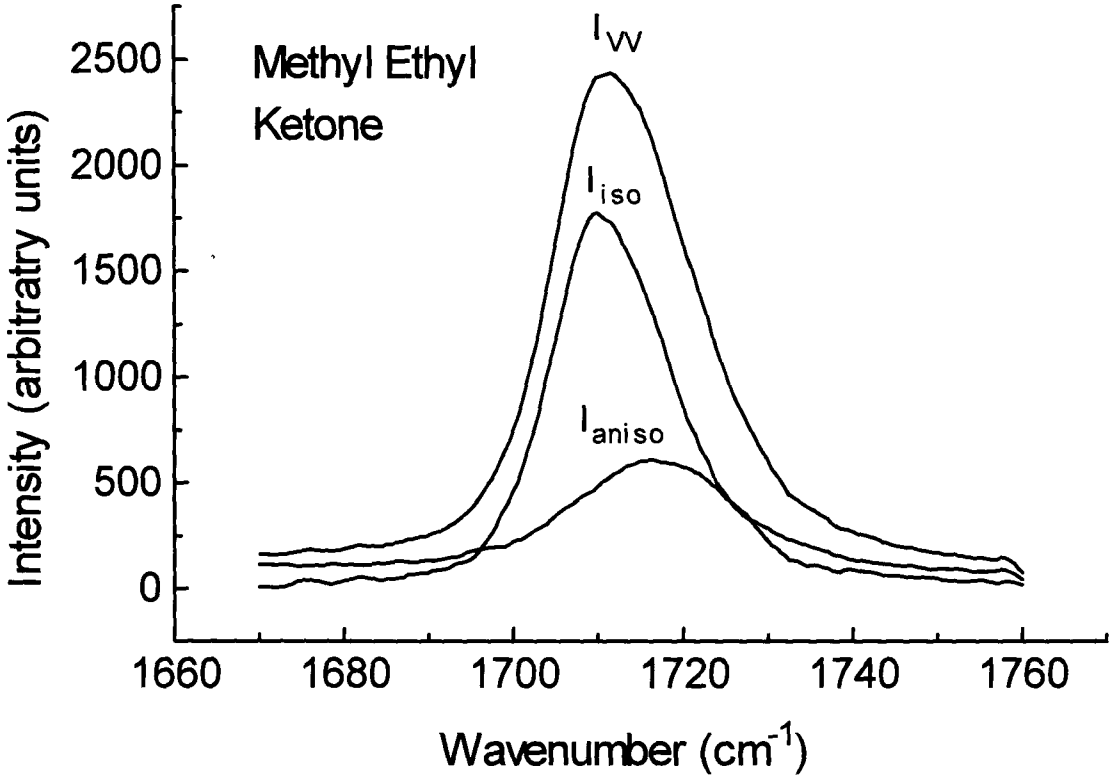

Fig. 4.1: Raman spectrum of neat liquid methyl ethyl ketone (MEK)

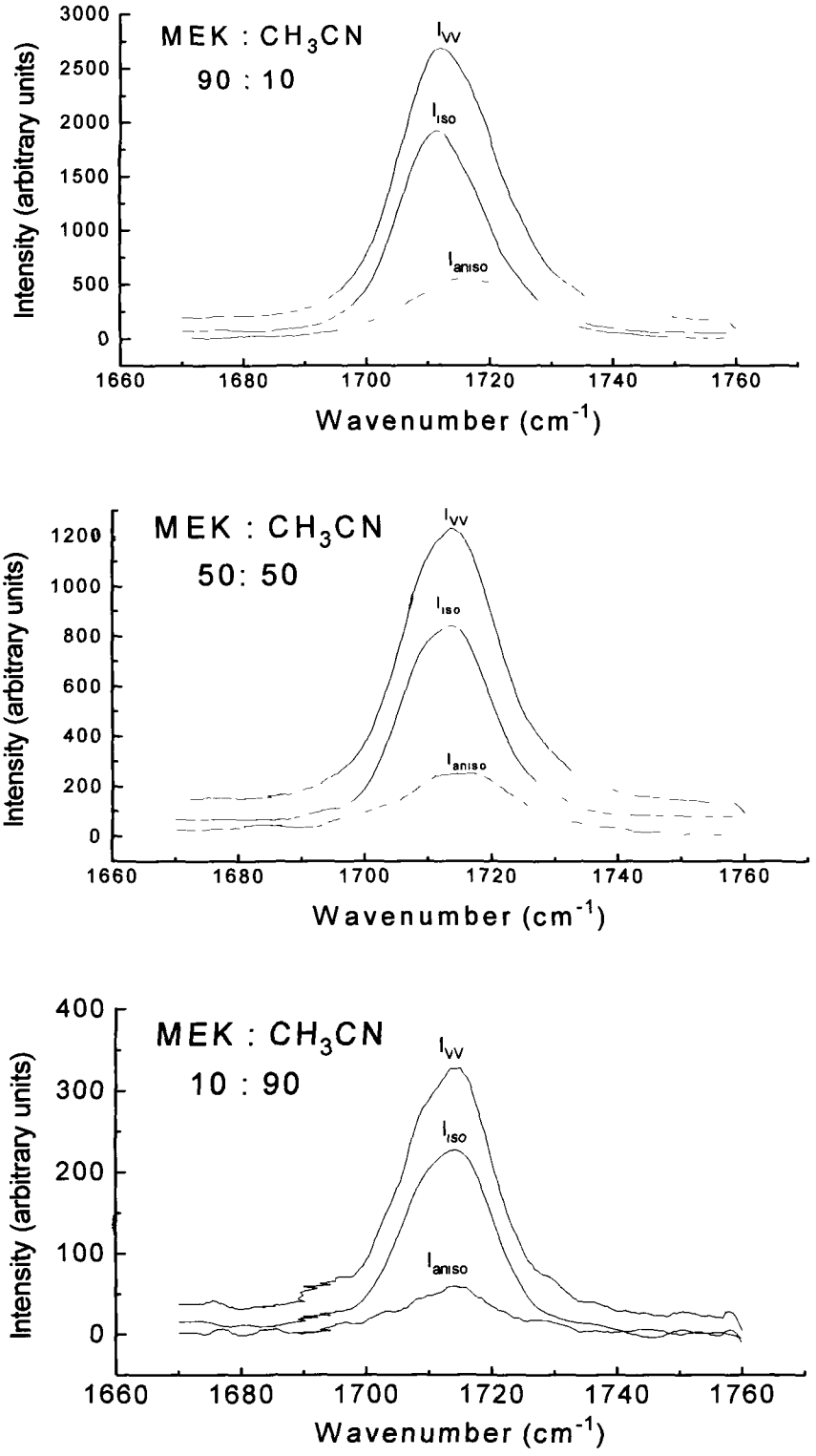

Fig 4.2: Raman spectra of MEK in CH_3CN solvent.

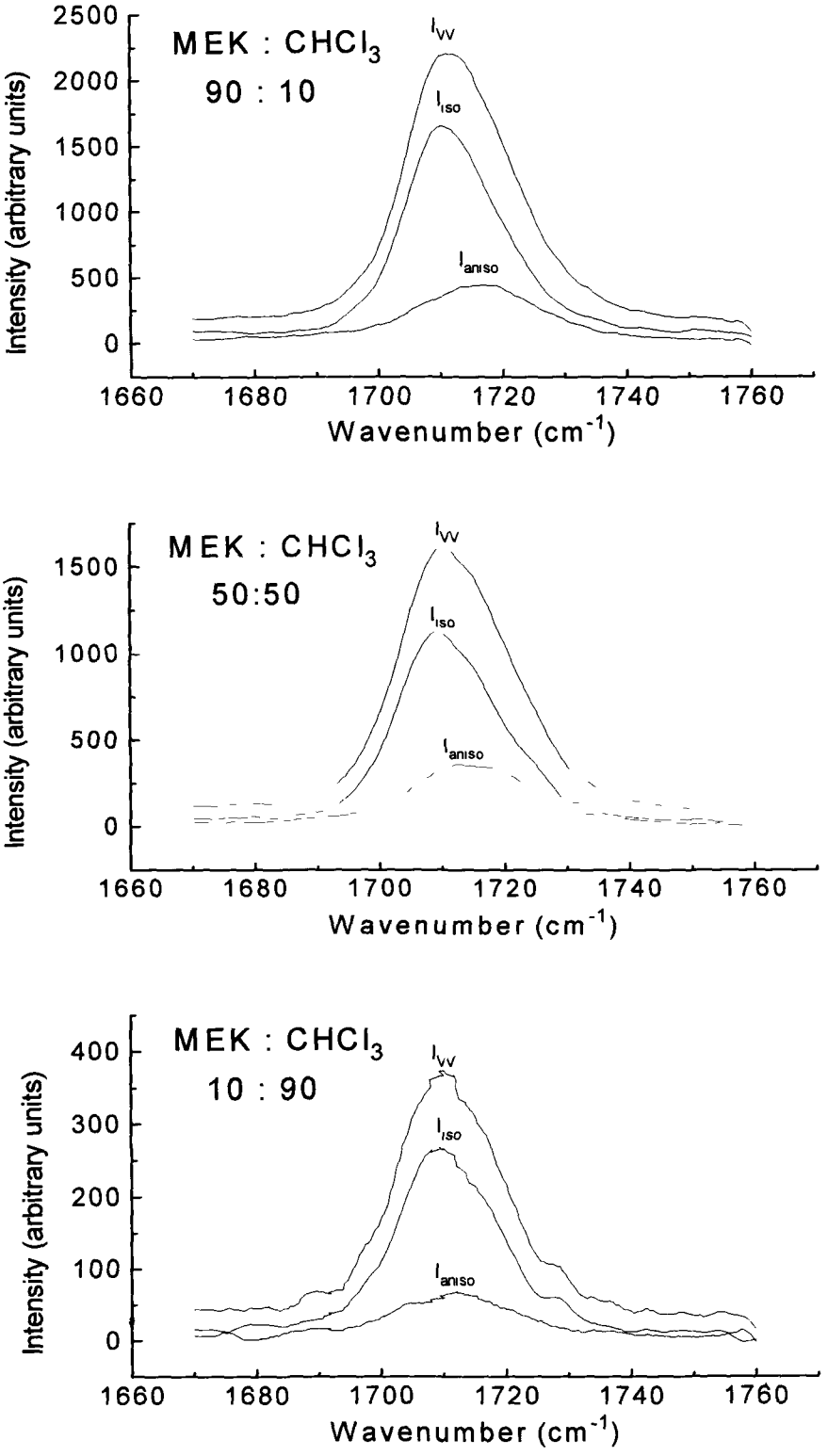

Fig 4.2: Raman spectra of MEK in $CHCl_3$ solvent.

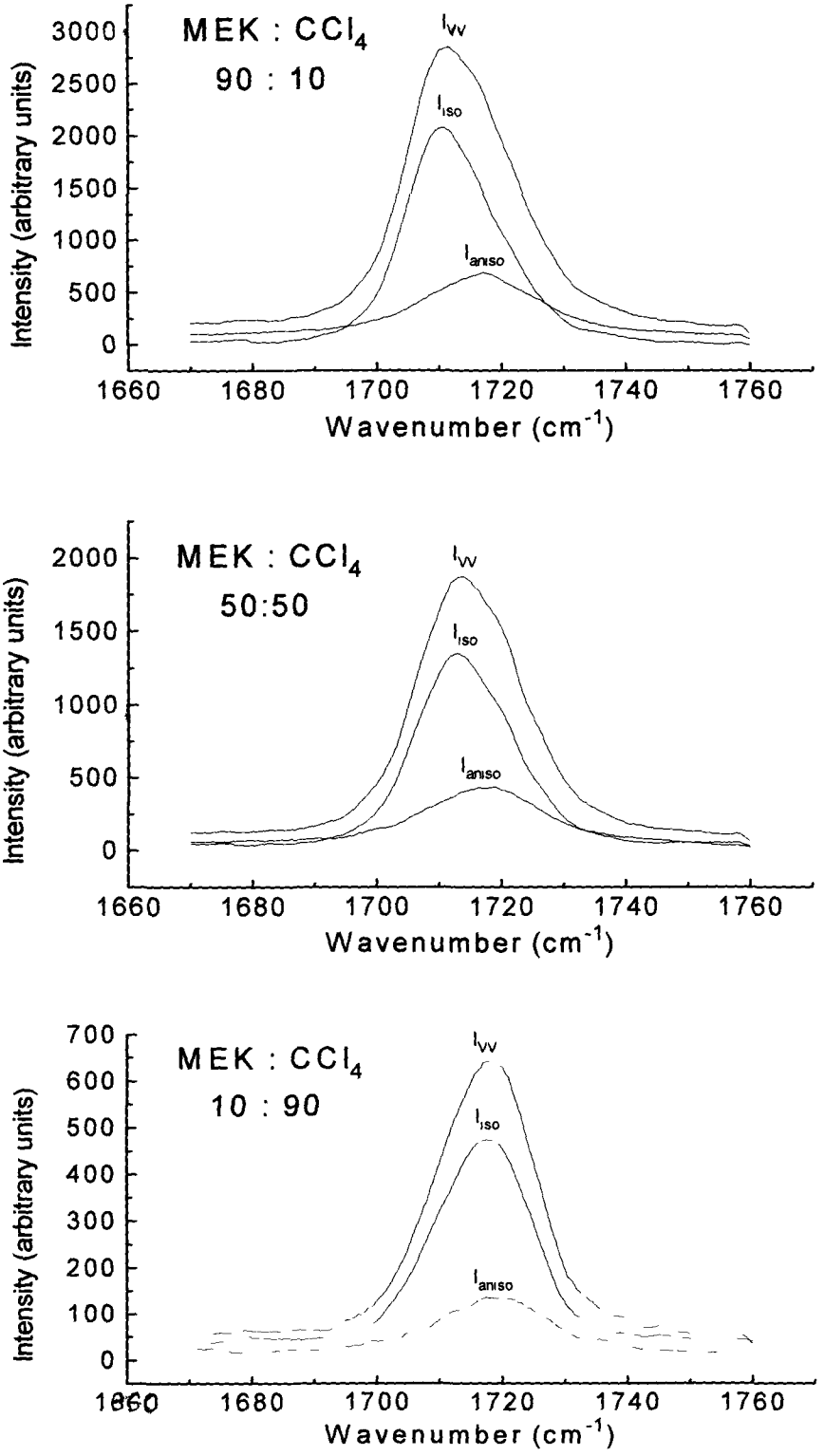

Fig 4.2: Raman spectra of MEK in CCl_4 solvent.

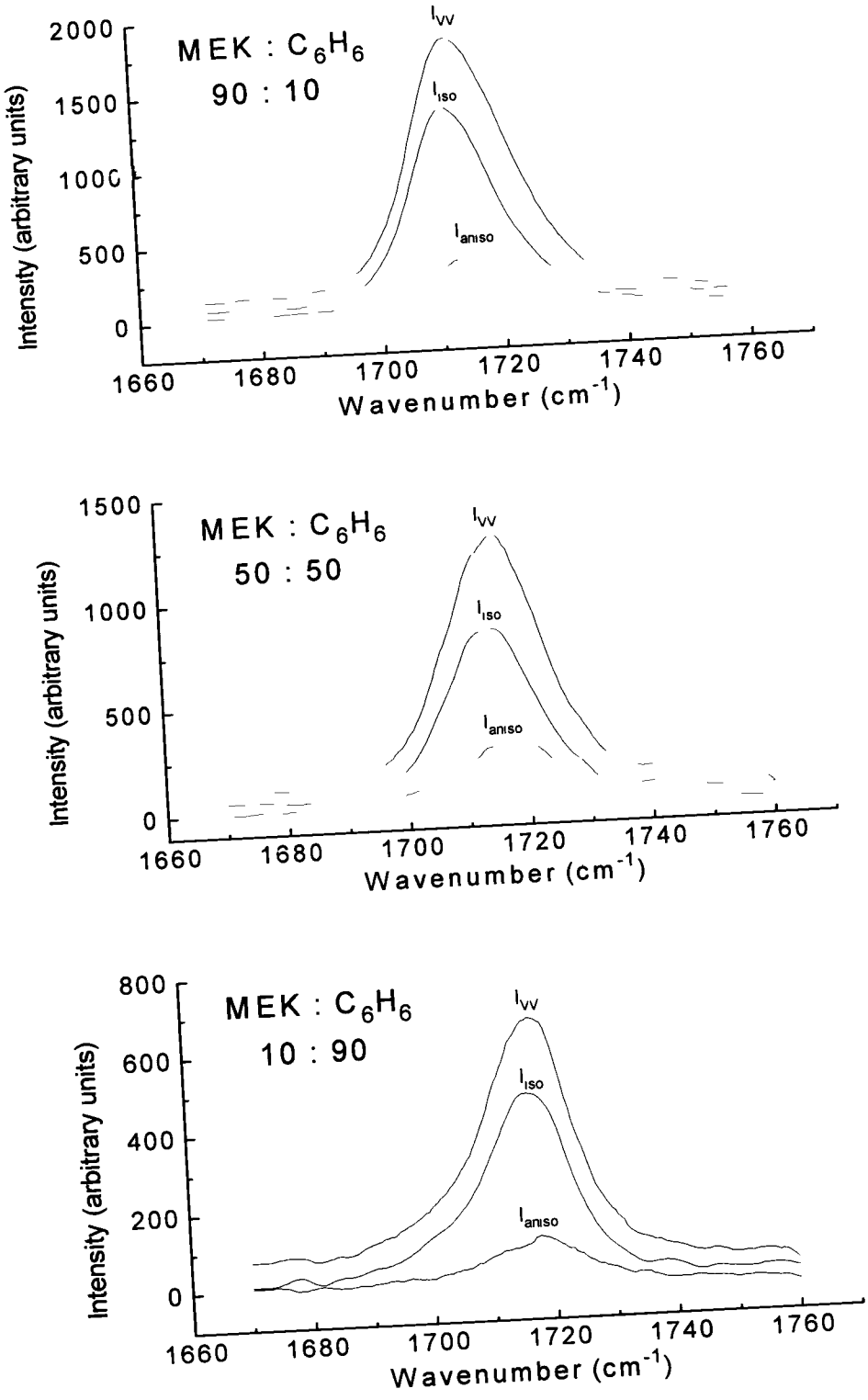

Fig 4.2: Raman spectra of MEK in C_6H_6 solvent.

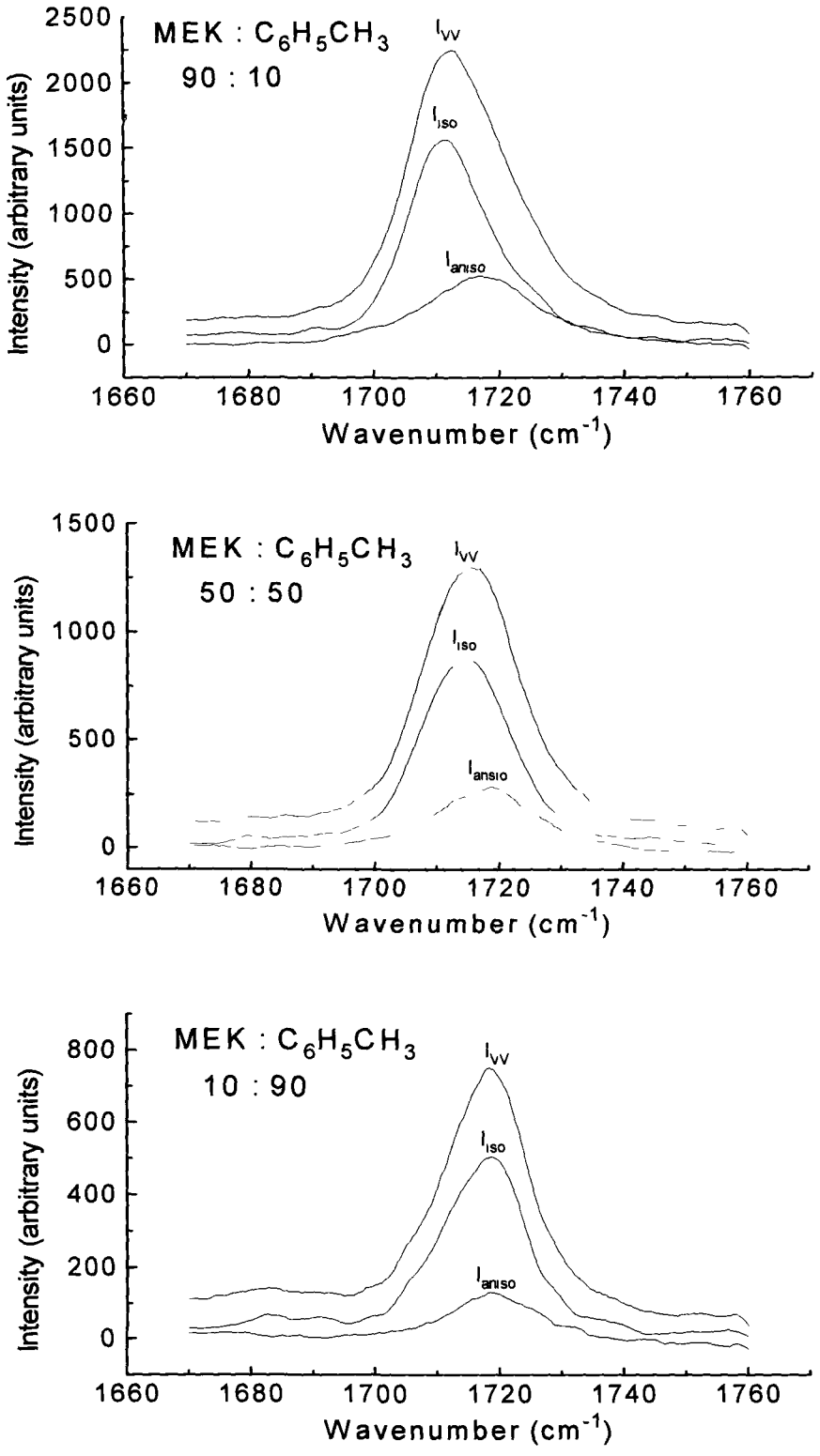

Fig 4.2: Raman spectra of MEK in $C_6H_5CH_3$ solvent.

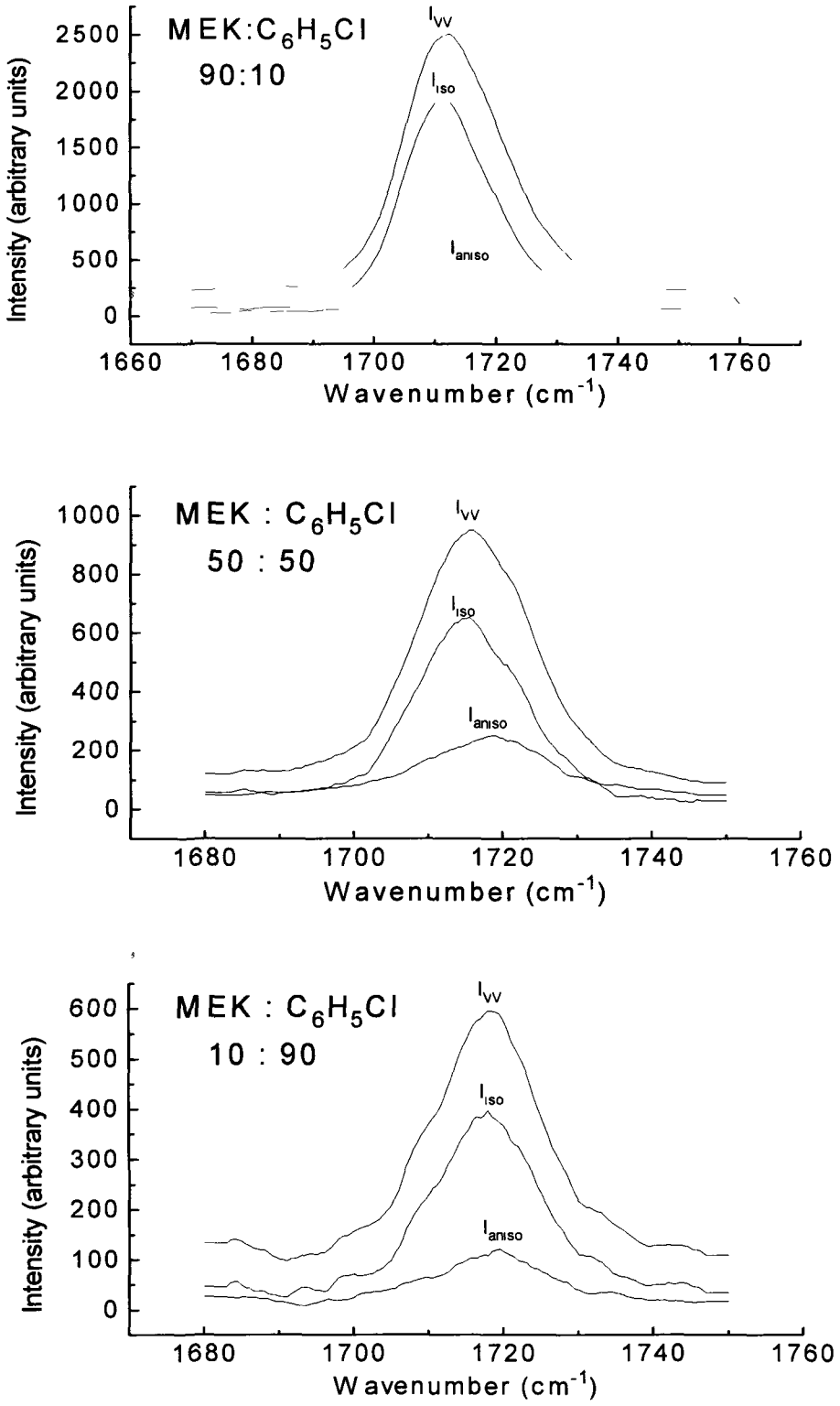

Fig 4.2: Raman spectra of MEK in C_6H_5Cl solvent.

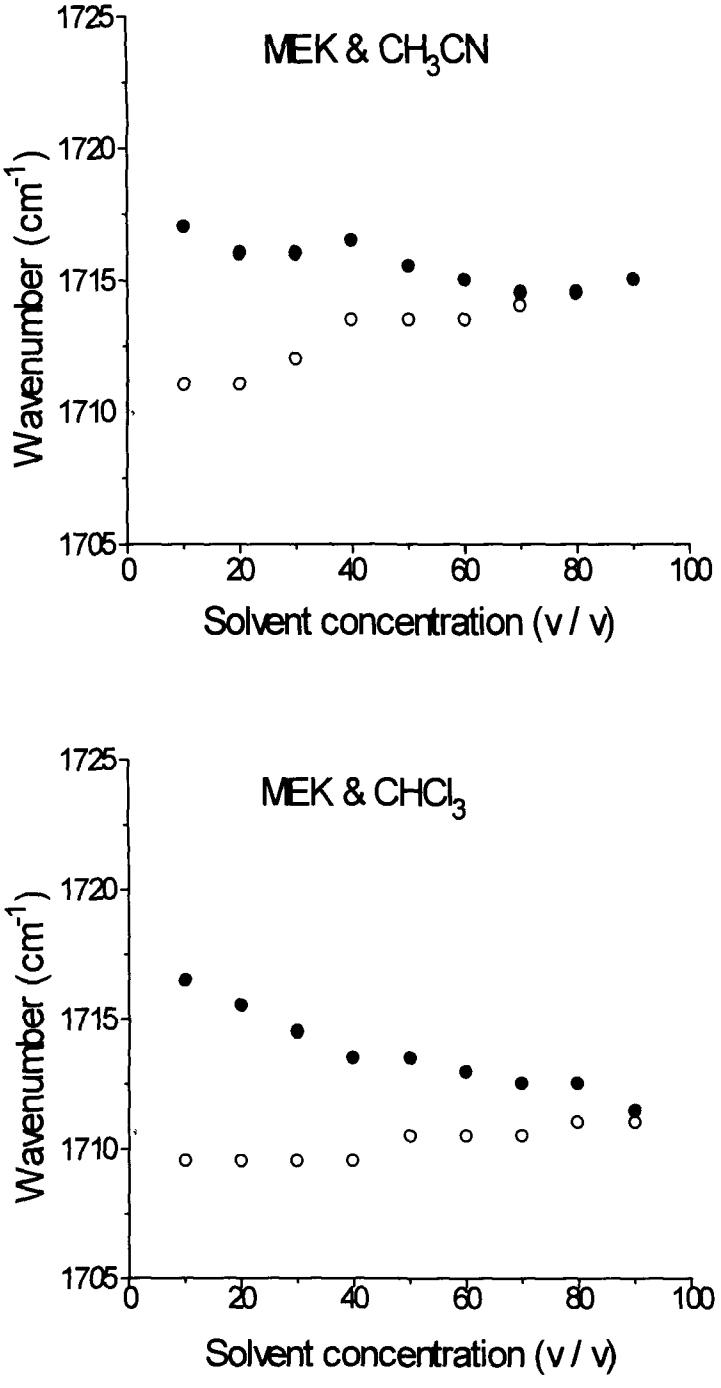

Fig. 4.3: Variation of peak frequencies of isotropic (o) and anisotropic (•) components as a function of concentration in CH_3CN and $CHCl_3$

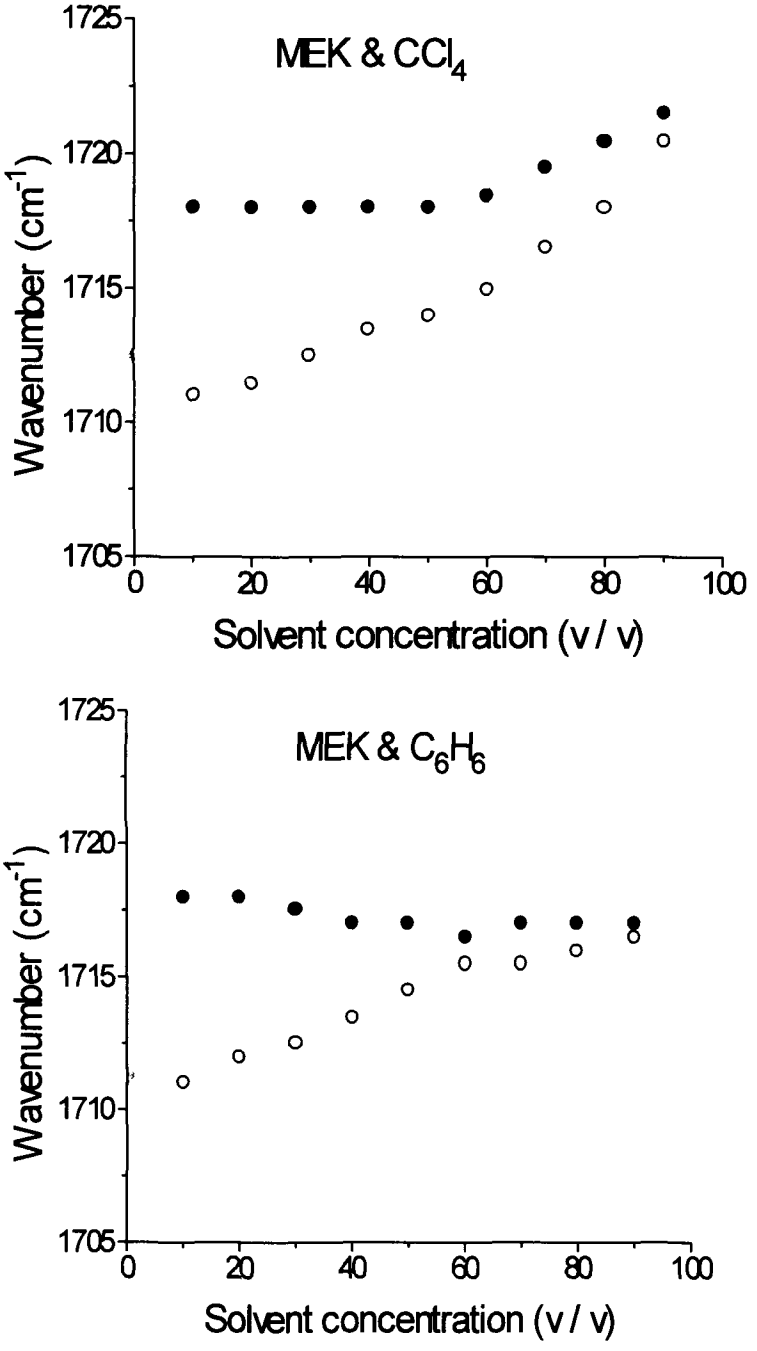

Fig. 4.3: Variation of peak frequencies of isotropic (o) and anisotropic (•) components as a function of concentration in CCl_4 and C_6H_6

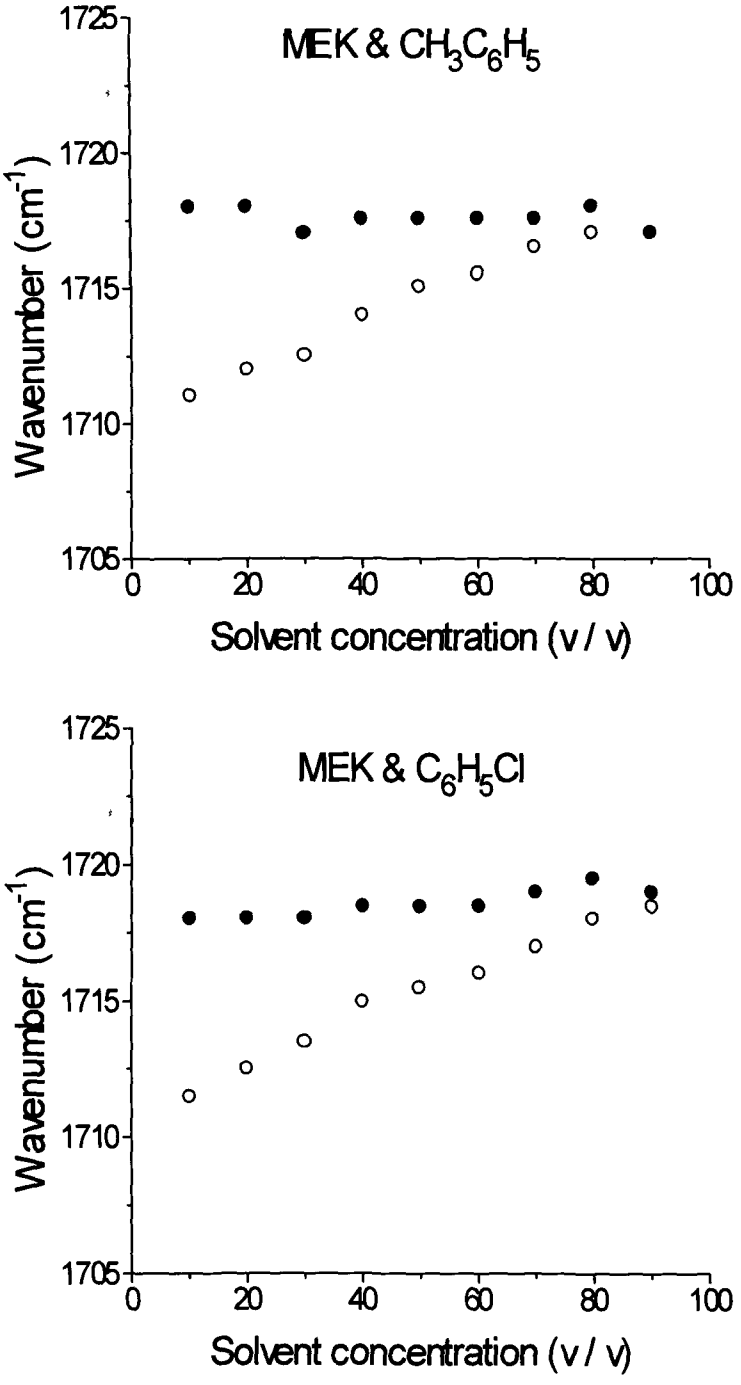

Fig. 4.3: Variation of peak frequencies of isotropic (o) and anisotropic (•) components as a function of concentration in $CH_3C_6H_5$ and C_6H_5Cl

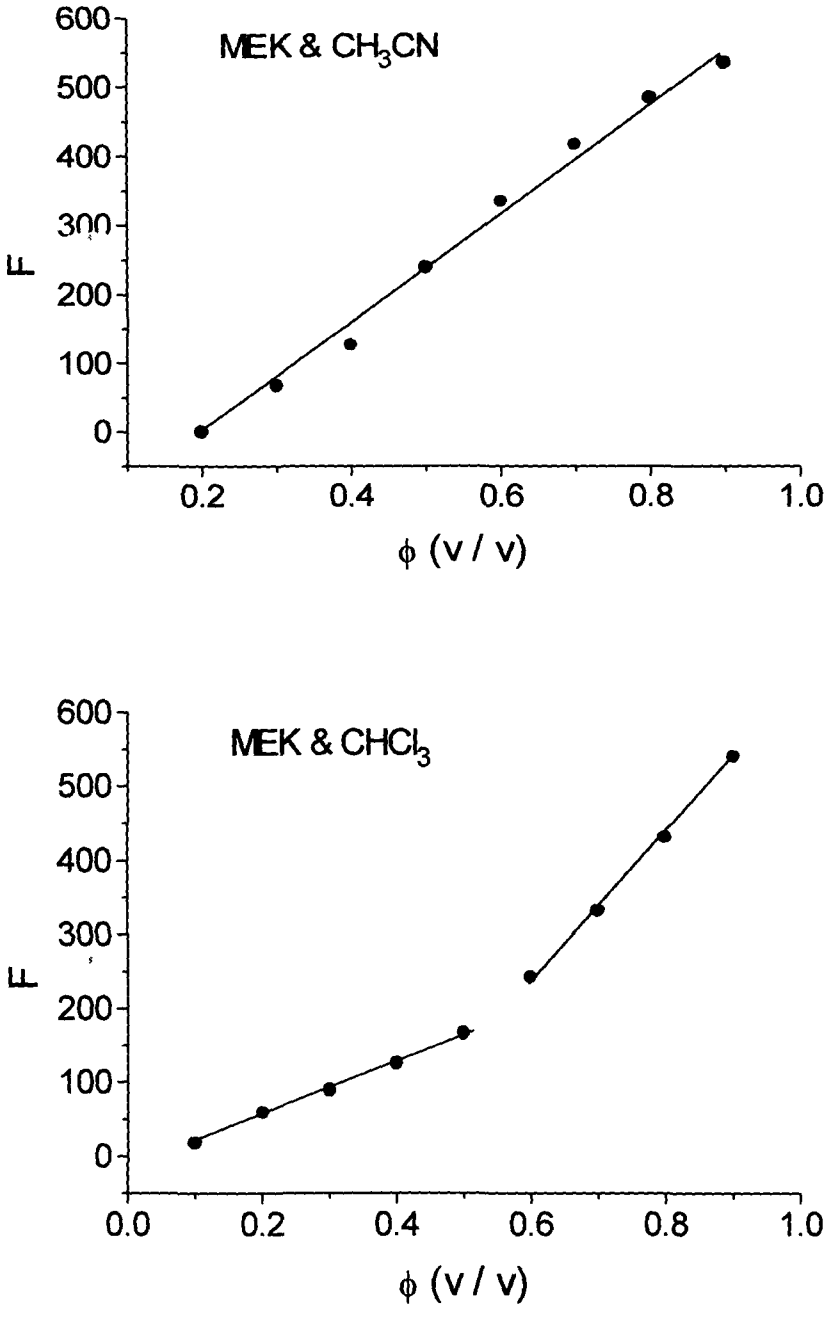

Fig. 4.4: Variation of the quantity F as a function of solute (MEK) concentration (φ) in CH_3CN and $CHCl_3$ solvents.

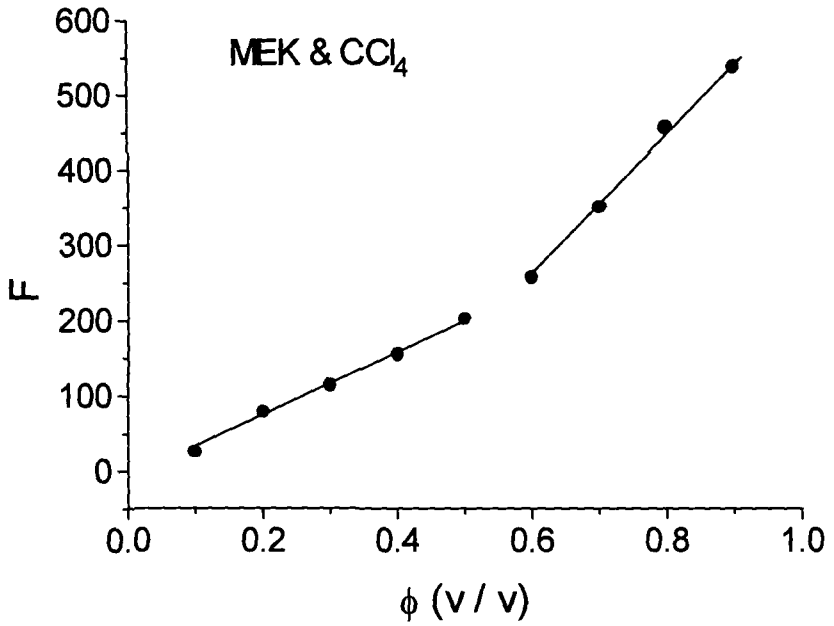

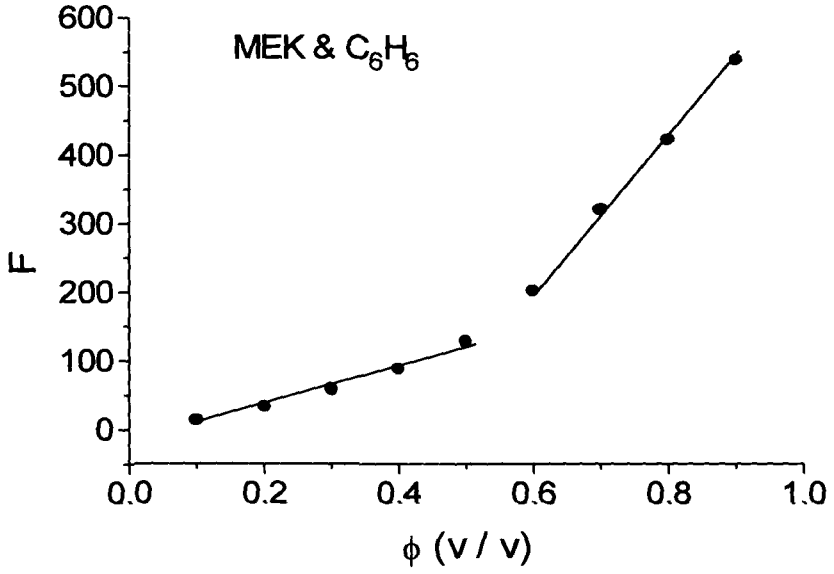

Fig. 4.4. Variation of the quantity F as a function of solute (MEK) concentration (φ) in CCl_4 and C_6H_6 solvents.

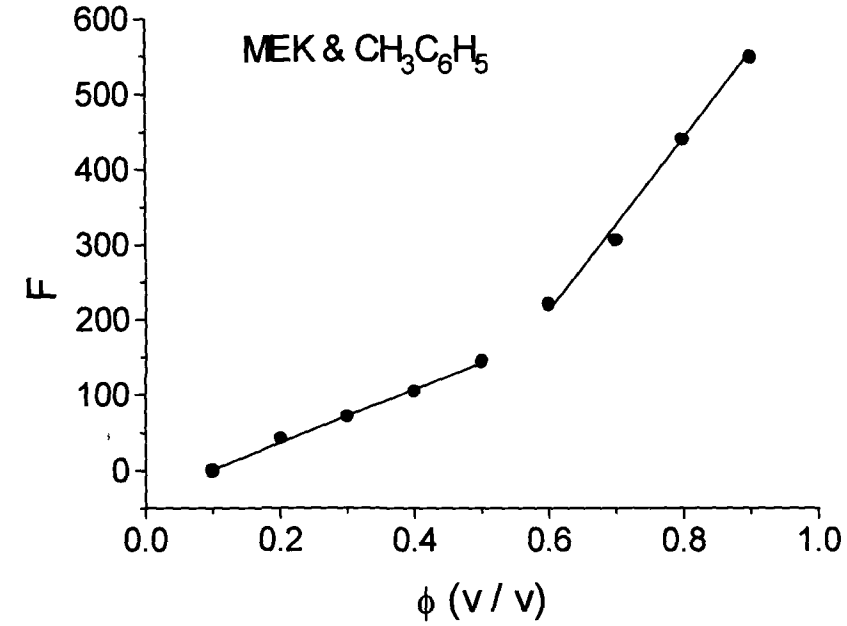

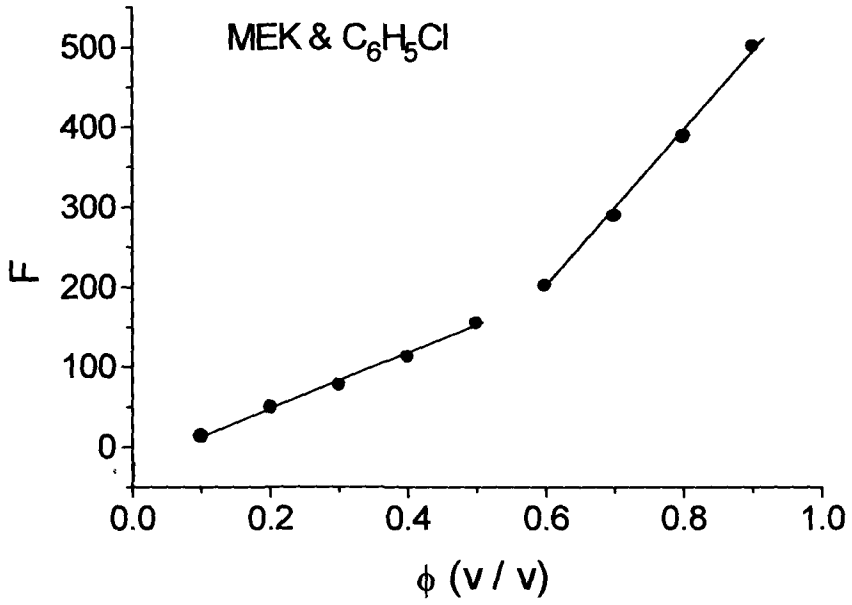

Fig. 4.4: Variation of the quantity F as a function of solute (MEK) concentration (φ) in $CH_3C_6H_5$ and C_6H_5Cl solvents.

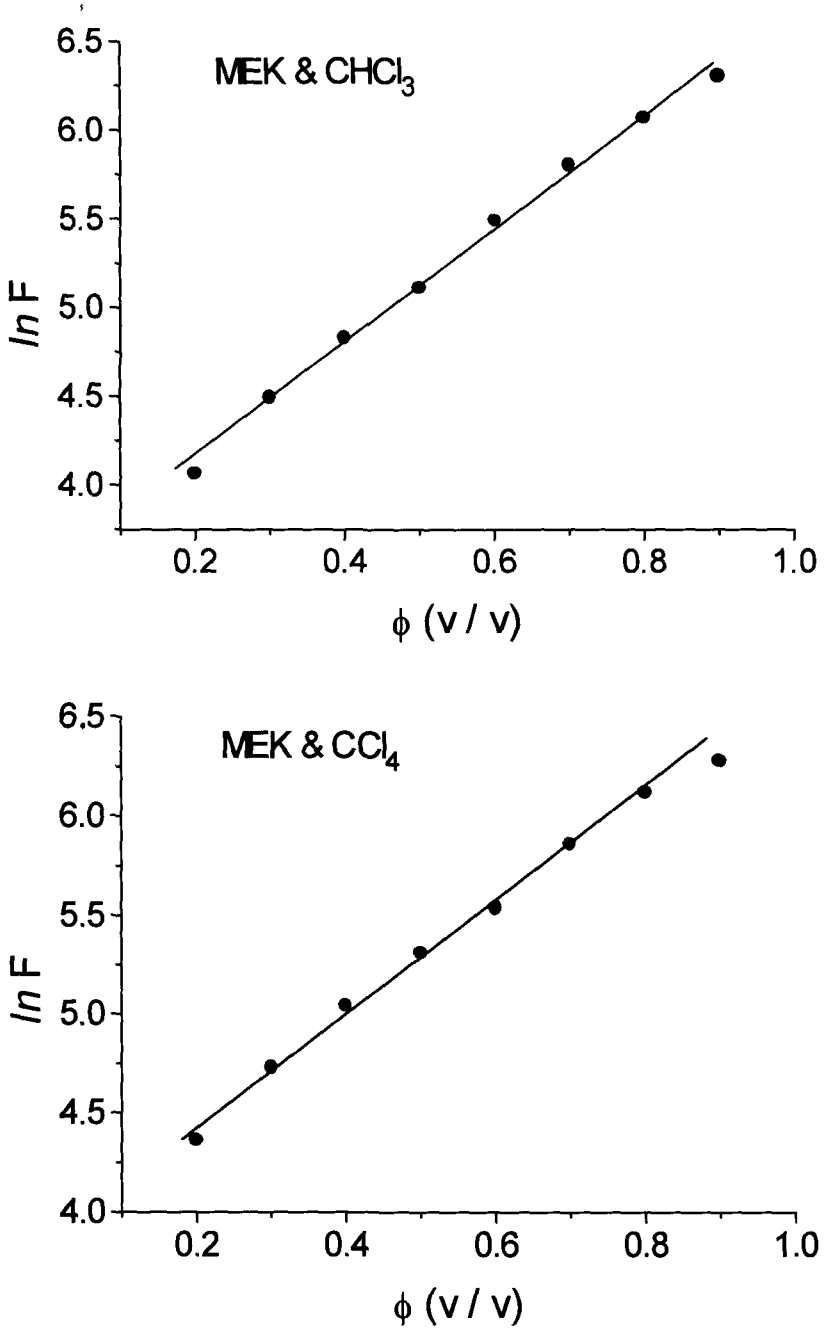

Fig. 4.5: Variation of *ln* F as a function of solute (MEK) concentration (φ) in $CHCl_3$ and CCl_4 solvents.

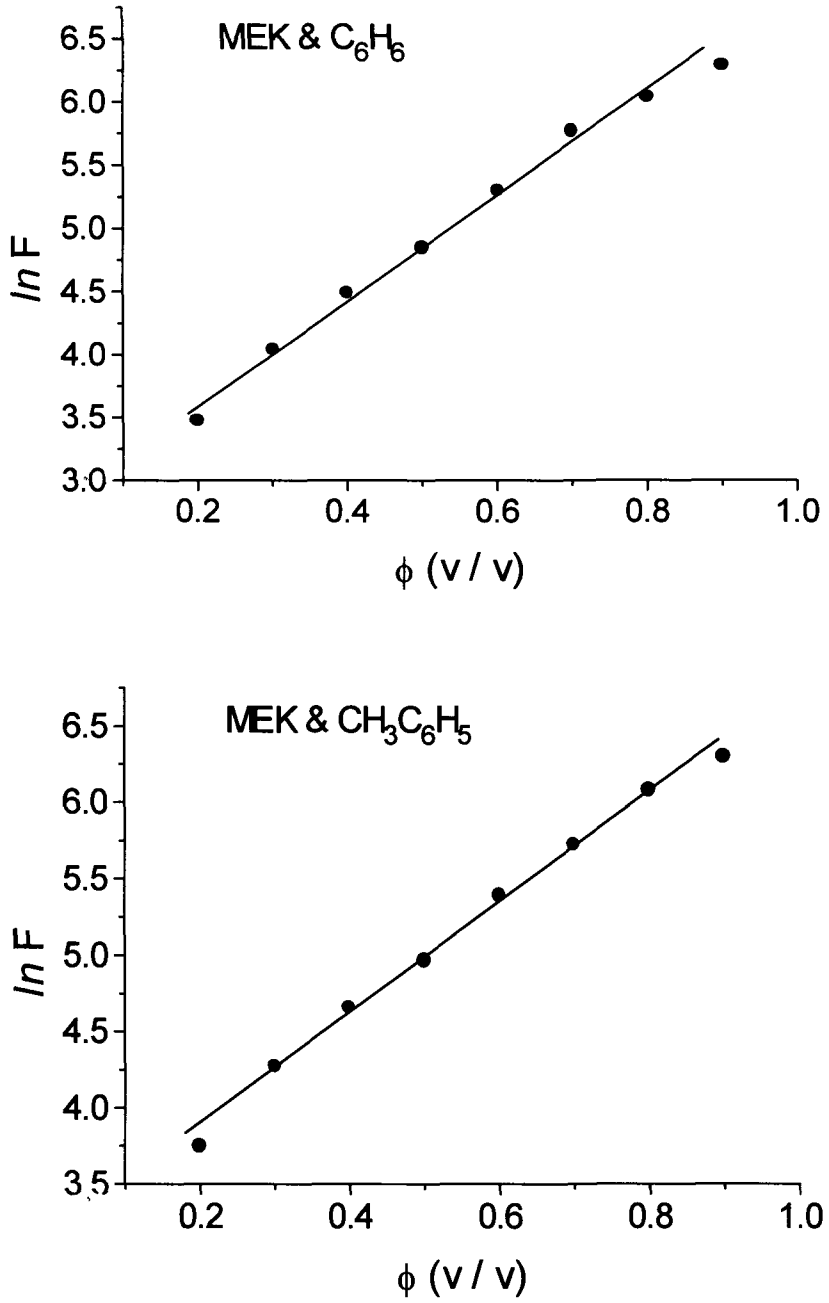

Fig. 4.5: Variation of *ln* F as a function of solute (MEK) concentration (φ) in C_6H_6 and $CH_3C_6H_5$ solvents.

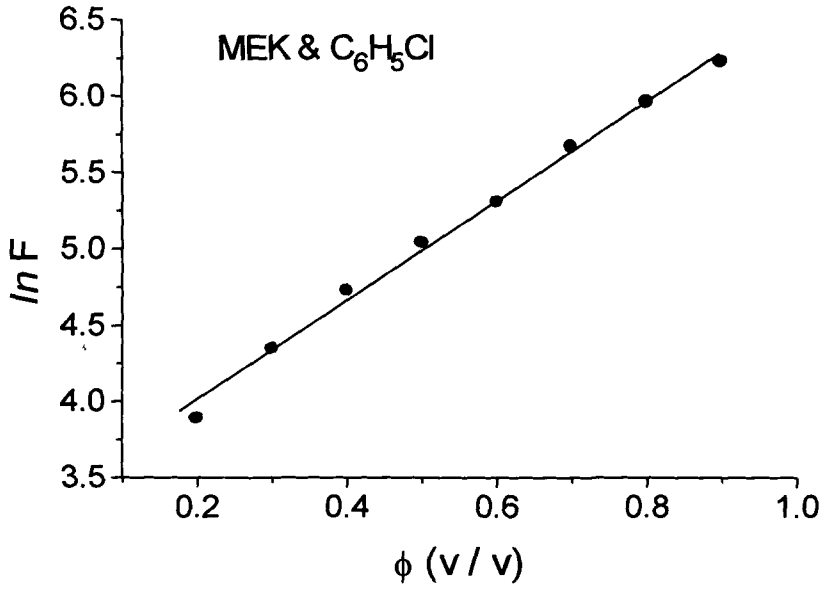

Fig. 4.5: Variation of *ln* F as a function of solute (MEK) concentration (φ) in C_6H_5Cl solvent.

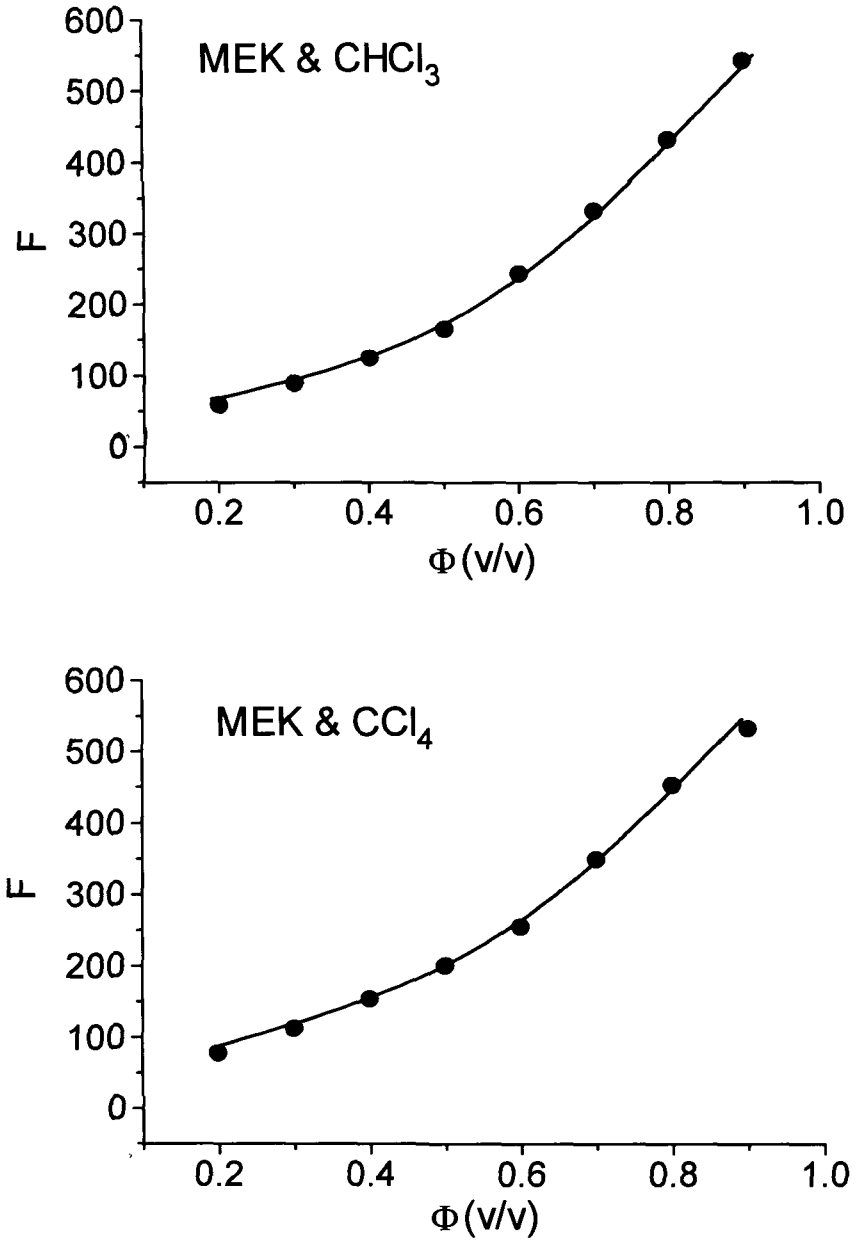

Fig. 4.6: Variation of the quantity F as a function of solute (MEK) concentration (φ) in $CHCl_3$ and CCl_4solvent.

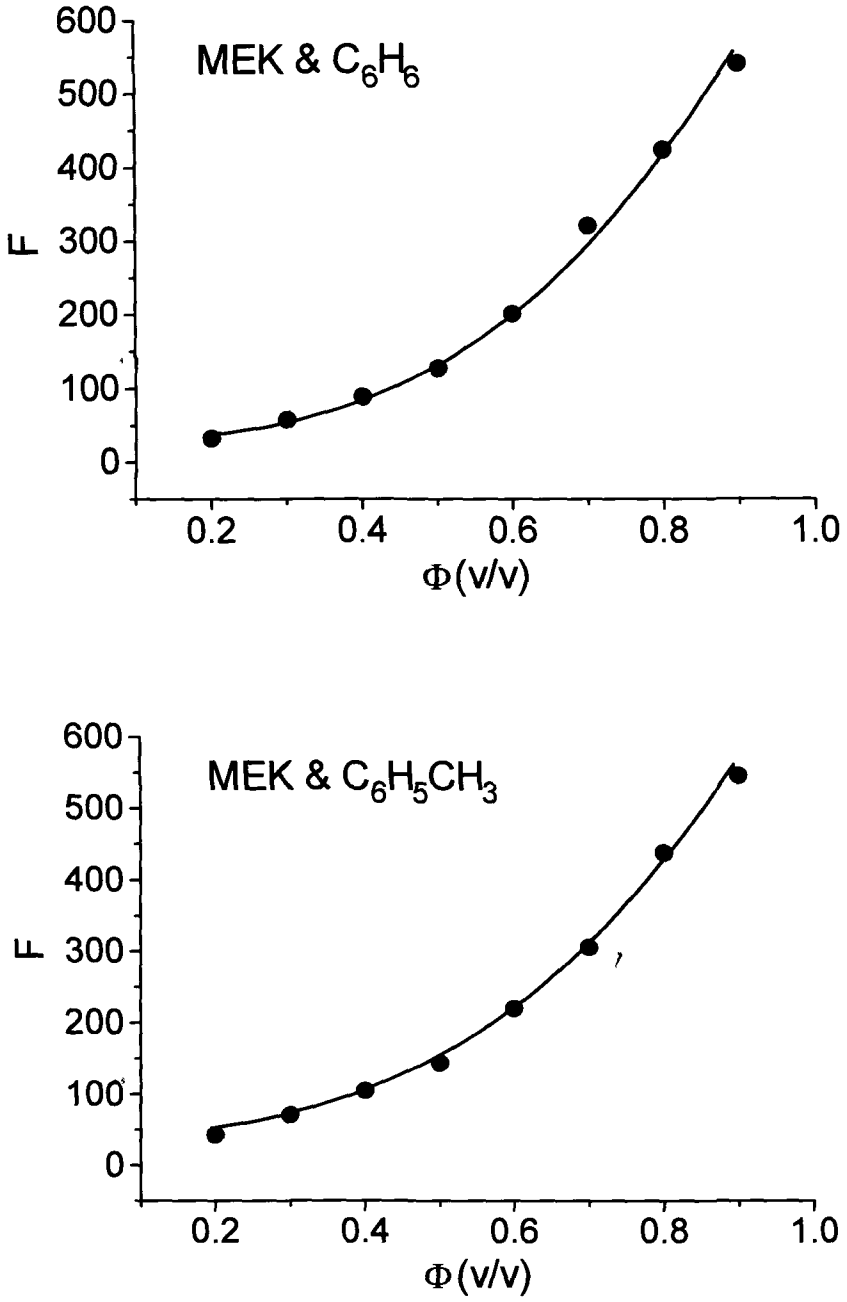

Fig. 4.6: Variation of the quantity F as a function of solute (MEK) concentration (φ) in C_6H_6 and $C_6H_5CH_3$ solvents.

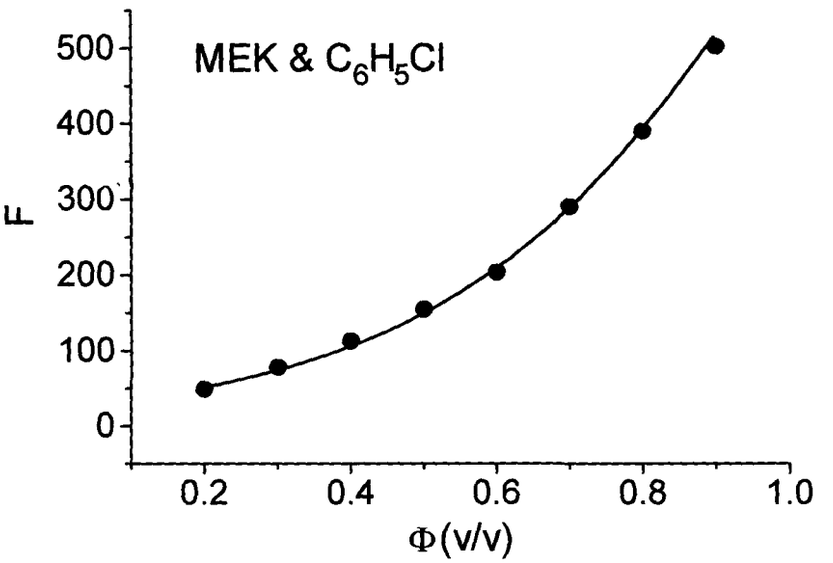

Fig. 4.6: Variation of the quantity F as a function of solute (MEK) concentration (φ) in C_6H_5Cl solvents.

CHAPTER 5

CHAPTER 5

VIBRATIONAL DEPHASING AND HYDRODYNAMIC EFFECTS ON VIBRATIONAL RELAXATION RATES IN ACETOPHENONE

5.1. INTRODUCTION

The vibrational relaxation processes in molecular liquids have been of considerable interest [1-22] for the last few decades. Raman spectra of molecular liquids are influenced by intermolecular interactions in several manners and are expected to be sensitive to various environmental fluctuations such as pressure, temperature, density and solvent concentrations [10,15-19]. The solvent contributions to vibrational frequencies and bandwidths are due to intermolecular interactions involving attractive and repulsive forces. Thus the changes in the band parameters may provide crucial information regarding the nature of interaction which may useful for studies related to such as chemical kinetics.

The dynamic fluctuations about the average force of interaction manifest the nature and shape of the relevant vibrational band. The local molecular interactions on individual molecule induces diagonal vibrational frequency modulation. It gives rise to inhomogenous broadening in slow modulation regime or dephasing in the intermediate or fast modulation regime and is seen more or less essentially in all vibrational bands [23].

According to Knapp and Fischer [24], the frequency shift and asymmetry of spectral line profile depend on the concentration fluctuations due to the interaction with nearest neighbours and their diffusion dynamics. Schweizer and Chandler [25] have shown the effects of repulsive and spatially slowly varying attractive forces on the band widths of the vibrational band in the molecular liquids. This model simultaneously examines both the broadening mechanisms and the frequency shifts. The theory of Schweizer and Chandler is more illustrated by the theory proposed by Ben-Amotz et al [26]. The line shape contribution from the rapidly changing repulsive forces would be homogeneously broadened leading to Lorentzian line shape whereas the lineshape contribution due to slowly changing attractive forces would be inhomogeneously broadened with the lineshape becoming Gaussian. The vibrational relaxation process is responsible for the line broadening of the isotropic Raman spectral component and is generally considered

to be due to contributions from vibrational dephasing, population relaxation and resonant energy transfer [27,28] and is expected to give detailed information about solution dynamics.

A starting point for a discussion of the aromatic solvent effect is the assumption that the solvation effect falls into two contributions [29]. Short-range solvation effects result from specific local interactions between solute and solvent molecules. This interaction depends on the microscopic parameters of the solvent molecules and also on the steric crowding around the solute molecule. The second solvation contribution arises from a long-range effect caused by the dielectric permittivity. However because of the orientation of solvent molecules in the vicinity of solute, the nearest region is characterized by a local ϵ which is lower than the bulk ϵ. The nearest region for a given solute depends [29] on the size and shape of the solvent molecule.

For the present study, acetophenone molecule has been chosen to investigate the sensitivity of Raman band corresponding to the carbonyl bond, to varying physico-chemical properties of solvents. The isotropic Raman component has been analyzed by calculating the correlation coefficient, assuming that the lineshape is predominantly Lorentzian in nature. The concentration dependence of the correlation coefficient in various solvents has been studied .The correlation coefficient is used to find where the lineshape is Lorentzian in nature.

The interaction energy for the solute and solvent molecules in the solution phase may arise as a result of contributions from various coupling mechanism like dipole-quadrupole quadrupole-quadrupole and higher multipolar interactions [30]. In addition, the hydrodynamic forces and the microenvironment may also be responsible for the variation in bandwidth and frequency. These type of interactions though complicated in nature deserve detailed investigation.. In order to have detailed knowledge about the effect of microenvironment on the active molecule, the molecules having different groups near carbonyl bond need to be investigated.

The acetophenone molecule is chosen here to get an insight into the different processes influencing the vibrational transition corresponding to C=O bond. This molecule is free from hydrogen bonding in neat liquid and has high dielectric constant as well as high dipole moment. The carbonyl group of this molecule is therefore expected to have strong interactions. This molecule has been studied by Giorgini etal. [31] from the point of view of non-coincidence effect in which they have found out the effect of solvents on anisotropy shift .Detailed and extensive work is required on this interesting molecule related to the band broadening and vibrational dephasing of the carbonyl band of acetophenone molecule. For this a set of chosen solvent molecules with varying dielectric constant, dipole moment and

shapes have been used to correlate the relaxation rate with the molecular properties.

The vibrational relaxation rate [VRR] serves as a good probe for the solute-solvent interactions. The interactions which influence the VRR are also important in determining a wide variety of closely related condensed properties such as chemical reaction rates [32]. The VRR have been the subject of numerous theoretical and experimental investigation [1-22]. The model [11-12] suggested by Purkayastha and Kumar has successfully explained the vibrational relaxation process under the condition of high dilution for amides, ketones and aldehydes [8,11-12]. In order to have better understanding of the complex mechanism of vibrational relaxation, we have measured the vibrational relaxation rate of the C=0 stretching mode of acetophenone and correlated their dependence on the solution properties.

The ketones are a class of molecules, which are very significant in physical chemistry and chemical dynamics. Acetophenone is an important molecule with a wide range of industrial applications. It is also the simplest aromatic ketone used as a component of perfumes and an intermediate for polymerization catalyst for the manufacture of pharmaceuticals. The C=O stretching of this molecule is suitable for probing the molecular environment as it is not perturbed by other vibrational modes.

5.2. EXPERIMENTAL

The Raman spectra of the C=O stretching mode of acetophenone were recorded in a spectral region of approximately 1600-1800 cm^{-1} as a function of solvent concentration in acetonitrile, carbon tetrachloride, benzene, chlorobenzene and methylbenzene solvents at room temperature. All the samples were of spectroscopic grade obtained commercially and were used without further purification. The laser line at 4880 Å from the Spectra Physics Model 165 Argon ion laser was used. The spectral measurements for Raman bands were carried out by means of a Spex Ramalog 1403 double monochromator equipped with a cooled RCA-C31034 photomultiplier tube and a photon counting arrangement. The spectrometer control and data processing were achieved with the help of a Datamate using DM-3000 software. The experiments were performed with a maximum power of about 300 mW. The slit width ~ 2.5 cm^{-1} was maintained for all recorded spectra. The spectra were recorded corresponding to a wavenumber step of 0.5 cm^{-1} and the integration time was set to 1s. All measurements were carried out at constant ambient temperature and pressure and spectral conditions were adjusted to get the best possible spectra. The accuracy of spectral data is believed to be ± 0.5 cm^{-1}.

The polarization of the incident laser light was vertical and the scattered light for both the vertical (I_{VV}) and horizontal (I_{VH}) polarization

were recorded using a polarization analyzer with a 90° scattering geometry. A polarization scrambler located just in front of the spectrometer entrance slit was used in all experiments to correct the polarization bias of the double monochromator (grating). The isotropic and anisotropic components of the spectrum were calculated from I_{VV} and I_{VH} using the standard equations as described in Chapter 2:

$$I_{iso}(\nu) = I_{VV}(\nu) - \frac{4}{3} I_{VH}(\nu) \qquad (5.1)$$

$$I_{aniso}(\nu) = I_{VH}(\nu) \qquad (5.2)$$

where $I_{VV}(\nu)$ and $I_{VH}(\nu)$ are the polarized and depolarized Raman spectra respectively and ν is the wave number in cm^{-1}.

The finite slit width effect on the observed bandwidth was corrected [33] according to the formula

$$\Gamma_c = \Gamma_o [1 - (S/\Gamma_o)^2] \qquad (5.3)$$

where Γ_o and Γ_c are the observed and corrected bandwidth and S is the spectral slit width in cm^{-1}.

5.3. RESULTS AND DISCUSSION

The isotropic components of the Raman bands were measured in neat liquid as well as in solutions using polar and non-polar solvents (acetonitrile, carbon tetrachloride, benzene, chlorobenzene and methylbenzene). Raman spectrum of neat liquid acetophenone is shown in figure 5.1. The experiments were carried out at solvent concentrations ranging from 10% to 90%. The band shapes were first checked for Lorentzian line shape by curve fitting method at each of the concentration. The analysis of the data shows that the bands have almost Lorentzian line shape under high dilution condition only.

A Lorentzian function $\omega(t)$ can be transformed into a linear equation of the form

$$1 / I_{iso} = K_1 (\omega - \omega_o) + K_2 \qquad (5.4)$$

where I_{iso} represent the intensity of the isotropic Raman component and $K_1$and K_2 being two constant terms.

The correlation coefficient '**r**' thus obtained essentially reflects the nature of band shape with reference to the Lorentzian character of the band. It exhibits concentration dependent features, which are interesting from the point of view of microscopic nature of the intermolecular interactions in solution phase. The dependence of '**r**' on the solvent properties as well as on the concentration being of

considerable value ,the correlation coefficient '**r**' was plotted as a function of solvent concentration (Fig 5.2). The data were found to fit in two different straight lines rather tha one with a sharp discontinuity in the intermediate region of solvent concentration, in all solvents. The data points also indicate that the band shape undergoes a change from non-Lorentzian to Lorentzian character from the region of low solvent concentration to high solvent concentration. The non-Lorentzian character appears to derive its major contribution through resonant energy transfer (RET) mechanism. The increase in solvent concentration leads to the weakening of the microscopic local order which results in the gradual fall of contribution from the RET process. This as a result imparts a gradual approach to the Lorentzian nature of the Raman band shape in the region of high solvent concentration.

It is surprising that in the region of 40% to 60% solvent concentration there is a pronounced deviation from the Lorentzian character in all the solvents. This is an interesting behaviour. This discontinuity in the intermediate region may be attributed to structure breaking effect and local fluctuations [34,35] when the solute and solvent molecules become comparable in number. The variation of chemical composition of the solvation shell surrounding the active molecule give rise to local fluctuations. The pair interaction gives rise to local orientational order because of dipole-dipole interactions in

identical molecules. On dilution with solvents, this order tends to break. The reduction in the structural order due to the effect of solvent is the structure breaking effect [35]. This indicates that structural characteristics of the solute molecule and the molecular fragments may play a significant role in determining the band shape. The microenvironment around the active site of the molecule may lead to the change of band shape in the intermediate region [30]. It is clear that the size and shape of the molecules are very significant in determining the lineshape of the Raman bands .

The vibrational frequency of a molecule is perturbed by random forces and has components, which fluctuates with time. Because of these random forces, the band will be broadened around the center by random modulation giving rise to a distribution of frequency. In neat liquid, local quasi-crystalline order due to strong interaction between permanent dipoles of identical molecules is present. However, on dilution, the randomization of vibrational phase due to elastic collisions with the solvent molecules leads to homogenous broadening. Hence a gradual approach towards Lorentzian line shape is observed in the high dilution regime. In the intermediate region, the interaction among solute and solvent molecules is random and it may be responsbile for the discontinuity in the plot (Fig 5.2). The resonant energy transfer mechanism leading to pair correlation in pure liquid is suppressed by

the solvent induced perturbations. The competitive short-range repulsive forces and the long-range attractions among the molecules invoke chaos in this region when the solute and solvent concentrations become comparable. The structural characteristics and the solute-solvent interactions arising from the various coupling terms such as dipole-dipole, dipole-induced-dipole, dipole-quadrupole, quadrupole-quadrupole and other multipolar interactions [6,30] are expected to contribute towards the determination of bandshape in the liquid mixtures. In case of aromatic molecules like acetophenone, the quadrupolar interactions are expected to be dominant. A detailed analysis is, however, required from the microscopic point of view to understand the effects of various complexities arising from the molecular aspects of such liquids. We therefore also studied the vibrational relaxation rates to understand the microenvironmental impact on an active oscillator.

The I_{VV}, I_{iso} and I_{aniso} components of Raman spectra of acetophenone molecule in various solvents at 80% solvent concentration are shown in figure 5.3.

The vibrational relaxation rate (τ_v^{-1}) is related to the isotropic band width (Γ_{iso}) of the Lorentzian band by the expression :

$$\tau_v^{-1} = \pi c \, \Gamma_{iso} \qquad (5.5)$$

where c is the velocity of light.

The vibrational relaxation rate (τ_v^{-1}) is also dependent upon viscosity (η), density (ρ) and the refractive index (n) and is expressed [13,14]in the following way:

$$\tau_v^{-1} = A\rho \frac{6\pi\eta r^6}{\mu^2}\left(\frac{n^2-1}{2n^2+1}\right)^{-1}$$

$$= C_m f(\rho,\eta, n) \qquad (5.6)$$

where $C_m = A\frac{6\pi r^6}{\mu^2}$ is a constant which depends mainly on the solute properties and $f(\rho,\eta, n) = \rho\eta\left(\frac{n^2-1}{2n^2+1}\right)^{-1}$

The parameter f (ρ,η,n) was calculated for acetophenone and correlated with the experimental values of the vibrational relaxation rate. The correlation is shown in Fig.5.4. Although the correlation is almost linear the data points for all the solvents do not fall on the straight line. It is probable that the discreteness of the medium due to solvent may be playing a role. Hence, a microscopic model was used in order to explain the microscopic environment. In this model, since the solute-solvent systems may not always be homogeneous and some heterogeneity may exist, the concept of microviscosity [36] was introduced and the parameter f (ρ,η,n) was modified

The modified parameter has the form

$$f_m = \rho\eta_m\left[\frac{n^2-1}{2n^2+1}\right]^{-1} \qquad (5.7)$$

where ρ is the density and n is the refractive index of the solvent molecule.

Here, the microviscosity factor η_m is given by

$$\eta_m = \eta\gamma$$

where γ is the microfriction factor which is responsible for the non-continuos nature of the visco-elastic medium and has the following form.

$$\gamma = \left[0.16 + 0.4\left(\frac{a}{b}\right)\right] \qquad (5.8)$$

'a' and 'b' are the solute and solvent molecular radii respectively.

Equation (5.7) therefore becomes

$$f_m = \rho\eta\ [0.16+0.4(a/b)]\ [(2n^2+1)/(n^2-1)] \qquad (5.9)$$

van der Waals' forces operate between portions of different molecules. The heterogeneity of the solute-solvent systems due to the associative nature of the molecules has to take into account the van der Waals' interactions. Based on this, the values of 'a' and 'b' for equation (5.9) are chosen. The entire molecular volume may not be effective in the interaction process due to the change in orientation of the active molecule on dilution. The acetophenone molecule may be assumed to

be planar and the main interaction is expected to occur through the C=O bond of this molecule when mixed with the CH_3CN and CCl_4 solvents. The molecular radius for the solute may therefore be chosen as the van der Waals' radius [37] of oxygen atom (1.40Å) for the acetophenone-CH_3CN and acetophenone-CCl_4 systems. The cylindrical structure of the C-C≡N fragment of the CH_3CN molecule is expected to determine the distance of closest approach of the solvent towards the solute. Due to steric effect and because of the symmetric top structure of CH_3CN molecule and the plate like structure of the acetophenone molecule, the interaction is most likely to be between the carbonyl bond and the nitrogen atom of the CH_3CN molcule. Therefore if the solvent molecular radius in this case is taken as the van der Waals' radius of nitrogen atom (1.50Å), it may explain the data. Due to the spherical nature of the CCl_4 molecule, the C-Cl bond distance (1.7Å) and the Cl atom van der Waals' radius (1.8Å) are summed up to obtain the molecular radius for this solvent. In case of C_6H_6, $CH_3C_6H_5$ and C_6H_5Cl molecules, the most favourable interaction between solvent and solute is likely to be between the benzene rings due to the flat nature of this fragment of the molecules. The molecular radius for the solute as well as the aromatic solvents may therefore be chosen as the van der Waals' radius of benzene (1.77 Å). The molecular parameters for the solute and solvents are shown in Table 5.1.

The variation of τ_v^{-1} as a function of f_m is shown in figure 5.5 which shows clearly a linear nature when the isotropic Raman components are obtained at 80% solvent concentration, where the band shape exhibits purely Lorentzian line shape. The concept of microviscosity and the consideration of other solvent parameters are of considerable help in explaining the Raman band shape of the solute-solvent systems in the acetophenone molecule. The hydrodynamic force parameter η assumes the form η_m after taking into account the microviscosity effects [11,12]. The present study shows that the modified hydrodynamic force parameter η_m and the dispersion force parameter $(2n^2+1)/(n^2-1)$ are playing major role in the line broadening mechanism in the acetophenone molecule.

The structural characteristics of molecular systems and the solvent induced perturbations at microscopic level are playing significant role in determining the nature and shape of Raman bands. The microviscosity considerations are crucial for complex molecular systems like acetophenone when dissolved in various solvents. The microenvironment around the solute molecule is found to play a vital role in determining the band width, hence vibrational relaxation rates.

TABLE 5.1: Molecular parameters for the acetophenone (AP) - solvent systems.

Molecular system	ρ (g/cm^3)	η (cP)	n	τ_v^{-1} (ps^{-1})	$f(\rho,\eta,n)$	$f_m(\rho,\eta_m,n)$
AP - CH_3CN	0.780	0.345	1.344	1.11	1.54	0.82
AP - $C_6H_5CH_3$	0.869	0.526	1.496	1.21	2.02	1.13
AP-C_6H_6	0.873	0.564	1.498	1.26	2.17	1.23
AP-C_6H_5Cl	1.107	0.631	1.524	1.36	2.98	1.67
AP-CCl_4	1.584	0.843	1.460	1.45	6.22	1.99

REFERENCES:

1. Th.G. Devi, K. Kumar, J. Raman Spectrosc. **35,** 835 (2004).
2. L. Bu, J.E. Straub, Biophysical Journal. **85**, 1429 (2003).
3. C.M. Cheatum, M.M. Heckscher, D. Bingemann, F.F. Crim, J. Chem. Phys. **115**, 7086 (2001).
4. A. Morresi, M. Paolantoni, P. Sassi, R.S. Cataliotti, G. Paliani, J. Phys. Condens. Matter **12,** 3631 (2000).
5. V. Deckert, B.P. Asthana, W. Kiefer, H.G. Burcker, A. Laubereau, J. Raman Spectrosc. **31**, 805 (2000).
6. A. Das, K. Kumar, Spectrochim. Acta **54A,** 793 (1998).
7. M. Kolodziejski, G.Waliszewska, H. Abramczyk, J. Phys. Chem. A **102**, 1918 (1998).
8. A. Bhattacharjee, A. Ghosh, T.N. Misra, S.K. Nandy, J. Raman Spectrosc. **27,** 457 (1996).
9. G. Moser, A. Asenbaum, G. Döge,J. Chem. Phys. **99**, 9389 (1993).
10. D.M. Campbell, M. Mackowiak, J. Jonas, J. Chem. Phys. **96**, 2717 (1992).
11. A. Purkaystha, R. Das, K. Kumar, Spectrochim. Acta **47A**, 525 (1991).
12. A. Purkaystha, K. Kumar, J. Raman Spectrosc. **22**, 721 (1991).

13. A. Purkaystha, R. Das, K. Kumar, Spectrochim. Acta **46A**, 1545 (1990).

14. A. Purkaystha, R. Das, K. Kumar, J. Raman Spectrosc. **21**, 227 (1990).

15. H.D. Thomas, J. Jonas, J. Chem. Phys. **90**, 4144 (1989).

16. A. Purkaystha, K. Kumar, J. Raman Spectrosc. **19**, 249 (1988).

17. A. Purkaystha, K. Kumar, Spectrochim. Acta **43A**, 1 (1987).

18. A.F.T. Chen, M. Schwartz, Spectrochim. Acta **43A**, 1151 (1987).

19. T.W. Zerda, H.D. Thomas, M. Bradley, J. Jonas, J. Chem. Phys. **86,** 3219 (1987).

20. R. Szostak, J.P. Hawraner, Spectrochim. Acta. **42A**, 799 (1986).

21. D. Schiebe, J. Raman Spectrosc. **13**, 103 (1982).

22. D.W. Oxtoby, J. Chem. Phys **70**, 2605 (1979).

23. H. Torii, J. Chem. Phys A **108**, 2103 (2004)

24. E. W. Knapp and S. F. Fischer, J. Chem. Phys. **76**, 4730(1982).

25. S. Schweizer, D. Chandler, J. Chem. Phys. **76**, 2296(1982).

26. D. Ben Amotz, M. R. Lee, S. Y. Cho, D. J. List, J. Chem. Phys. **96**, 8781 (1992).

27. D. W. Oxtoby, J. Phys. Chem. **87**, 3028(1983).

28. J. Jonas, Act. Chem. Res. **17,** 74 (1984).

29. Z. Pawelka, T. Kue, Polish J. Chem. **75**, 845 (2001)

30. A. Das, K. Das, K. Kumar, Spectrochim. Acta **58A**, 1583 (2002).

31. M.G. Giorgini, G. Fini, J. Chem. Phys, **79**, 639 (1983).

32. J.S. Brader, B.J. Berne, J. Chem. Phys, **100**, 8359 (1994).

33. G. Tarjus, S. Bratos, Mol. Phys. **42**, 307 (1981).

34. S. Bratos, G. Tarjus, Phys. Rev. A. **24**, 1591 (1981).

35. K. Tanabe, J. Hiraishi, Specrtochim. Acta. **36A**, 341 (1980).

36. V.V. Frolov, in "Nuclear Magnetic Resonance" Edited by P.M. Borodin, Amerind, New Delhi (1975).

37. A. Bondi, J. Phys. Chem. **68**, 441 (1964).

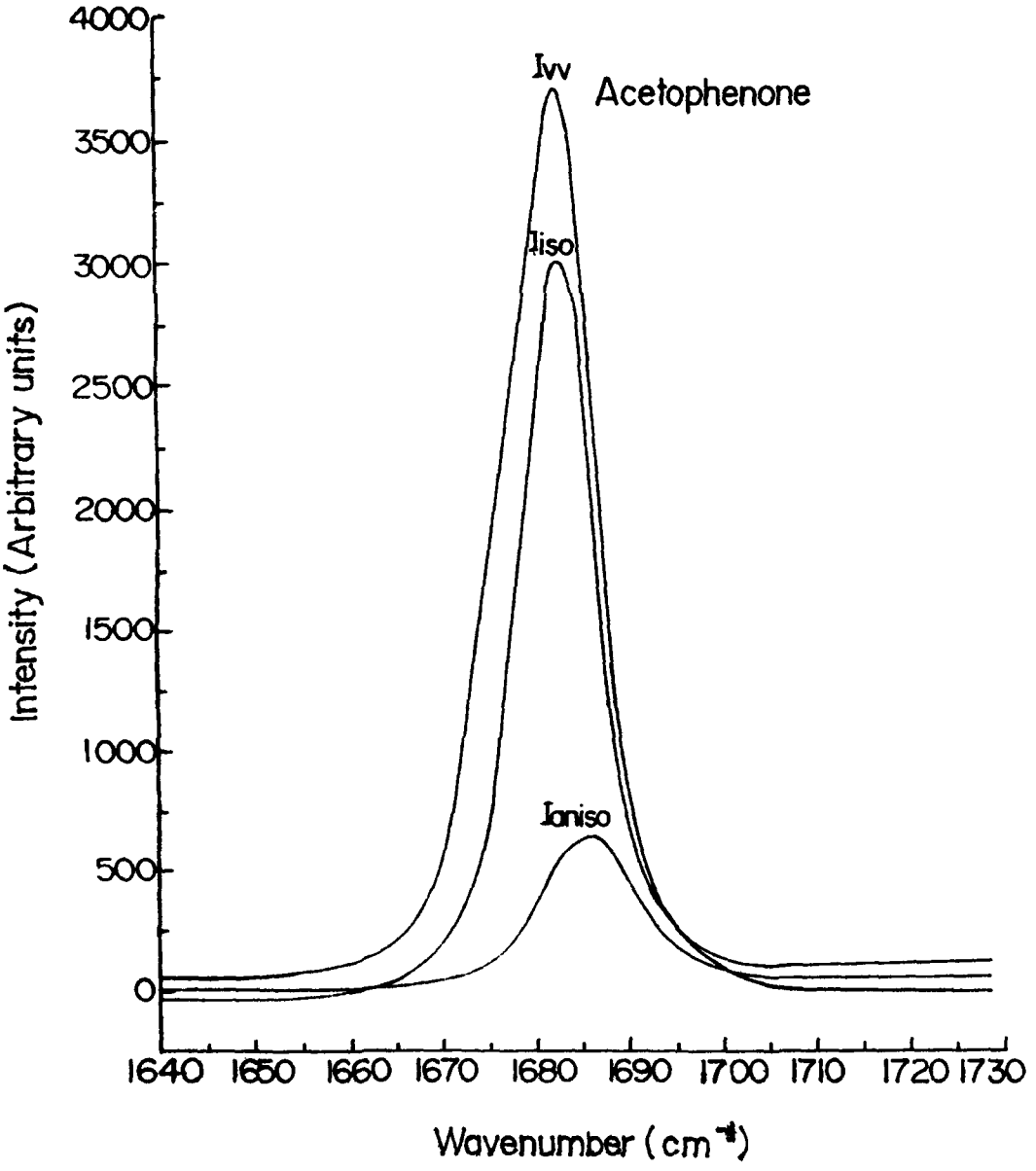

Fig. 5.1: Raman spectrum of neat liquid Acetophenone

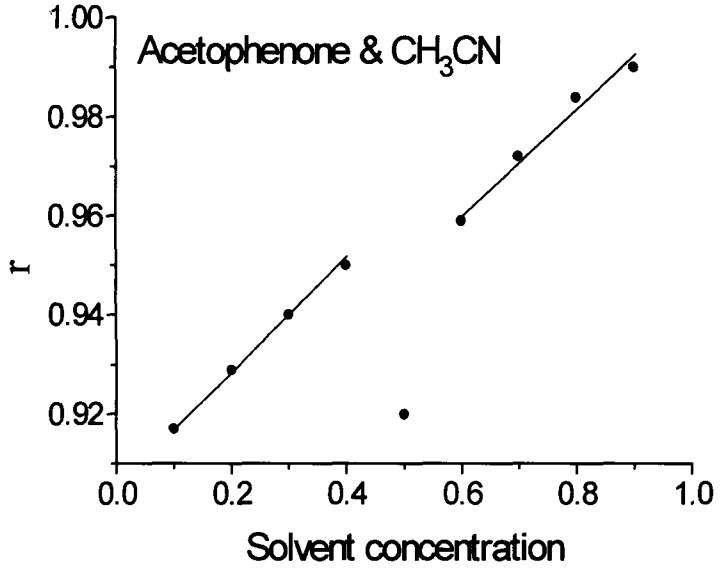

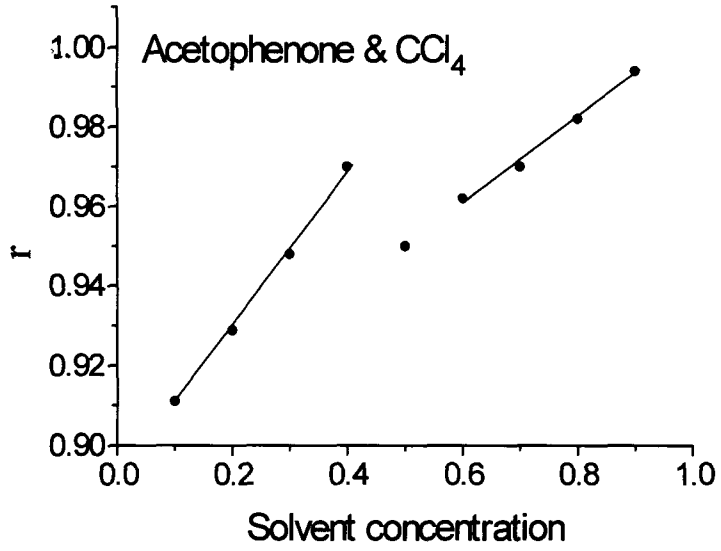

Fig. 5.2: Variation of correlation coefficient 'r' as a function of solvent(s) concentration in CH_3CN and CCl_4 solvents.

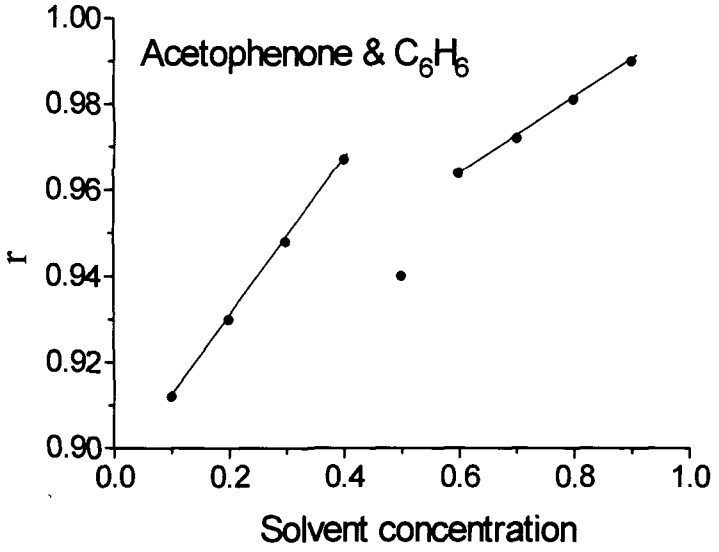

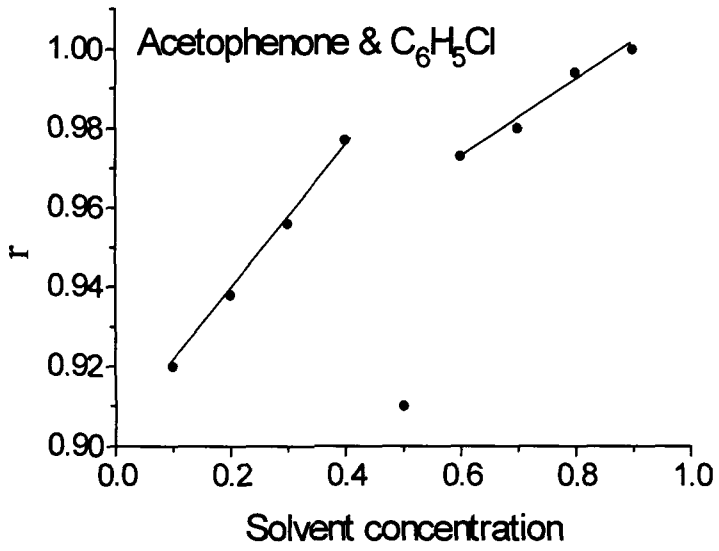

Fig. 5.2: Variation of correlation coefficient 'r' as a function of solvent(s) concentration in C_6H_6 and C_6H_5Cl solvents.

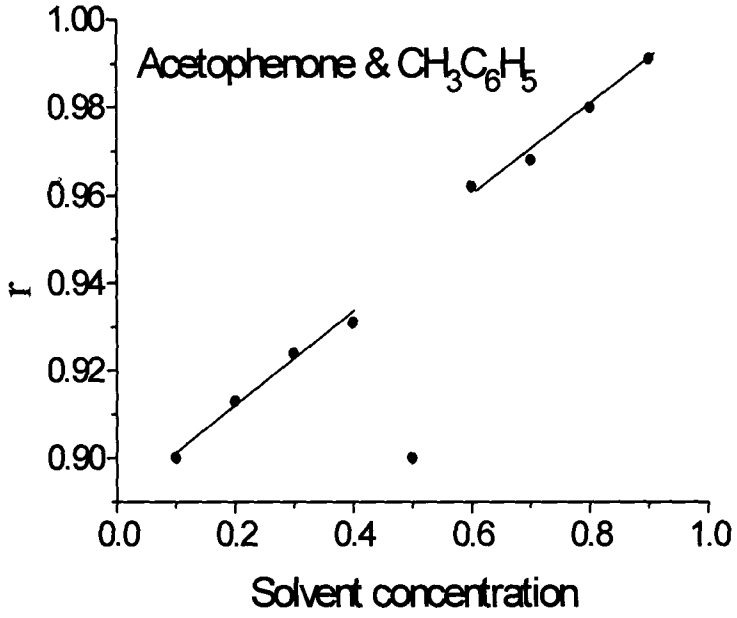

Fig. 5.2: Variation of correlation coefficient 'r' as a function of solvent concentration in $C_6H_5CH_3$ solvent.

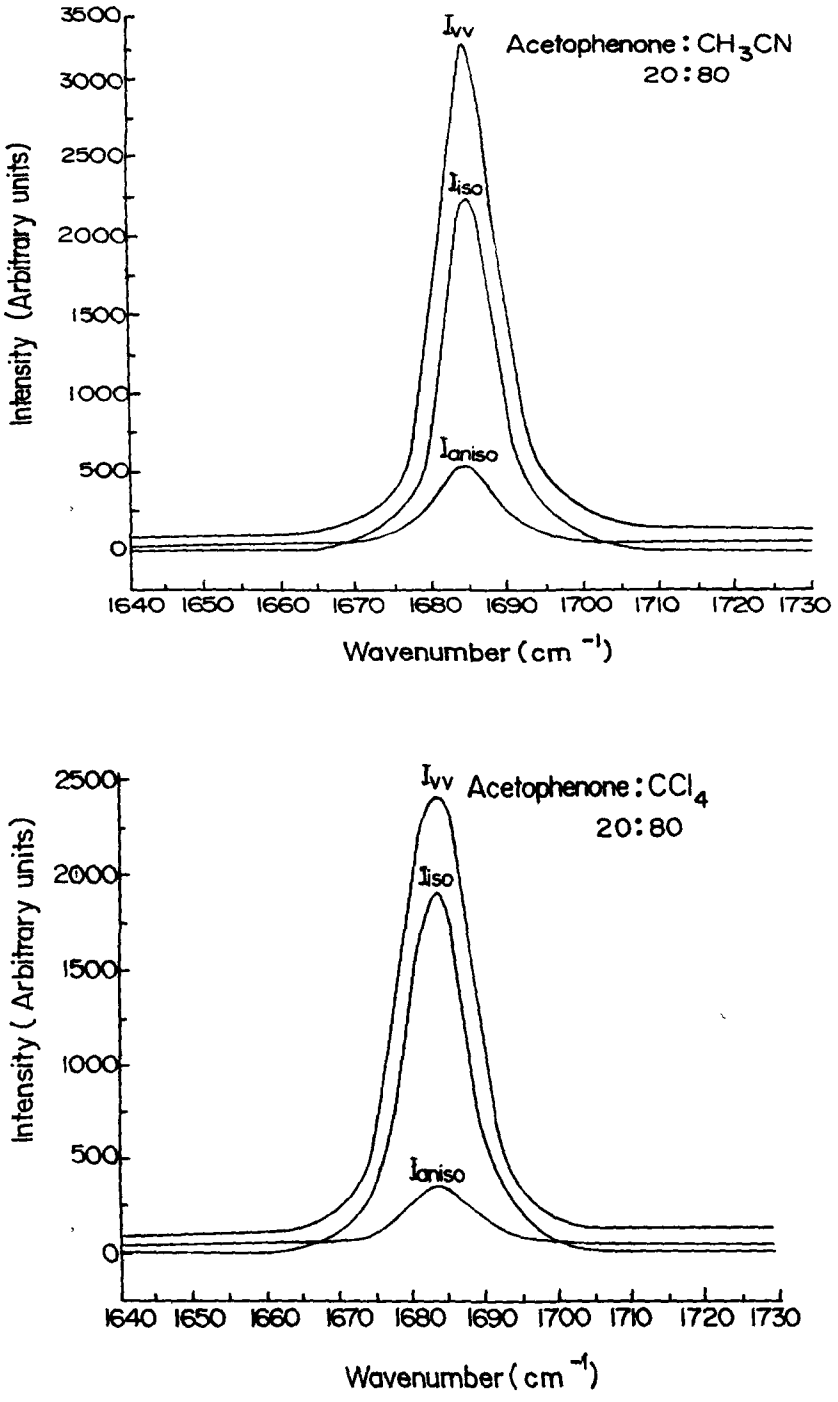

Fig 5.3: Raman spectra of Acetophenone in CH_3CN and CCl_4 solvents.

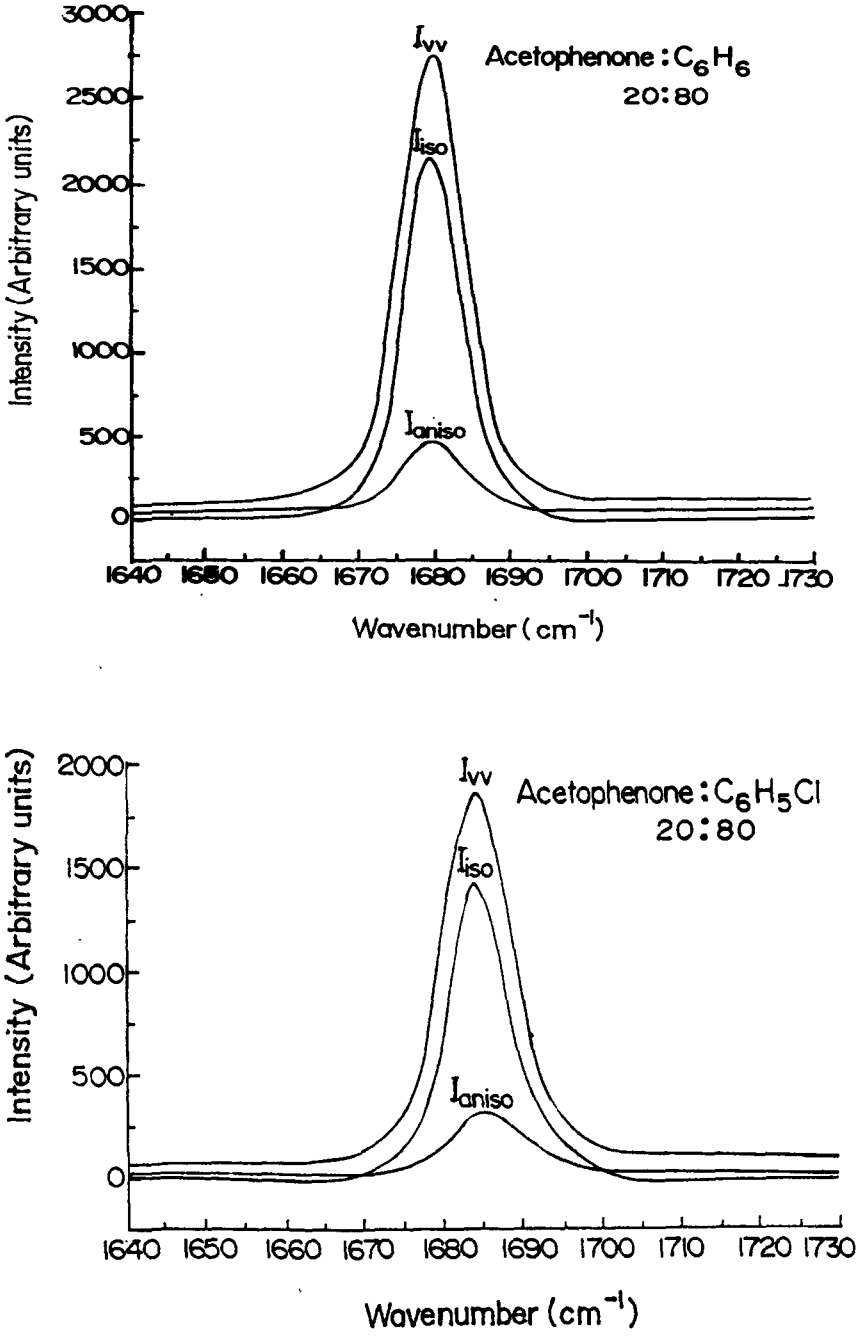

Fig 5.3: Raman spectra of Acetophenone in C_6H_6 and C_6H_5Cl solvents.

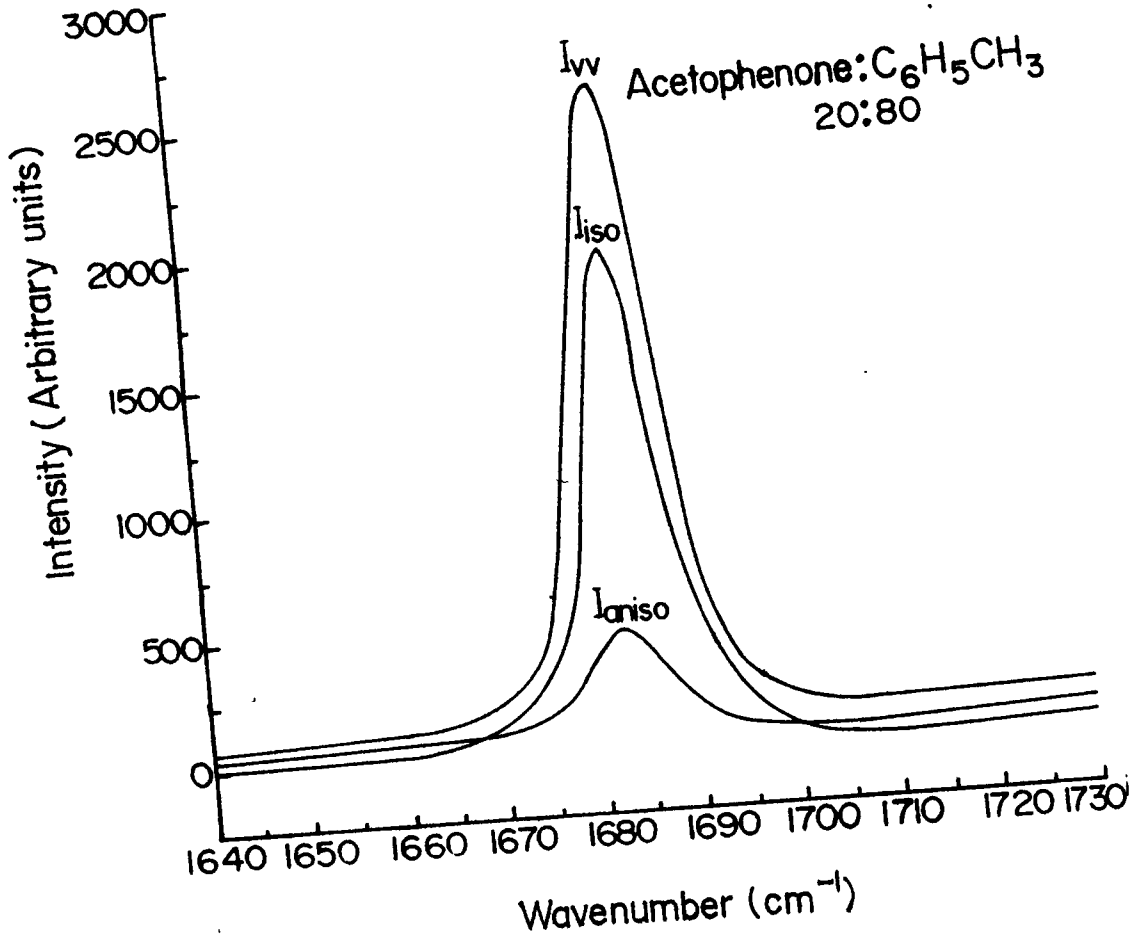

Fig 5.3: Raman spectra of Acetophenone in $C_6H_5CH_3$ solvent.

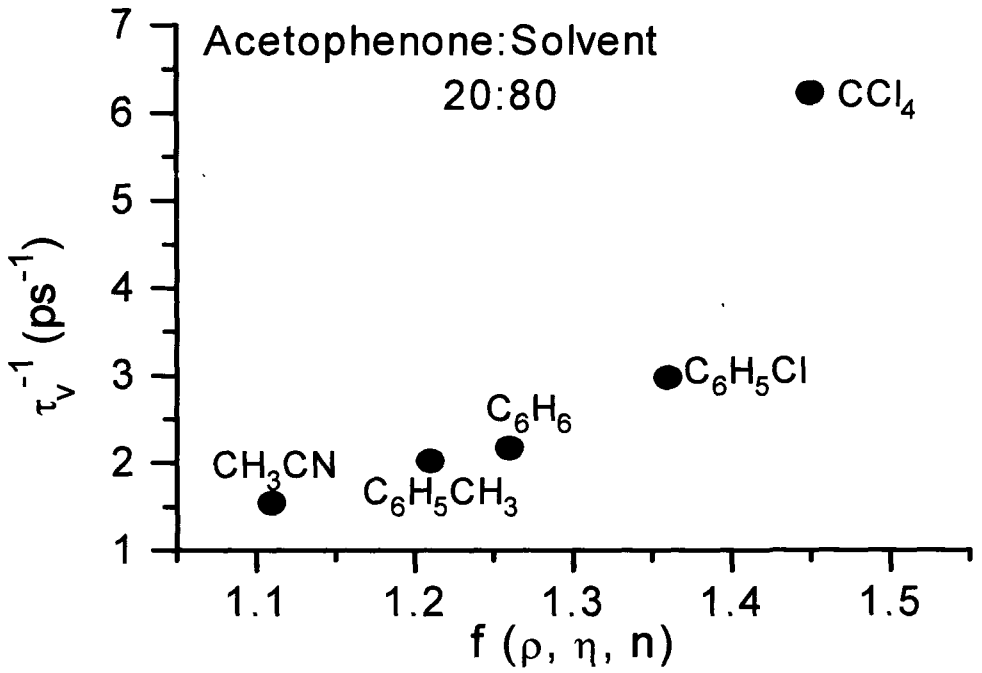

Fig. 5.4: The variation of τ_v^{-1} as a function of parameter f for Acetophenone molecule.

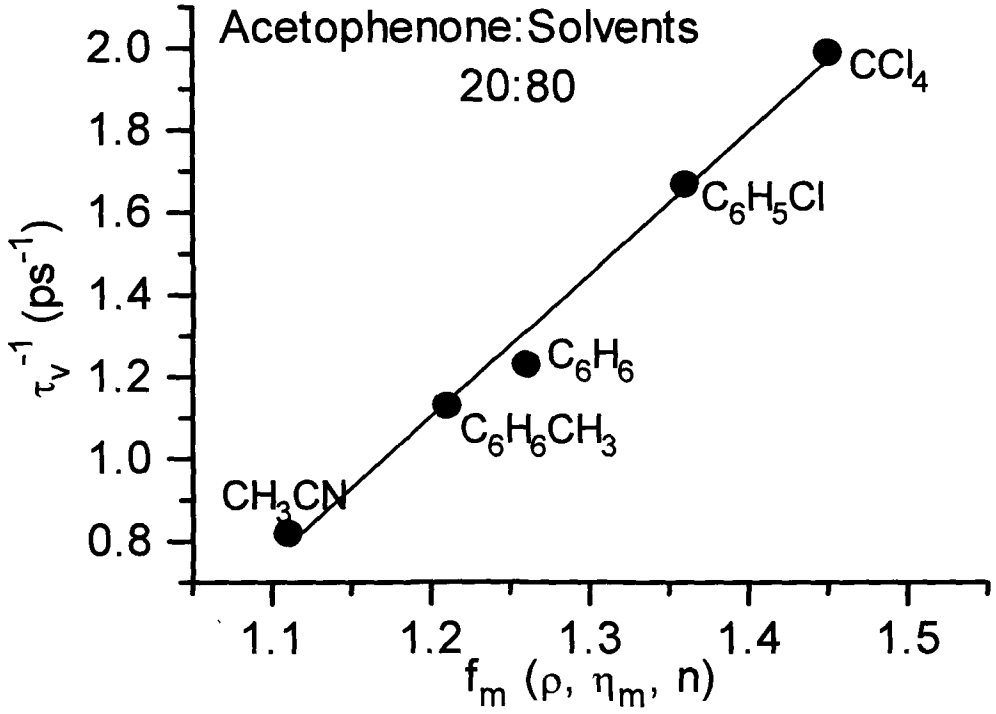

Fig. 5.5: The variation of τ_v^{-1} as a function of parameter f_m for Acetophenone molecule.

CHAPTER 6

CHAPTER 6

VIBRATIONAL RELAXATION STUDIES IN METHYL ACETATE: ROLE OF MICROENVIRONMENT AND HYDRODYNAMIC FORCES

6.1. INTRODUCTION

During the past few decades, vibrational relaxation processes has been studied by analyzing the isotropic and anisotropic profiles of a Raman band [1-30]. Conceptually, vibrational relaxation provides a critical testing ground for the theoretical models for intermolecular interactions in condensed phase as various mechanisms contribute to vibrational relaxation in liquids. The vibrational relaxation in molecular liquids is playing a very important role in analyzing the band shape of complex molecular systems. This process is responsible for the line broadening of the isotropic Raman spectral component and is generally considered to be due to contributions from vibrational dephasing, population relaxation and resonant energy transfer [3-4] and is expected to give

detailed information in the study of solution dynamics. The solvent contributions to vibrational frequencies and band widths are due to intermolecular interactions involving repulsive and attractive forces [7]. In solution, the solute molecule is surrounded by solvent molecules and the solvent cage exerts forces directed against the expansion of the solute molecule. The lingering of a molecule near another because of the hindering presence of solvent molecules is solvent cage effect. Lee and Richards [31] while explaining the interacting situations of solute and solvents showed that the centres of the atoms of the surrounding molecules are allowed to be placed near the probe (C=O). According to Eisenberg and Mclachlan [32], the solvent accessible areas and volumes of molecules may be used to quantify their interaction with the solvent. Moser et al [33] proposed a stochastic model which describes the exchange processes of two particles in the nearest neighbour shell of the reference molecule responsible for the line broadening. However, the vibrational relaxation process for complex molecular systems, sometimes cannot be explained on the basis of a macroscopic perception of the interacting systems.

It is interesting and useful to study the effects of different solvents on an active molecule through the changes in Raman vibrational bandwidth and frequency. The sensitivity of Raman bandwidth and frequency on the environmental conditions of the liquid

provides information not only about the intermolecular forces but also its microenvironment [14-20]. The interaction energy in the solution phase may arise as a result of contributions from various coupling mechanisms like dipole-dipole, dipole-quadrupole, quadrupole-quadrupole and higher multipolar interactions [11-12]. Besides, the hydrodynamic forces and the microenvironment are also responsible for the variation in bandwidths and frequencies. These types of interactions are interesting and complicated in nature and need to be investigated carefully.

Although studies of such type have been carried out in past few decades, the effect of microenvironment on the active molecule need to be investigated more thoroughly. Esters are very significant molecules in chemical physics, physical chemistry and biochemical reactions. In an attempt to characterize the role of the intermolecular interactions on the band parameters of the C=O stretching mode in esters, we have undertaken the study of vibrational relaxation rate, making use of the Raman band corresponding to the C=O stretching mode of the methyl acetate (MA) molecule. In MA the *trans*-configuration is the most stable, hence there is no possibility of rotational isomerism in this molecule. The microscopic parameters of such molecular systems could help chemists in increasing the reaction output and physicists to explain the intermolecular interactions in condensed states. The chemical dynamics

between molecules may depend upon the presence of solvents. The reaction between molecules and reaction products may be influenced by the presence of solvents. The microenvironment created by solvent may lead to the increase of the product formation if the reaction is diffusion controlled. The diffusion coefficient is going to play a significant role in such a situation as it depends upon microviscosity, which involves the solvent properties. Proper choice of the solvent will help in increasing the reaction products. The symmetric C=O stretching mode is suitable for probing the molecular environment as it is not perturbed by other vibrational modes.

6.3. EXPERIMENTAL

The Raman spectra of Methyl acetate in CH_3CN, CCl_4, $CHCl_3$, C_6H_6, C_6H_5Cl and $CH_3C_6H_5$ solvents have been recorded in a spectral region of ~ 1600-1800 cm^{-1}. All the samples were spectroscopic grade commercial compounds and were used without further purification. The spectral measurements for Raman bands were carried out by means of a Spex Ramalog 1403 double monochromator equipped with a photomultiplier tube and a photon counting arrangement. The spectrometer control and data processing were achieved with the help of a datamate using DM-3000 software. The excitation source was the 488 nm radiation from a Spectra Physics Model 165 argon ion laser with a power ~300 mW. All

measurements were done at ambient pressure and temperature. The slit width was kept at 3 cm^{-1} for recording all the spectra. The polarization of the laser light was vertical and the scattered light for both the vertical (I_{VV}) and horizontal (I_{VH}) polarization were recorded using a polarization analyzer with a 90° scattering geometry. A polarization scrambler located just in front of the spectrometer entrance slit was used in all experiments to correct the polarization bias of the double monochromator (grating).

The isotropic and anisotropic components of Raman band were found according to the formula:

$$I_{iso}(\nu) = I_{VV}(\nu) - \frac{4}{3} I_{VH}(\nu) \qquad (6.1)$$

$$I_{aniso}(\nu) = I_{VH}(\nu) \qquad (6.2)$$

where $I_{VV}(\nu)$ and $I_{VH}(\nu)$ are the polarized and depolarized Raman spectra respectively and ν is the wave number in cm^{-1}.

The corrections to the observed bandwidth were made using the relation [28] given by Tanabe and Hiraishi

$$\Gamma_t = \Gamma_a [1 - (S/ \Gamma_a)^2] \qquad (6.3)$$

where Γ_t and Γ_a are the true and apparent band width and S is the spectral slit width. All spectral conditions were adjusted to get the best

possible spectra and the accuracy of the spectral data is believed to be ± 0.5 cm^{-1}.

6.3. RESULTS AND DISCUSSION

The analysis of Raman band profile provides valuable clues about intermolecular forces, especially the study of isotropic component of the band is a probe for vibrational phase relaxation. In this study, we present the results of Raman studies on vibrational relaxation in MA as a function of the properties of solvents CH_3CN, CCl_4, $CHCl_3$, C_6H_6, C_6H_5Cl and $C_6H_5CH_3$ at a dilution of 80%. This particular concentration has been used as the anisotropy shift due to non–coincidence effect almost vanishes at this point in the above mentioned solvents. As a result the broadening due to resonant energy transfer process may be neglected. The Raman spectra of neat MA is shown in fig. 6.1. Although there is non-coincidence effect in neat liquid, the anisotropic band exhibits a broad feature therefore the variation of anisotropy shift in different solvents was not attempted in this molecule.

The relaxation rate serves as a probe of solute-solvent interactions. According to Kubo model [30], the vibrational relaxation rate [τ_v^{-1}] is proportional to the isotropic bandwidth (Γ_{iso}) for which the equation has the form

$$\tau_v^{-1} = \pi c \Gamma_{iso} \qquad (6.4)$$

The hydrodynamic model suggested by Purkayastha and Kumar [15] showed the dependence of isotropic bandwidth and hence relaxation rate on solvent parameters viz. dynamic viscosity (η), density (ρ) and dispersion force parameter $[(2n^2+1)/(n^2-1)]$ as follows:

$$\tau_v^{-1} = C_m f(\rho,\eta, n) \tag{6.5}$$

where C_m is a constant depending on solvent properties and

$$f(\rho,\eta, n) = \rho\eta\left(\frac{n^2-1}{2n^2+1}\right)^{-1} \tag{6.6}$$

Since the relaxation rate equation (6.4) is valid only for Lorentzian lineshape, the bandwidths in various solvents were measured for 80% solvent concentration where the bands exhibited Lorentzian lineshape. The Raman spectra of MA in CH_3CN, CCl_4, $CHCl_3$, C_6H_6, C_6H_5Cl and $C_6H_5CH_3$ solvents at 80% concentration of solvent are shown in fig 6.2.

Following this, the correlation between relaxation rate (τ_v^{-1}) and the parameter f (ρ,η,n) were plotted (Fig. 6.3). The plot shows that all data points do not fall on the straight line. The dynamic viscosity (η) is a macroscopic property of the solvent. In order to take care of the microenvironment, the concept of microviscosity [14-20] was introduced where the molecular size is shown to play an important role. It is possible that owing to the heterogeneity of the solute-solvent system, only a certain fragment of the solvent may interact with the solute

rather than the molecule as a whole. In the viscosity, the microfriction factor involving interaction between portions of solute and solvent would be more appropriate rather than the mere consideration of dynamic viscosity.

The theory of microviscosity takes into account the discreteness of the medium starting from the view that it is impossible to have various liquid layers separated by a distance less than the molecular size [34]. This is where lies the difference between the microviscosity theory and the Stokes theory in which infinitesimally close layers moving with different velocities are assumed. Introduction of the finite limiting distance of closeness between molecular layers in Strokes formalism leads to expression for coefficient of friction in the theory of microviscosity [35] as:

$$\beta = 6\pi\eta a\gamma = 6\pi\eta a\,[(3b/2a) + (1 + b/a)^{-1}]^{-1}$$

$$\approx 6\pi\eta a\,(0.19 + 0.31a/b) \qquad (6.7)$$

Here γ is the so-called microfriction factor for translational molecular motion which has the form

$$\gamma = [0.16 + 0.4(a/b)]$$

'b' is the radius of the molecule surrounding the molecule of radius 'a' considered.

The notion of microviscosity was introduced by Gierer, Spernol and Wirtz for establishing relations between Debye's correlation time τ_l and the coefficient of diffusion, on one hand and viscosity on the other hand [34]. They simultaneously carried out experimental verification of the relation (6.7) for dilute solutions, in which in place of relation (6.7) the empirical formula for the microviscosity was obtained [34] as follows

$$\eta_m = \eta\left[0.16 + 0.4\left(\frac{a}{b}\right)\right] \tag{6.8}$$

In the experimental verification, the molecular sizes were determined from the assumption of the closest packing of molecular spheres in the liquid (space factor 0.74).

By introducing this microfriction factor the equation (6.5) for the relaxation rate assumes the form:

$$\tau_v^{-1} = C f_m(\rho, \eta_m, n)$$

$$= C\eta\rho[0.16+0.4(a/b)][(2n^2+1)/(n^2-1)] \tag{6.9}$$

where 'a' and 'b' are the molecular radii of the interacting fragments of solute and the solvent molecules respectively. A proper choice of the parameters 'a' and 'b' may allow describing the contribution of environmental effects of neighboring solvent molecules.

Short-range solvation effect result from specific interaction of the solute with the solvent molecules as a result of which an ordered region

with specific microstructure in the vicinity of the dipole of solute (dipole is the probe here) is formed. The extent of this region is determined to a first approximation, by the size of the solvent molecules. The surface of a molecule bears information about how it interacts with other molecules and its solvent. The areas and volumes of the probe of the solute or solvent accessible surface may be used to quantify their interaction with the solvent [36]. It is the interaction (attraction) between the solute and solvent that is responsible for the friction in solution phase. The effective fluid friction will depend upon the orientation of the solute molecule, which does not remain fixed in the liquid. The values of 'a' and 'b' for the different types of solute-solvent systems were chosen according to the following considerations.

The dipole moment of the entire molecule is expected to be concentrated on the C=O bond, therefore, the primary interaction is associated with the dipole of the C=O bond. The solute van der Waals' radius in all cases is taken equal to the radius of the sphere of influence of the C=O bond as 2.8Å. This is obtained from [37] the sum of the C=O bond length (1.28 Å) and the van der Waals' radius of the oxygen atom (1.52 Å)

MA - CH_3CN system:

The CH_3CN molecule has symmetric top structure. The interaction of this top with the planar solute molecule MA, may be approximated as if the cylinder like C-C≡N portion of the solvent occupies a position near the cylinder like probe C=O bond. The strength of the coupling depends on the relative orientation of the two dipoles. The dipoles will try to orient because of dipole-dipole interaction. They are under thermal motion and also possess entropy. Both MA and CH_3CN have high dipole moments and the interaction is mainly through the dipole moment of the probe C=O bond of the solute molecule and the C-C≡N portion of the solvent. They may tend to align in parallel, antiparallel, head to tail or head to head configurations. In view of the fact that the antiparallel and head to tail are attractive configurations, one of them is likely. The layers are moving in the liquid and there is continuous motion of the molecules, therefore, antiparallel configuration is more likely. The entire C-C≡N portion has been considered to determine the radius of sphere of influence of CH_3CN as the orientation is not fixed in the liquid state. Therefore the solvent radius is taken as the radius of the sphere of influence of the C-C≡N portion [37] which is equal to sum of the C-C bond length (1.54 Å), C≡N bond length (1.15 Å) and the van der Waals' radius of nitrogen atom (1.55 Å).

MA - $C_6H_5CH_3$, MA - C_6H_6 and MA - C_6H_5Cl systems:

In the systems, where the solvents have a benzenoid portion, the C=O probe of the solute will be floating near the plate like benzenoid structure of the solvent molecules. The plate like structure is likely to be formed between the solute and solvent molecules. However, the interactions of such a simple type may not be feasible due to the presence of the π - electron of the benzenoid portion. The dipole of the C=O may not be oriented in a particular direction due to the non-dipolar nature of the benzenoid ring. The main interaction, which may contribute towards the viscosity, may therefore be due to the dipole-induced dipole interactions. This viscosity being due to the microenvironment is going to be responsible for the change in the vibrational relaxation rate. The carbon atom of the benzene ring may limit the distance of closest approach. The van der Waals' radius of carbon atom of the benzene ring is 1.77 Å and the same value is chosen as the solvent molecular radius here [37].

MA - CCl_4 system:

The CCl_4 is a non-polar molecule. It has a spherical shape and highly polarizable. It has recently been shown that the Cl atom of this molecule acquires a positive charge instead of behaving like an electronegative atom [38] due to polarization and as a result an

electrostatic potential is developed in the vicinity of the molecule whose value decreases with the increasing distance between the molecules (solute and solvent). The polarization effect is a result of electrical quadrupoles of the Cl atom in CCl_4. The spherical shape of the molecule may help it roll over the solute molecule, which has a planar structure. The sphere of influence of the C-Cl portion will therefore determine the distance of closest approach in the case of solvent. In view of the spherical shape, it is reasonable to consider that the radius of the molecule comprising of the C-Cl bond length (1.77 Å) and the Cl atom van der Waals' radius (1.75 Å) is considered [37] as the solvent radius.

MA – $CHCl_3$ system:

The hydrogen atom present in $CHCl_3$ is acidic in nature, and it may form a weak hydrogen bond with the C=O bond of the solute molecule. This appears to be reasonable due to the relatively large bandwidth (FWHM) in case of this solvent. It may be weakly associated with the C=O bond and the oscillations between oxygen and carbon atoms may not be as in the case of strongly hydrogen bonded systems. Nevertheless, the interaction may be sufficient to weaken the pair interaction at sufficiently high concentration of the solvent where several $CHCl_3$ molecules may surround the solute in a cage effect fashion. In such a hydrogen bonded system, the layer of $CHCl_3$

molecule may be formed over MA molecule. The C-H bond of the $CHCl_3$ may prefer an orientation in a head to tail configuration with the C=O bond of MA molecule forming a $H^+...O^-= C^+$ interacting system. If this configuration is preferred, hydrogen bonding may be the main interaction for the MA-$CHCl_3$ system. Therefore, in this case the value of the solvent radius is taken as 1.2 Å, representing the van der Waals' radius of hydrogen atom [37].

The molecular parameters for the solute and solvents are presented in Table 6.1.

The vibrational relaxation rate (τ_v^{-1}) is plotted (Fig. 6.4) as a function of the parameter $f_m(\rho,\eta_m,n)$ and the plot exhibits a straight line. This indicates that the data points fit better with the modified parameter $f_m(\rho,\eta_m,n)$ and also the dependence of relaxation rate on microscopic properties of solute-solvent systems. The correlation coefficients were calculated for the data points in the plots τ_v^{-1} vs. $f(\rho,\eta,n)$ and τ_v^{-1} vs. $f_m(\rho,\eta_m,n)$ and were found to be 0.638 and 0.993 respectively. So the parameter $f_m(\rho,\eta_m,n)$ provides a better correlation, hence is a better parameter to explain vibrational relaxation rate. This result supports the hydrodynamic-microviscosity model and is in agreement with our previous findings [11-20].

In the present study the solvent effect on the active molecule has been discussed in terms of solvation contributions arising from the local

complex molecule interactions. The shape of a molecule appear to be trivial in determining the vibrational relaxation rate. For example, both CH_3CN and $CHCl_3$ have a similar symmetric top structure but their bandwidths exhibit fairly large variations. This may be due to the difference in their hydrodynamic properties like density, viscosity and refractive index and also the mode of interactions of the solvents with the probe. It may be concluded that the fragments of solute and solvent molecules taking part in the interaction process are vital for the band broadening and the interactions related to these fragments are crucial for the vibrational relaxation rate. The interactions, which contribute to the vibrational relaxation, are important for variety of closely related condensed phase properties like chemical reaction rates. The vibrational relaxation rate of the C=O stretching fundamental vibration depends strongly on the solvents and its macroscopic as well as microscopic properties.

TABLE 6.1: Molecular parameters for the methyl acetate (MA)- solvent systems.

Molecular system	ρ (g/cm^3)	η (cP)	n	τ_v^{-1} (ps^{-1})	$f(\rho,\eta,n)$	$f_m(\rho,\eta_m,n)$
MA - CH_3CN	0.780	0.345	1.344	0.86	1.54	0.653
MA-$C_6H_5CH_3$	0.869	0.526	1.496	1.01	2.02	1.603
MA-C_6H_6	0.873	0.564	1.498	1.06	2.17	1.722
MA-C_6H_5Cl	1.107	0.631	1.524	1.16	2.98	2.363
MA-CCl_4	1.584	0.843	1.460	1.26	6.22	2.974
MA-$CHCl_3$	1.489	0.580	1.450	1.65	4.10	4.48

REFERENCES

1. H. Torii, J. Phys. Chem. A **108**, 2103 (2004).
2. M.G. Giorgini, Pure Appl. Chem. **76**, 157 (2004).
3. D. W. Oxtoby, J. Phys. Chem. **87**, 3028 (1983).
4. J. Jonas, Act.. Chem. Res. **17,** 74 (1984).
5. C.M. Cheatum, M.M. Heckscher, D. Bingemann, F.F. Crim, J. Chem. Phys. **115**, 7086 (2001).
6. M. Kolodziejski, G.Waliszewska, H. Abramczyk, J. Phys. Chem. A **102**, 1918 (1998).
7. G.R. Remar, R.A. Macphail, J. Chem. Phys. **103**, 4381 (1995).
8. J.S. Bader, B.J. Berne, J. Chem. Phys. **100**, 8359 (1994).
9. H. Torii, M. Tasumi, J. Raman Spectrosc. **22**, 601 (1991).
10. T.F. Sun, J.B. Chan, S.L. Wallen, J. Jonas, J. Chem. Phys. **94**, 7486 (1991).
11. A. Das, R. Das, K. Kumar, Spectrochim. Acta **58A**, 1583 (2002).
12. A. Das, K. Kumar, J. Raman Spectrosc. **30**, 547 (1999).
13. A. Purkayastha , K. Kumar, J. Raman Spectrosc. **19**, 249 (1988).
14. A. Purkayastha , K. Kumar, Spectrochim. Acta **43A**, 1269 (1987).
15. A. Das, K. Kumar, Spectrochim. Acta **54A**, 793 (1998).
16. A. Purkayastha, K. Kumar, J. Raman Spectrosc. **22**, 721 (1991).

17. A. Purkayastha , R. Das, K. Kumar, Spectrochim. Acta **47A**, 525 (1991).

18. A. Purkayastha , R. Das, K. Kumar, Spectrochim. Acta **46A**, 1545 (1990).

19. A. Purkayastha, R. Das, K. Kumar, J. Raman Spectrosc. **21,** 227 (1990).

20. Th.G. Devi, K. Kumar, J. Raman. Spectrosc. **35**, 835 (2004).

21. N. Meinander, M..M. Strube, A.N. Johnson, J. Laane, J. Chem. Phys. **86**, 4762 (1987).

22. A.F.T. Chen, M. Schwartz, Spectrochim. Acta **43A**, 1151 (1987).

23. T. Kato, J. Chem. Phys. **84**, 3409 (1986).

24. K. Tanabe, S. Tsuzuki, Spectrochim. Acta **42A**, 611 (1986).

25. S. Bratos, G. Tarjus, Phys. Rev. A **32**, 2431 (1985).

26. E.W. Knapp, J Chem. Phys. **81**, 643 (1984).

27. E.W. Knapp, S.F. Fischer, J Chem. Phys. **76**, 4730 (1982).

28. K. Tanabe, J. Hiraishi, Spectrochim. Acta. **36A**, 341 (1980).

29. R.J. Bartholomew, D.E. Irish, J. Raman Spectrosc. **29**, 115 (1997).

30. R. Kubo, J. Phys. Soc. Jpn. **17**, 1100 (1962).

31. Lee B., F. M. Richards, J. Mol. Biol., **55**, 379 (1971).

32. Eisenberg. D, A. D. Mclachlan, Nature, **319**, 199(1986).

33. G. Moser, A. Asenbaum, J. Barton and G. Döge, J. Chem. Phys. **102**, 1173 (1995).

34. V.V. Frolov, in "Nuclear Magnetic Resonance" Edited by P.M. Borodin, Amerind, New Delhi (1975).

35. A. Gierer, K. Wirtz, Zs. Naturforschung, **8a**, 522 (1953).

36. D. Eisenberg, A.D. McLachlan, Nature **319**, 199 (1986).

37. A. Bondi, J. Phys. Chem. **68**, 441 (1964).

38. H. Torii . J. Chem. Phys. **119**, 2192 (2003).

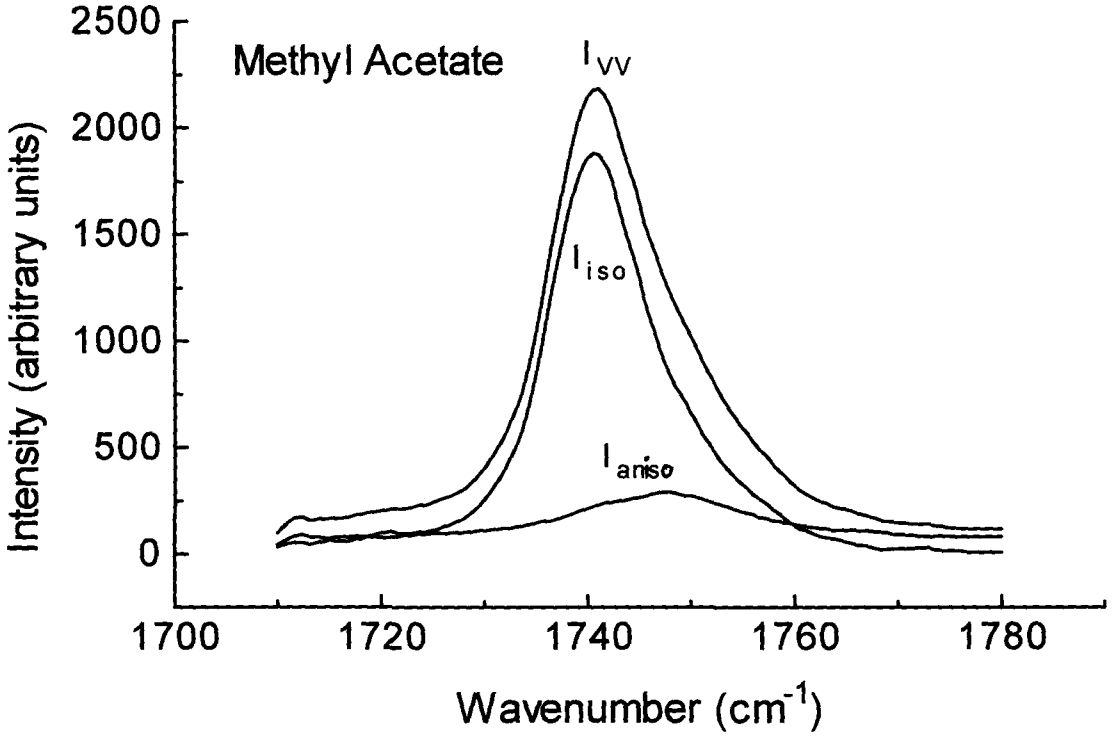

FIG 6.1: RAMAN SPECTRUM OF NEAT LIQUID METHYL ACETATE (MA)

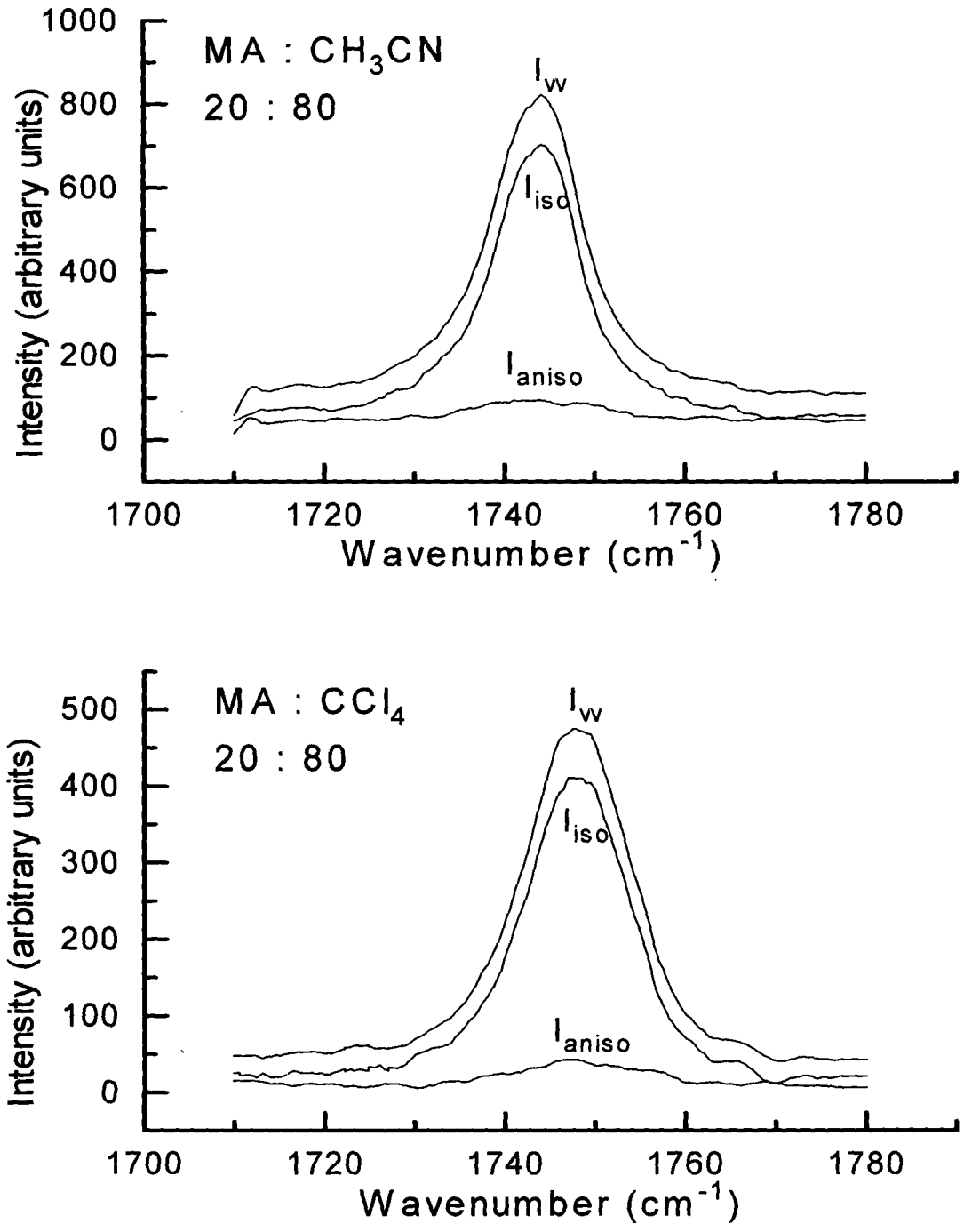

Fig 6.2: Raman spectra of MA in CH_3CN and CCl_4

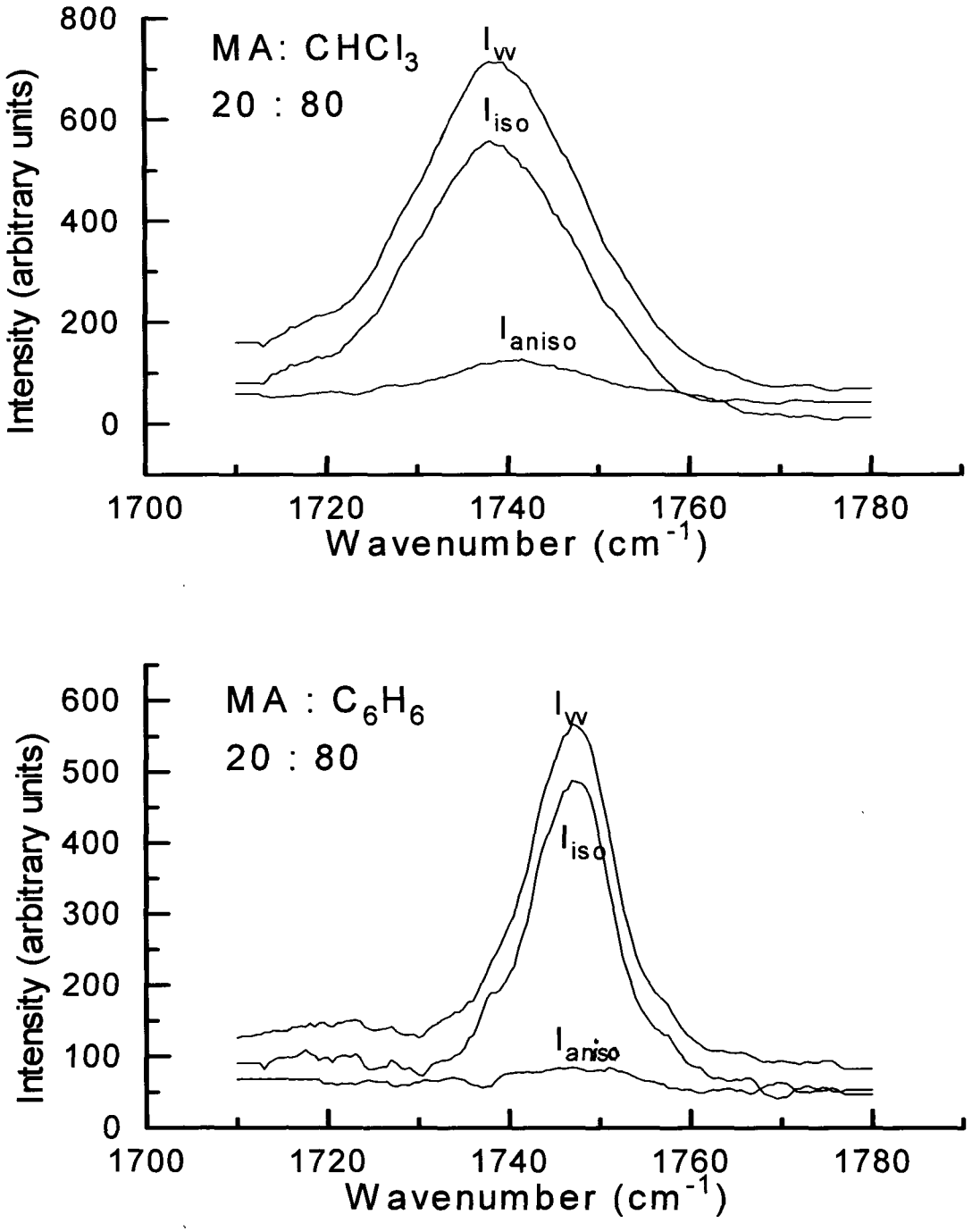

Fig 6.2: Raman spectra of MA in$CHCl_3$ and C_6H_6

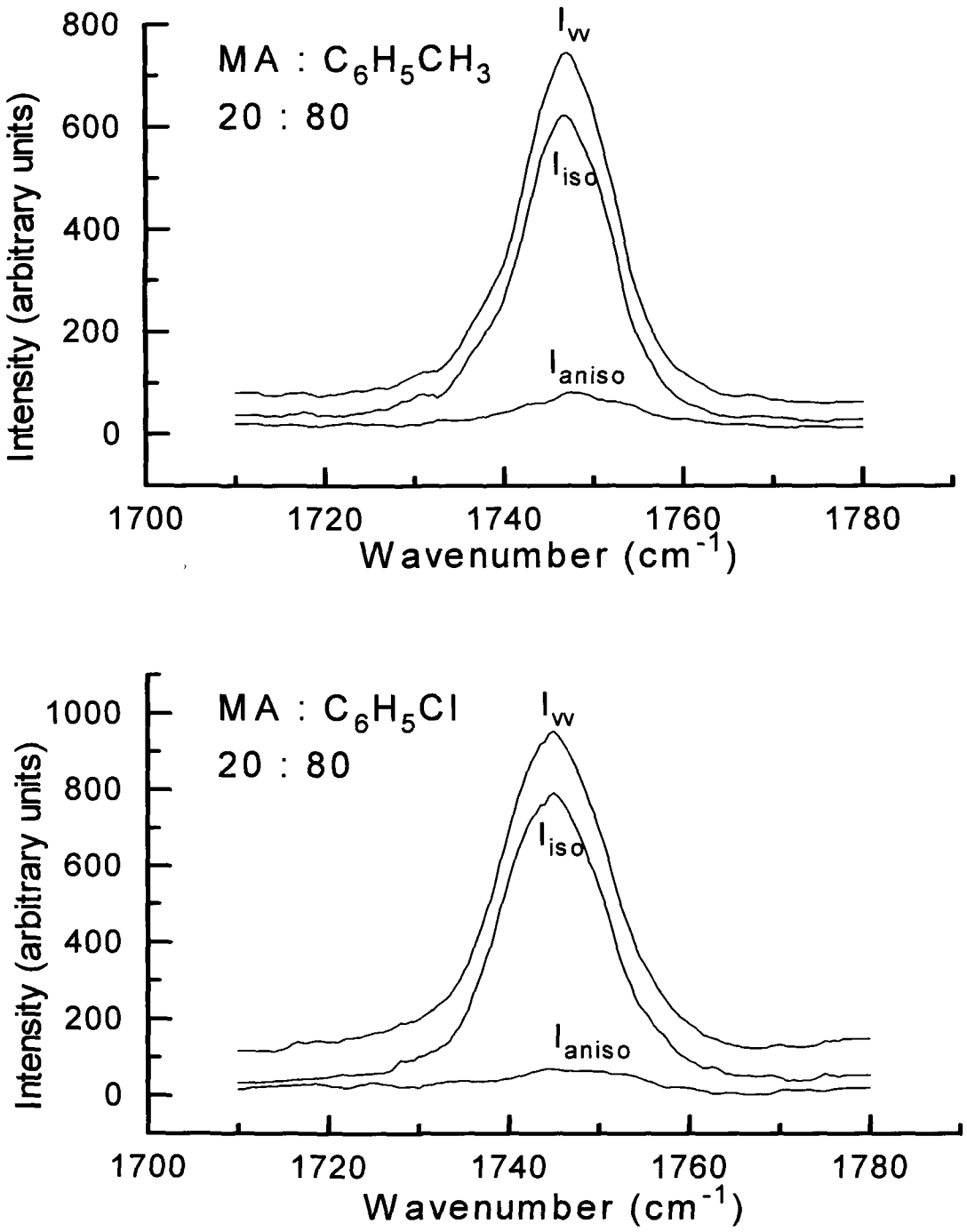

Fig 6.2: Raman spectra of MA in C_6H_5Cl and C_6H_5Cl

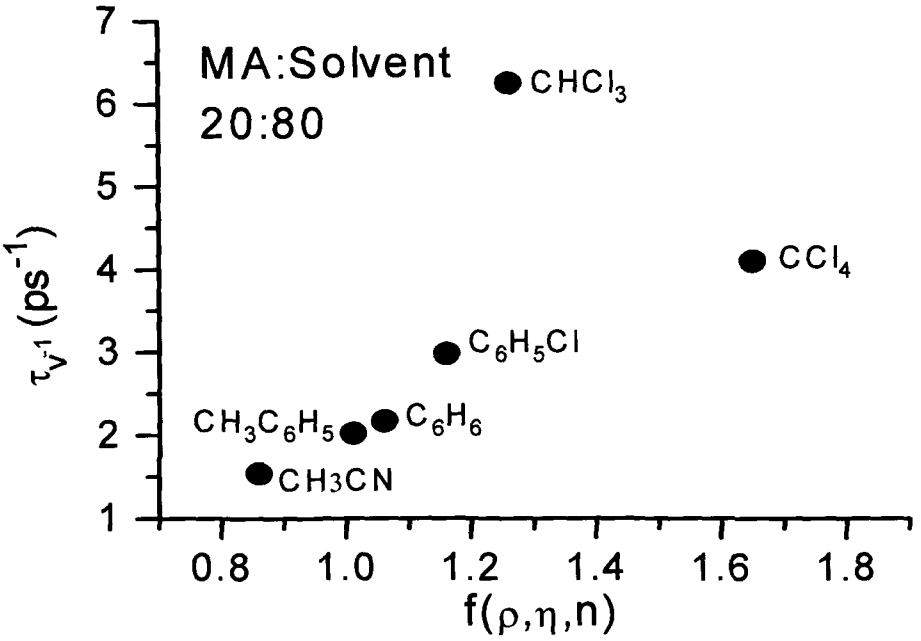

Fig. 6.3: The variation of τ_v^{-1} as a function of f(ρ,η,n)

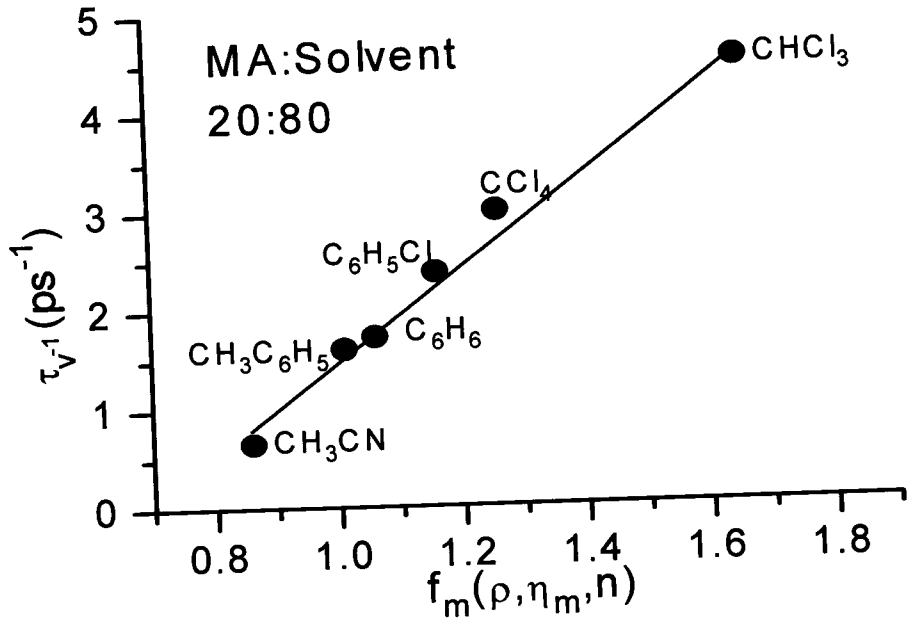

Fig. 6.4: The variation of τ_v^{-1} as a function of $f_m(\rho,\eta_m,n)$

CHAPTER 7

CHAPTER 7

CONCLUSION

Vibrational dynamics and spectra of molecules in the liquid phase are affected by intermolecular interactions in various ways. The Raman scattering experiments are well suited to investigate the structure and dynamic processes in the liquid phase. It is possible to get the information about the chosen molecular system according to the shape and position of the spectral bands in varying environment. The analysis of the non-coincidence effect, a spectroscopic manifestation of the intermolecular coupling in molecular liquids has been carried out and presented. Besides the lineshape analysis of vibrational transitions have been recognized as a powerful tool for extracting information on molecular dynamics in condensed phases. The contributions of vibrational dephasing have been examined in detail in varying environmental conditions and are presented in the thesis.

The Raman studies have been carried out for the C=O symmetric stretching vibration of methyl ethyl ketone (MEK), acetophenone and methyl acetate (MA) molecules as solutions in solvents of varying dipole

moments, dielectric constants and refractive indices. The size and shape of the solvent molecules are also chosen to be different. The intermolecular interactions and the dependence of the Raman band shape on the solvent properties were studied. The solvent induced perturbations, which lead to fluctuations in the solute vibrational frequency, mainly contribute to the band broadening and vibrational relaxation rate.

The stretching vibration of the carbonyl bond of MEK molecule has been studied mainly with regard to non-coincidence effect (NCE) and the entire dipole moment is supposed to be on the C=O bond. The Raman spectra for MEK were recorded in CH_3CN, CCl_4, $CHCl_3$, C_6H_6, $C_6H_5CH_3$ and C_6H_5Cl solvents at different concentrations ranging from 10% to 90%. The isotropic and anisotropic Raman components show non-coincidence with the anisotropic component shifted to higher wavenumber position. The local order of the solute molecules is mainly due to orientation dependent dipole-dipole interactions. The dominant mechanism responsible for the NCE (anisotropy shift) is however, because of the Transition dipole-Transition dipole interaction. The anisotropy shift goes on reducing as the concentration of the solvent is increased which may be due to the reduction of the interaction between solute molecules.

The NCE was studied by taking into account the screening factor

related to the permanent and transition dipoles. The Onsager - Fröhlich dielectric continuum model was employed to study the behaviour of anisotropy shift at various solvent concentrations. The plot of the anisotropy shift function $F = \Delta\nu\ (2\varepsilon + n^2)^2\ \varepsilon^{-1}$ as a function of solute volume fraction Φ, for different solvent shows that the data points fit well in exponential curves for all solvents except CH_3CN. The dielectric continuum theory is applicable and may explain the MEK-CH_3CN system. It may be due to the high dielectric constant of the CH_3CN solvent. For all other solvents under study, the observation reveals that the Onsager-Fröhlich dielectric continuum model based upon the transition dipole coupling mechanism does not hold good. At the most it may be expected to be valid only for dilute solutions. The concentration dependence of shift may be due to several interactions such as dipole-dipole, dipole-quadrupole, quadrupole-quadrupole and higher multipole interactions in the solute-solvent systems. In these systems, discreteness of the medium also exists. The effect of dispersion forces and various multipolar interactions are likely to vary from solvent to solvent. Hence it is clear that the dielectric screening may not be as effective as envisaged by the Onsager-Fröhlich continuum model in such systems. The fitting of the data to exponential curves indicates that an exponential factor is coming into play, which may be due to the presence of repulsive forces. By considering the molecular interactions

as hard sphere interaction model, it may be inferred that the repulsive potential function of the type $e^{-\alpha R}$ (where R is the appropriate distance of closest approach and α is a constant) is playing a dominant role, in most of the solute-solvent systems. Fluctuations of dipole moments and polarizabilities may arise as a result of concentration fluctuations. The steric effects and atomic quadrupole effects may be responsible for the repulsive nature of the intermolecular forces.

The vibration of a reference mode is influenced by solvent and concentration dependent fluctuations. The Raman isotropic component of C=O stretching mode of acetophenone molecule dissolved in CH_3CN, CCl_4, C_6H_6, $C_6H_5CH_3$ and C_6H_5Cl solvents were studied.

The shape of the band was studied at various concentrations ranging from 10% to 90% for all the solvents mentioned earlier in order to see the behaviour of the line shape as a function of concentration. A Lorentzian function $\omega(t)$ can be transformed into a linear equation of the form

$$1 / I_{iso} = K_1 (\omega - \omega_o) + K_2$$

where I_{iso} represent the intensity of the isotropic Raman component and $K_1$and K_2 being two constant terms. The correlation coefficient 'r' was estimated for the isotropic Raman band with reference to Lorentzian line shape. The correlation coefficient 'r' thus obtained essentially reflects the nature of bandshape with reference to the Lorentzian

character of the band. It is observed to exhibit concentration dependent features, which are interesting from the point of view of microscopic nature of the intermolecular interactions in solution phase. The observed data are found to be highly concentration dependent. Therefore the correlation coefficient 'r' was plotted as a function of solvent concentration. The data points are found to fit well in two straight lines with a sharp discontinuity in the intermediate region of solvent concentration. The data points also indicate that the band shape undergoes a change from non-Lorentzian to Lorentzian character in all solvents. The resonant energy transfer mechanism leading to pair correlation in pure liquid is suppressed by the solvent induced perturbations. The non-Lorentzian character appears to derive its major contribution through resonant energy transfer mechanism. The increase in solvent concentration leads to the weakening of the microscopic local order which results in the gradual fall of contribution from the RET process. This as a result imparts a gradual approach to the Lorentzian nature of the Raman band shape in the region of high solvent concentration. The discontinuity in the intermediate region may be attributed to structure breaking effect and local fluctuations when the solute and solvent molecules become comparable in number. The size and shape of the molecule may be significant in explaining this

interesting feature of change from non-Lorentzian to Lorentzian bandshape.

The molecular ensemble sees a different environment, and the vibrational frequency is, therefore, perturbed by various interaction potentials depending upon geometric relationship. The microscopic processes involved are also responsible for the dephasing. The vibrational dephasing process in molecular liquid leads to the broadening of the isotropic Raman spectral component. The Raman isotropic components at 80% solvent concentration were obtained for acetophenone and methyl acetate molecules. It was seen that the isotropic component exhibited Lorentzian line shape at this concentration. The isotropic band width [Γ_{iso}] was measured at 80% dilution in different solvents to find the dephasing rate (τ_v^{-1}) which is given as:

$$\tau_v^{-1} = \pi c \Gamma_{iso}$$

where c is the velocity of light. The theoretical explanation for the dephasing process may be given by correlating the vibrational relaxation rate (τ_v^{-1}) with some molecular parameters taking into account the effect of solvent electric field on the solute molecule. The various models proposed for explaining the dephasing process take into account the dynamic viscosity (η), a macroscopic property. The finer

details of the liquid structure, however, require a model incorporating the microviscosity (η_m).

The microviscosity may be calculated from the dynamic viscosity by estimating the appropriate values of solute and solvent radii. These radii have been estimated keeping in view the relative orientation of the molecular fragments. The intermolecular interactions as well as hydrodynamic properties of the liquid have also been kept in mind. At sufficiently high concentration of the solvent, the solute molecule may be considered to be in a cage of solvent molecules with an occasional escape to the adjacent position. The solvent microviscosity [η_m] is defined taking into account the distance of closest approach of the solute-solvent molecules as:

$$\eta_m = \eta\ [0.16+0.4(a/b)]$$

where 'a' and 'b' are the molecular radii of the interacting fragments of the solute and solvent respectively. This value is substituted in place of the dynamic viscosity and a new parameter [f_m] was obtained as

$$f_m(\rho,\eta_m,n) = f\ (\rho,\eta,n)\ [0.16+0.4(a/b)]$$

The vibrational relaxation rate is

$$\tau_v^{-1} \propto f_m\ (\rho,\eta_m,n)$$

The variation of τ_v^{-1} with respect to f_m was then plotted. This graph showed linear behaviour, which indicates that the discreteness of the

medium due to solvents has a significant influence on the dephasing process in complex molecular systems. The microenvironment around the solute molecule is vital for the band broadening. The interactions related to the molecular fragments are also significant in determining the vibrational relaxation rate.

LIST OF PUBLICATIONS

1. Non-coincidence effect in methyl ethyl ketone: a solvent dependent Raman study,
   Soma Datta and K. Kumar, *J. Raman Spectrosc.* **36**, 50 (2004)

2. Vibrational dephasing and hydrodynamic effects on vibrational relaxation rates in acetophenone: Raman bandshape analysis,
   Soma Datta and K. Kumar, *Spectrochim. Acta*, **62A**, 413 (2005)

3. Vibrational relaxation studies in methyl acetate: Role of microenvironment and hydrodynamic forces,
   Soma Datta and K. Kumar, *Spectrochim. Acta Part A* (in press)

4. Solvent dependent study of anisotropy shift in methyl isobutyl ketone,
   Soma Datta and K. Kumar, in *Proceedings of the XVth national conference on Atomic and Molecular Physics*, p-56, PRL, Ahmedabad (2004)

5. Dependence of Raman anisotropic bandwidth on van der Waals' volume of the complex interacting systems,
   Th.G. Devi, Soma Datta and K. Kumar, in *Proceedings of IVth DAE-BRNS National Laser Symposium,* edited by B. M. Suri, V. K. Mago and Alok. K. Ray, p. 454, Allied Publishers Pvt. Ltd., New Delhi (2005)

6. Solvent dependent Raman bandshape analysis of C=O stretching mode of Methyl Ethyl Ketone,
   Soma Datta, Th.G. Devi and K. Kumar, in *Proceedings of DAE-BRNS National Laser Symposium,* edited by B. M. Suri, V. K. Mago and Alok. K. Ray, p. 718, Allied Publishers Pvt. Ltd., New Delhi (2005)

Particulars of the Candidate

Name of the Candidate	**: Ms. Soma Datta**
Degree	**: Ph. D.**
Department	**: Physics**
Title of the Dissertation	**: Vibrational band shape analysis and intermolecular interactions in some complex molecules**
Date of payment of admission fee	**: 24. 10. 2002**
Approval of Research proposal School Board	**: 28. 10. 2003**
Registration No. and Date	**: 756 of 28. 10. 2003**
Extension (if any)	**: No**

P. Nongkynrih

(Prof. P. Nongkynrih)
Head
Department of Physics
NEHU, Shillong

Prof. & Head,
Physics Department,
N.E.H.U. Shillong-793022.